UNIVERSITAT
POLITÈCNICA
DE VALÈNCIA

Mesoporous silica nanoparticles targeting tumor microenvironment as a tool for breast cancer treatment

PhD THESIS

Ana Catarina Trigo Lameirinhas

PhD supervisors:

Dr. Pilar Eroles Asensio

Prof. Ramón Martínez Máñez

Dr. Iris Garrido Cano

Valencia, June 2024

“Science knows no country,
because knowledge belongs to humanity,
and is the torch which illuminates the world.”
Louis Pasteur

Dedicated to my loved ones.

The work presented in this doctoral thesis was carried out in the Breast Cancer Biology Group at INCLIVA Health Research Institute from January 2020 to June 2024 under the supervision of Dr. Pilar Eroles Asensio, Prof. Ramón Martínez Máñez, and Dr. Iris Garrido Cano.

This work has been supported by the following fellowships and grants:

— Asociación Española contra el Cáncer AECC predoctoral fellowship to Ana Lameirinhas.

Publications

The following scientific publications results from the results obtained from this PhD Thesis and contributions to other studies:

- Marta Tapia, Cristina Hernando, María Teresa Martínez, Octavio Burgués, Cristina Tebar-Sánchez, **Ana Lameirinhas**, Anna Ágreda-Roca, Sandra Torres-Ruiz, Iris Garrido-Cano, Ana Lluch, Begoña Bermejo, Pilar Eroles. (2023) Clinical Impact of New Treatment Strategies for HER2-Positive Metastatic Breast Cancer Patients with Resistance to Classical Anti-HER Therapies. Cancers.
- Iris Garrido-Cano, Anna Adam-Artigues, **Ana Lameirinhas**, Juan F. Blandez, Vicente Candela-Noguera, Ana Lluch, Begoña Bermejo, Felix Sancenón, Juan Miguel Cejalvo, Ramón Martínez-Máñez, Pilar Eroles. (2023) Delivery of miR-200c-3p Using Tumor-Targeted Mesoporous Silica Nanoparticles for Breast Cancer Therapy. ACS Applied Materials & Interfaces.
- Sandra Torres-Ruiz, Eduardo Tormo, Iris Garrido-Cano, **Ana Lameirinhas**, Federico Rojo, Juan Madoz-Gúrpide, Octavio Burgués, Cristina Hernando, Begoña Bermejo, María Teresa Martínez, Ana Lluch, Juan Miguel Cejalvo, Pilar Eroles. (2023) High VEGFR3 Expression Reduces Doxorubicin Efficacy in Triple-Negative Breast Cancer. International Journal of Molecular Sciences.
- Birlipta Pattanayak, **Ana Lameirinhas**, Sandra Torres-Ruiz, Octavio Burgués, Ana Rovira, María Teresa Martínez, Marta Tapia, Sandra Zazo, Joan Albanell, Federico Rojo, Begoña Bermejo, Pilar Eroles. (2022) Role of SALL4 in HER2+ breast cancer progression: regulating PI3K/AKT pathway. International Journal of Molecular Sciences.
- Iris Garrido-Cano, Anna Adam-Artigues, **Ana Lameirinhas**, Juan F Blandez, Vicente Candela-Noguera, Federico Rojo, Sandra Zazo, Juan

ABSTRACT

Madoz-Gúrpide, Ana Lluch, Begoña Bermejo, Felix Sancenón, Juan Miguel Cejalvo, Ramón Martínez-Máñez, Pilar Eroles. (2022) miR-99a-5p modulates doxorubicin resistance via the COX-2/ABCG2 axis in triple-negative breast cancer: from the discovery to *in vivo* studies. Cancer Communications.

- Iris Garrido-Cano, Birlipta Pattanayak, Anna Adam-Artigues, **Ana Lameirinhas**, Sandra Torres-Ruiz, Eduardo Tormo, Raimundo Cervera, Pilar Eroles. (2021) MicroRNAs as a clue to overcome breast cancer treatment resistance. Cancer and Metastasis Reviews.
- Anna Adam-Artigues*, Iris Garrido-Cano*, Juan Antonio Carbonell-Asins, **Ana Lameirinhas**, Soraya Simón, Belén Ortega-Morillo, María Teresa Martínez, Cristina Hernando, Vera Constâncio, Octavio Burgues, Begoña Bermejo, Rui Henrique, Ana Lluch, Carmen Jerónimo, Pilar Eroles, Juan Miguel Cejalvo. (2021) Identification of a Two-MicroRNA Signature in Plasma as a Novel Biomarker for Very Early Diagnosis of Breast Cancer. Cancers (* equal contribution).
- Anna Adam-Artigues, Iris Garrido-Cano, Soraya Simón, Belen Ortega, Santiago Moragón, **Ana Lameirinhas**, Vera Constâncio, Sofia Salta, Octavio Burgués, Begoña Bermejo, Rui Henrique, Ana Lluch, Carmen Jerónimo, Pilar Eroles, Juan Miguel Cejalvo. (2021) Circulating miR-30b-5p levels in plasma as a novel potential biomarker for early detection of breast cancer. ESMO Open.

Iris Garrido-Cano, Vera Constâncio, Anna Adam-Artigues, **Ana Lameirinhas**, Soraya Simón, Belen Ortega, María Teresa Martínez, Cristina Hernando, Begoña Bermejo, Ana Lluch, Paula Lopes, Rui Henrique, Carmen Jerónimo*, Juan Miguel Cejalvo*, Pilar Eroles*. (2020) Circulating miR-99a-5p Expression in Plasma: A Potential Biomarker for Early Diagnosis of Breast Cancer. International Journal of Molecular Sciences (* equal contribution).

Abstract

Most of the breast cancer therapies currently used in the clinical practice are focused on targeting tumor cells. Nevertheless, new advances in the immunology field uncovered the main role of the tumor microenvironment in tumor modulation. Specifically, cancer-associated fibroblasts play an important role in tumor progression, tumor immunity modulation, and therapy resistance. Hence, this Ph.D. thesis entitled "Mesoporous silica nanoparticles targeting tumor microenvironment as a tool for breast cancer treatment" is focused on the design of a nanodevice targeting cancer-associated fibroblasts and on the evaluation of its potential as a new therapeutic strategy for breast cancer treatment.

A nanoparticle was designed and synthesized using mesoporous silica nanoparticles as support, loaded with doxorubicin, and functionalized with a FAP-α ligand peptide (NP-FAP-DOX). NP-FAP-DOX's characterization showed controlled cargo release and an *in vitro* nontoxic profile.

The *in vitro* studies evaluated the nanoparticle efficacy to target FAP-α, cellular cytotoxicity, and tumor penetration in breast cancer cell lines, cancer-associated fibroblasts derived from triple-negative breast cancer patient biopsies, and breast cancer patient-derived organoids. These studies probed that the NP-FAP-DOX efficiently targeted and produced a cytotoxic effect in breast cancer cells with FAP-α positive expression as well as in cancer-associated fibroblasts. Moreover, the NP-FAP-DOX presented good penetration efficiency in patient-derived organoids, while maintaining the targeting and cytotoxic effect in this 3D model.

Finally, the NP-FAP-DOX's *in vivo* efficacy was evaluated in a murine triple-negative breast cancer model. The NP-FAP-DOX showed a tumor-targeting ability and effective drug delivery, resulting in an *in vivo* antitumoral effect. Moreover, the NP-FAP-DOX *in vivo* treatment efficiently

targeted and depleted cancer-associated fibroblasts, leading to tumor microenvironment re-modulation and activation of tumor immune response. Specifically, this treatment promoted lymphocyte infiltration, increased the percentage of natural killer cells, and decreased the M2-like macrophages leading to an increased M1/M2 ratio in tumors. Besides, the nanoparticles improved the therapeutic and safety profile of the free drug, preventing doxorubicin-induced cardio and systemic toxicity.

Overall, these results demonstrated the potential of the designed nanodevices as a new targeted drug delivery system for breast cancer treatment. These nanoparticles can improve drug delivery efficacy, overcome adverse side effects, and enhance therapy efficacy through the modulation of the tumor microenvironment.

Resumen

La mayoría de las terapias contra el cáncer de mama que se utilizan actualmente en la práctica clínica se centran en atacar las células tumorales. Sin embargo, los nuevos avances en el campo de la inmunología han resaltado el papel principal del microambiente tumoral en la modulación tumoral. Específicamente, los fibroblastos asociados al cáncer desempeñan un papel importante en la progresión tumoral, la modulación de la inmunidad tumoral y la resistencia a la terapia. Por ello, esta tesis doctoral titulada “Nanopartículas de sílice mesoporosas dirigidas al microambiente tumoral como herramienta para el tratamiento del cáncer de mama” se centra en el diseño de un nanodispositivo dirigido a los fibroblastos asociados al cáncer y en la evaluación de su potencial como nueva estrategia terapéutica para el tratamiento del cáncer de mama.

Se diseñó y sintetizó una nanopartícula utilizando nanopartículas mesoporosas de sílice como soporte, cargadas con doxorrubicina y funcionalizadas con un péptido ligando de FAP-α (NP-FAP-DOX). La caracterización de NP-FAP-DOX mostró una liberación controlada de la carga y un perfil no tóxico *in vitro*.

Los estudios *in vitro* evaluaron la eficacia de las nanopartículas para dirigirse a FAP-α, la citotoxicidad celular y la penetrabilidad tumoral en las líneas celulares de cáncer de mama, en los fibroblastos asociados al cáncer derivados de biopsias de pacientes con cáncer de mama triple negativo y en los organoides derivados de pacientes con cáncer de mama. Estos estudios demostraron que NP-FAP-DOX se dirigió eficazmente y produjo un efecto citotóxico en células de cáncer de mama con expresión positiva de FAP-α, así como en fibroblastos asociados al cáncer. Además, la NP-FAP-DOX presentó una buena eficiencia de

penetración en los organoides derivados de paciente, manteniendo así la acción dirigida y el efecto citotóxico en este modelo tridimensional.

Finalmente, se evaluó la eficacia de NP-FAP-DOX *in vivo* en un modelo murino de cáncer de mama triple negativo. La NP-FAP-DOX mostró una buena capacidad para atacar tumores y una administración eficaz de fármacos, lo que dio como resultado un efecto antitumoral *in vivo*. Además, el tratamiento *in vivo* con NP-FAP-DOX se dirigió eficazmente a los fibroblastos asociados al cáncer y los eliminó, lo que llevó a la remodulación del microambiente tumoral y a la activación de la respuesta inmunitaria del tumor. Específicamente, este tratamiento promovió la infiltración de linfocitos, aumentó el porcentaje de células asesinas naturales y disminuyó los macrófagos M2, lo que llevó a un aumento de la proporción M1/M2 en los tumores. Además, las nanopartículas mejoraron el perfil terapéutico y de seguridad del fármaco libre, previniendo la toxicidad cardíaca y sistémica inducida por doxorrubicina.

Con todo, estos resultados demostraron el potencial de los nanodispositivos diseñados como un nuevo sistema de administración de fármacos dirigido para el tratamiento del cáncer de mama. Estas nanopartículas pueden mejorar la eficacia de la administración de fármacos, superar los efectos secundarios adversos y mejorar la eficacia de la terapia mediante la modulación del microambiente tumoral.

Resum

La majoria de les teràpies contra el càncer de mama que s'utilitzen actualment en la pràctica clínica, es centren en atacar les cèl·lules tumorals. Tanmateix, els nous avanços en el camp de la immunologia han ressaltat el paper principal del microambient tumoral en la modulació tumoral. Específicament, els fibroblasts associats al càncer tenen un paper important en la progressió tumoral, la modulació de la immunitat tumoral i la resistència a teràpia. Per això, aquesta tesi doctoral titulada "Nanopartícules de sílice mesoporoses dirigides al microambient tumoral com a ferramenta per al tractament del càncer de mama" es centra en el disseny d'un nanodispositiu dirigit als fibroblasts associats al càncer i en l'avaluació del seu potencial com a nova estratègia terapèutica per al tractament del càncer de mama.

Es va dissenyar i sintetitzar una nanopartícula utilitzant nanopartícules mesoporoses de sílice com a suport, carregades amb doxorubicina i funcionalitzades amb un pèptid lligand de FAP-α (NP-FAP-DOX). La caracterització de NP-FAP-DOX va mostrar un alliberament controlat de la càrrega i un perfil no tòxic *in vitro*.

Els estudis *in vitro* van avaluar la eficàcia de les nanopartícules en l'acció dirigida a FAP-α, la citotoxicitat cel·lular i la penetrabilitat tumoral en les línies cel·lulars de càncer de mama, en els fibroblasts associats al càncer derivats de biòpsies de pacients amb càncer de mama triple negatiu i en els organoides derivats de pacients amb càncer de mama. Aquests estudis van demostrar que NP-FAP-DOX es dirigia eficaçment i produïa un efecte citotòxic en les cèl·lules de càncer de mama amb expressió positiva de FAP-α, així com en fibroblasts associats al càncer. A més, la NP-FAP-DOX va presentar una bona eficiència de penetració

en els organoides derivats de pacient, mantenint així l'acció dirigida i l'efecte citotòxic en aquest model tridimensional.

Finalment, es va avaluar la eficàcia de NP-FAP-DOX *in vivo* en un model murí de càncer de mama triple negatiu. La NP-FAP-DOX va mostrar una bona capacitat per a atacar tumors i una administració eficaç de fàrmacs, el que va donar com a resultat un efecte antitumoral *in vivo.* Addicionalment, el tractament *in vivo* amb NP-FAP-DOX es va dirigir eficaçment als fibroblasts associats al càncer generant la seua depleció i així, la remodelació del microambient tumoral i l'activació de la resposta immunitària del tumor. Específicament, aquest tractament va promoure la infiltració de limfòcits, va augmentar el percentatge de cèl·lules citocides naturals i va disminuir els macròfags M2, el que va conduir a un augment en la proporció M1/M2 en els tumors. A més, les nanopartícules van millorar el perfil terapèutic i de seguretat del fàrmac lliure, prevenint la toxicitat cardíaca i sistèmica induïda per la doxorubicina.

Amb tot, aquests resultats demostraren el potencial dels nanodispositius dissenyats com un nou sistema d'administració de fàrmacs dirigits per al tractament del càncer de mama. Aquestes nanopartícules poden millorar l'eficàcia de l'administració de fàrmacs, reduir els efectes secundaris adversos i millorar l'eficàcia de la teràpia mitjançant la modulació del microambient tumoral.

Table of contents

Figure index

Table index

Abbreviations

ACK – ammonia-chloride-potassium

ACN – acetonitrile

ADAMTS1 – a disintegrin and metalloproteinase (ADAM) with thrombospondin motifs 1

AKT – AKT serine-threonine kinase

ANGPTL4 – angiopoietin-like 4

ATCC – American Type Culture Collection

ATM – ataxia telangiectasia mutated

ATP – adenosine triphosphate

AUF1 – high heterogeneous nuclear ribonucleoprotein D

BC – breast cancer

BRCA – breast cancer gene

BRIP1 – BRCA1 interacting helicase 1

BSA – bovine serum albumin

CAF – cancer-associated fibroblast

Cav-1 – caveolin-1

cCASP3 – cleaved caspase-3

CCL – C-C motif chemokine ligand

CDH1 – cadherin-1

CDK – cyclin-dependent kinase

CHEK2 – checkpoint kinase 2

Chi3L1 – chitinase 3 like 1

ABBREVIATION

CLU – clusterin

c-Met – MET proto-oncogene, receptor tyrosine kinase

CSF-1 – monocyte chemotactic protein-1

CSF-1R – colony-stimulating factor-1 receptor

CTABr – N-cetyltrimethylammonium bromide

CTGF – connective tissue growth factor

CTHRC1 – collagen triple helix repeat containing-1

CTLA-4 – cytotoxic T-lymphocyte antigen 4

CXCL – chemokine (C–X–C motif) ligand

DAPI – 4',6-diamidino-2-phenylindole

DAPI – 4',6-diamidino-2-phenylindole (DAPI

DIC – ductal invasive carcinoma

Dll1 – delta-like canonical Notch ligand 1

DLS – dynamic light scattering

DMSO – dimethyl sulfoxide

DOX – doxorubicin

ECM – extracellular matrix

EDC – *N*-Ethyl-*N*′-(3-dimethylaminopropyl)carbodiimide hydrochloride

EGFR – epidermal growth factor receptor

EMT – epithelial-to-mesenchymal transition

ER – estrogen receptor

ERK – extracellular signal-regulated kinase

FAP-α – fibroblast activation protein alpha

FBS – fetal bovine serum

FFPE – formalin-fixed paraffin-embedded

FGF – fibroblast growth factors

FISH – fluorescence *in situ* hybridization

FOSL2 – FOS-like 2

FSP1 – fibroblast-specific protein 1

FTIR – fourier transform infrared spectroscopy

GREM1 – gremlin 1

GRO-α – growth-regulated oncogene alpha

GSH – glutathione

H&E – hematoxylin and eosin

H_2O_2 – hydrogen peroxide

HDAC6 – histone deacetylase 6

HER2 – human epidermal growth factor receptor 2

HIF-1α – hypoxia-inducible factor 1 alpha

HMGB1 – high-mobility group box 1

HR – hormone receptor

ICP-MS – inductively coupled plasma mass spectroscopy

IDO1 – indoleamine 2,3-dioxygenase 1

IL – interleukin

LIC – lobular invasive carcinoma

LOX – lysyl oxidase

MCP-1 – monocyte chemotactic protein-1

MCT4 – monocarboxylic acid transporter 4

MDCS – myeloid-derived suppressor cells

MMP – matrix metalloproteinase

MSN – mesoporous silica nanoparticle

mTOR – mammalian target of rapamycin

MYH7 – myosin heavy chain β (MHC-β)

NaOH – sodium hydroxide

NG2 –chondroitin sulfate proteoglycan 4

NK – natural killer

NLRP3 – NLR family pyrin domain containing 3

NP – nanoparticle

OPN – osteopontin

P/S – penicillin/streptomycin

P4H – prolyl 4-hydroxylase

PALB2 – partner and localizer of BRCA2

PARP – poly-ADP-ribose polymerase

PBS – phosphate-buffered saline

PD-1 – programmed cell death 1

PDGF – platelet-derived growth factor

PDGFR – platelet-derived growth factor receptors

PD-L1 – programmed cell death receptor ligand 1

PDOs – patients-derived organoids

PDPN – podoplanin

PEG – polyethylene glycol

PEI – polyethyleneimine

PIK3 – phosphatidylinositol-4,5-bisphosphate 3-kinase

PR – progesterone receptor

PTEN – phosphatase and tensin homolog

PTFE – polytetrafluoroethylene

PTX3 – pentraxin 3

PVR – polio virus receptor

ROS – reactive oxygen species

RT-qPCR – real-time quantitative polymerase chain reaction

S100A4 – S100 calcium-binding protein A4

SD – standard deviation

SDF-1 – stromal cell-derived factor 1

SDS-PAGE – sodium dodecyl sulfate-polyacrylamide gel electrophoresis

SEM – standard error of the mean

STAT – signal transducer and activator of transcription

STC-1 – stanniocalcin-1

STEM-EDX – electronic energy-dispersive X-ray spectroscopy

STK11 – serine/threonine kinase 11

TAM – tumor-associated macrophages

TBS/T – tris-buffered saline/0.1% Tween20

TDO2 – tryptophan 2,3-dioxygenase 2

TEM – transmission electron microscopy

TEOS – tetraethyl orthosilicate

TGA – thermogravimetric analyses

TGF – transforming growth factor

TIMP-1 – tissue inhibitor of metalloproteinase 1

Tlr4 – toll-like receptor 4

TMAH – tetramethylammonium hydroxide solution

TME – tumor microenvironment

TNM – tumor–node–metastasis

TP53 – tumor protein p53

UCIM-UV – Central Medicine Research Unit of Universitat de Valencia

VEGF – vascular endothelial growth factor

WHO – World Health Organization

α-SMA – alpha-smooth muscle actin

CHAPTER 1 |

INTRODUCTION

1.1. Breast cancer

1.1.1. Epidemiology

Nowadays, cancer ranks as a leading cause of premature death worldwide, and its incidence is rapidly growing [1]. Breast cancer (BC) is the second most diagnosed cancer, with an estimated 2.3 million new cases (11.6% of total cases), and the fourth cause of cancer-related deaths, with 665 thousand deaths (6.9% of total deaths) (**Figure 1A**). In women, BC accounts for 1 in 4 cancer cases being the most incident and the leading cause of cancer-related deaths (1 in 6 cancer deaths) (**Figure 1B**) [2]. In contrast, it is considered a rare disease in men since it accounts for 1% of all BC-diagnosed cases [3].

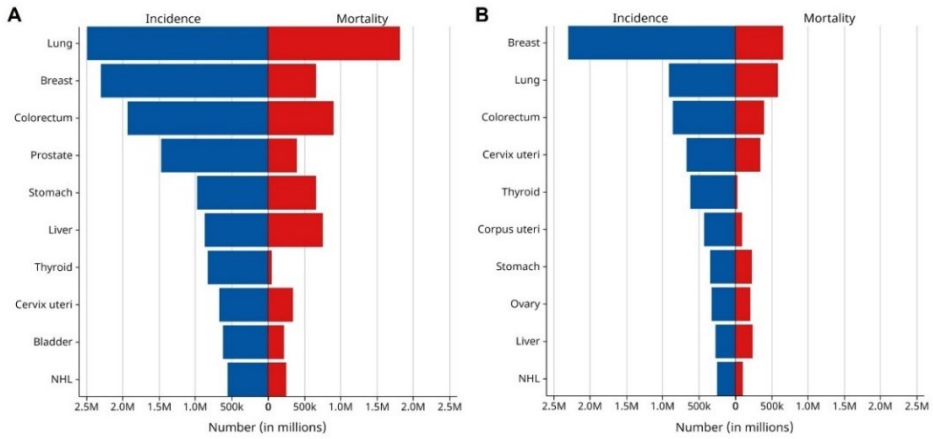

Figure 1. Estimated number of incident cases and deaths for the top 10 most common cancers **(A)** among both sexes or **(B)** in women in 2022, worldwide. Source: GLOBOCAN 2022. Abbreviations: NHL – Non-Hodgkin lymphoma.

Worldwide, population aging and growth, together with risk factors associated with socioeconomic development are predicted to raise cancer incidence and mortality, particularly in low and middle-income countries

[4]. The BC incidence rate is 76% higher in transitioned countries than in transitioning countries (**Figure 2**) [2]. These data reflect the higher prevalence of risk factors in developed countries such as lifestyle, hormonal and reproductive factors [5]. In contrast, the BC mortality rate in transitioning countries is 35% higher than in transitioned countries, probably due to the lack of early detection by mammographic screening, which considerably reduces mortality [2, 6].

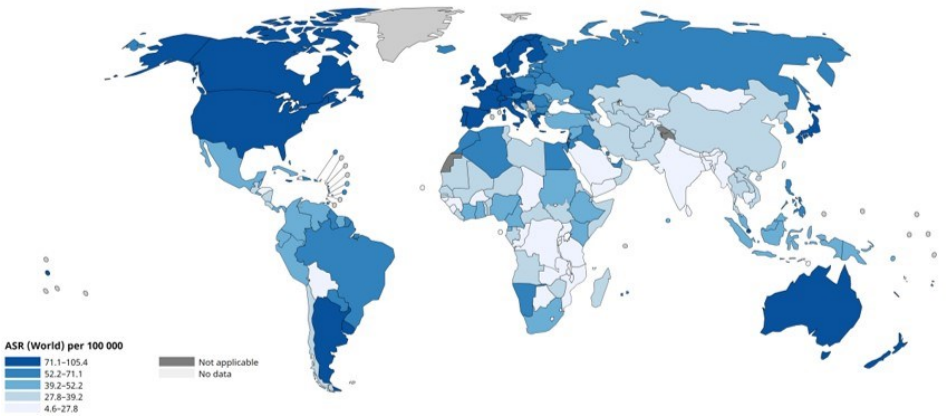

Figure 2. World map representative of breast cancer incidence in women age-standardized rates (ASR) per 100,000 in 2022. Source: GLOBOCAN 2022.

1.1.2. Risk factors

Most of the BC cases occur in women, being gender the strongest risk factor due to enhanced hormonal stimulation [7, 8]. Besides gender, age is an important factor in BC development. In women over 40 years of age the incidence is markedly higher, being most of the cases diagnosed between the ages of 50 and 70 [9]. Nevertheless, BC can also appear in younger women (younger than 40 years) being associated with more aggressive subtypes [10].

Moreover, lifestyle factors, such as smoking, alcohol consumption, lack of physical activity, and overweight, also contribute to a higher risk of BC [11]. Besides, a history of previous radiation therapy [12], former BC, or other non-cancerous alternations in breast tissue, like fibrosis, calcifications, atypical hyperplasia, or carcinoma *in situ*, lead to a greater risk of renewed breast lesions [13, 14].

Reproductive factors have also been related to BC development. On the one hand, extended reproductive lifespan (early menstruation and late menopause) [15], as well as administration of hormonal contraception [16] or hormone replacement therapy after menopause [17], increase the time of exposure to hormones, resulting in a higher probability of developing BC. Besides, pregnancy at an early age (particularly before 30 years) [18] and prolonged breastfeeding [19] contribute to reducing BC risk.

Although approximately 85% of women diagnosed with BC have no known family history of the disease, around 5-10% of the cases are linked to genetic factors [20, 21]. A family history of BC is significantly associated with an increased risk of BC, whereas a family history of ovarian cancer might also have a positive impact [22, 23]. The risk of developing BC is two times higher when women have first-degree relatives affected with BC and increases with the number of cases in the family [24]. Hereditary genetic mutations highly increase BC risk. Highly penetrance mutations in the *breast cancer gene* (*BRCA*) *1* and *BRCA2* tumor suppressor genes increase the risk of BC by approximately 65% and 45% (at 70 years), respectively, and the susceptibility to other cancer types such as ovarian cancer [25]. Moreover, these mutations are strongly associated with BC in younger women [26]. Other germline mutations involved in the induction of breast carcinogenesis can occur in highly penetrant genes like *cadherin-1* (*CDH1*), *phosphatase and tensin homolog* (*PTEN*), *serine/threonine kinase 11* (*STK11*), and *tumor protein p53* (*TP53*), or in

moderate-penetrance genes like *Ataxia Telangiectasia Mutated* (*ATM*), *BRCA1 interacting helicase 1* (*BRIP1*), *checkpoint kinase 2* (*CHEK2*), and *partner and localizer of BRCA2* (*PALB2*) [27].

1.1.3. Screening and diagnosis

BC early detection is a critical factor that influences patients' prognosis and survival. In patients diagnosed at early stages (stage I and II) the 5-year survival rate is higher than 90%, however, survival rates decrease to 75% for stage III, and 29% for stage IV (metastatic disease) [9]. Therefore, it is important to highlight the importance of screening programs that allow the detection and diagnosis at early stages, thus improving the patients' outcome.

BC screening programs have been implemented to detect asymptomatic early-stage BC in women with an average risk of developing the disease. The European Commission Initiative on Breast Cancer, following the recommendations from the World Health Organization (WHO), recommends mammography-based screening every two years for women with average risk aged between 50 and 69 years [28]. Moreover, for women with a family history of BC screening should be initiated at younger ages after risk assessment [29].

Several studies demonstrate the benefits of mammography screening in terms of reduced BC mortality. Women who attended screening programs reduced the risk of death from BC by up to 50% compared to women who were not screened [30, 31]. However, mammographic screening presents some disadvantages including false-positive or false-negative results and the long-term effects of radiation exposure [32]. The false-positive results lead to overdiagnosis and overtreatment and are usually associated with high breast tissue density [33]. Moreover,

screening mammography has lower sensitivity and specificity in women with dense breasts. Therefore, supplementary screening methods such as magnetic resonance imaging can be used in high-risk women with high breast density but are not recommended for women without a BC family history [34].

The diagnosis of women with positive mammography or those who experience BC symptoms is based on clinical examination in combination with imaging and a needle biopsy carried out before any treatment. Afterwards, a standard pathology report is provided, and patient's treatment options are discussed [35, 36].

1.1.4. Classification and staging

BC pathological evaluation provides a complete histomorphology, immunohistochemical, and, if necessary, molecular evaluation of the tumor. In this way, three classification systems (histological and anatomical classification, pathological classification, and molecular classification) are integrated to determine the best treatment strategy for each patient, as well as the patient's prognosis.

1.1.4.1. Histological and anatomical classification

The final pathological assessment, as well as the disease stage, is made according to the 4th edition of the WHO classification of tumors and the 8th edition of the Union for International Cancer Control tumor–node–metastasis (TNM) staging system [28].

Considering histological classification, according to WHO classification, breast invasive carcinomas can be divided into several histological tumor types [37, 38]. The most common histological subtype

is “no special type carcinoma” commonly referred to as “ductal invasive carcinoma” (DIC). DICs represent around 70-75% of BC cases, being their names assigned due to cellular morphology and epithelial origin once tumors originated in the mammary ducts. The “lobular invasive carcinoma” (LIC) subtype is the second most frequently diagnosed, representing 10-15% of BC, and includes tumors with lobular origin [39, 40].

The anatomical classification defines the tumor stage considering the TNM staging system. TNM system evaluates the size and local extension of the primary tumor (T), involvement of regional lymph nodes (N), and presence of distant metastases (M) (**Table 1**), and defines four anatomic stage groups (from stage I, early-stage to stage IV, advanced or metastatic stage) (**Table 2**) [41].

Table 1. Summary of clinical classification of breast tumors according to the 8th edition of the Union for International Cancer Control tumor–node–metastasis (TNM) staging system to breast cancer anatomical classification.

Primary tumor	T0	No evidence of a primary tumor
	Tis	Non-invasive primary tumor
	T1	Tumor size ≤ 20 mm
	T2	Tumor size > 20 mm and ≤ 50 mm
	T3	Tumor size ≥ 50 mm
	T4	Tumor of any size with direct extension to chest wall and/or skin
Lymph Nodes	N0	No lymph node metastasis
	N1	Metastasis in movable axillary lymph node
	N2	Non-movable axillary lymph node metastasis or metastasis in internal mammary lymph nodes
	N3	Metastasis in the infraclavicular/supraclavicular lymph nodes or internal mammary lymph nodes
Metastases	M0	No distant metastasis
	M1	Distant metastasis

Table 2. Staging of breast tumors according to the 8th edition of the Union for International Cancer Control tumor–node–metastasis (TNM) staging system to breast cancer anatomical classification.

Stage		T	N	M
Stage 0		Tis	N0	M0
Stage I	**A**	T1	N0	M0
	B	T0, T1	N1 micrometastases	M0
Stage II	**A**	T0, T1	N1	M0
		T2	N0	M0
	B	T2	N1	M0
		T3	N0	M0
Stage III	**A**	T0, T1, T2	N2	M0
		T3	N1, N2	M0
	B	T4	N0, N1, N2	M0
	C	Any T	N3	M0
Stage IV		Any T	Any N	M1

In the 8th edition of the TNM staging system, histological grade and immunohistochemistry biomarkers (estrogen receptor (ER), progesterone receptor (PR), human epidermal growth factor receptor 2 (HER2), and Ki67) were incorporated into the traditional anatomic TNM classification [42]. This change provided a more accurate prognosis and clinical management based on the biomarkers' status [43].

The histological grade is determined according to the Nottingham Grading System which analyses three morphological tumor features: nuclear pleomorphism, degree of tubular formation, and mitotic activity. According to this, tumors can be scored from 1 to 3: grade 1 (well differentiated), grade 2 (moderately differentiated), and grade 3 (poorly differentiated) [44, 45]. The grade score is associated with the patient's prognosis, once reflects the tumor aggressiveness [46].

1.1.4.2. Pathological classification

In the clinical context, the pathological classification is based on the immunohistochemical analysis of the biomarkers ER, PR, HER2, and the proliferation marker Ki67, and provides important information for treatment decisions [47-49]. Formalin-fixed paraffin-embedded (FFPE) tissue samples of tumor core biopsies are used to determine the biomarkers' status, according to international guidelines. Beyond immunohistochemical analysis, in borderline positive cases, HER2 status can also be determined by fluorescence *in situ* hybridization (FISH) [28, 50].

Based on these biomarkers' expression, the pathological classification recognizes four surrogate intrinsic BC subtypes: luminal A (ER^+, PR^+, $HER2^-$, $Ki67^{low}$), luminal B (ER^+, $PR^{+/-}$, $HER2^{+/-}$, $Ki67^{high}$), HER2-positive (ER^-, PR^-, $HER2^+$, $Ki67^{high}$), and triple-negative (ER^-, PR^-, $HER2^-$, $Ki67^{high}$) (**Table 3**) [51].

Table 3. Pathological classification of Breast cancer subtypes.

BC subtype	ER	PR	HER2	Ki67
Luminal A	+	+/-	-	<14%
Luminal B	+	+/-	+/-	≥14%
HER2-positive	-	-	+	≥14%
Tiple-negative	-	-	-	≥14%

Following pathological classification, luminal A and luminal B together represent approximately 65% of all BC cancer tumors (50% and 15%, respectively). These subtypes present the best prognosis, with a 5-year survival rate above 90%. HER2-positive is the second most frequent subtype of BC (approximately 20%), being also considered a good prognosis subtype with a 5-year survival rate of approximately 80%.

Triple-negative tumors are the less frequent (approximately 15%), however, these tumors exhibit aggressive behavior and the worst prognosis with a 5-year survival rate of around 77%, due to the lack of targeted therapies [9, 52].

1.1.4.3. Molecular classification

In the last few years, a molecular classification of BC based on gene expression profiling has been developed and provides optimal management of patients' treatment and predicts more accurate prognosis [53].

In 2000, for the first time, a multigenetic study proposed that BC tumors could be divided into intrinsic molecular subtypes based on their genetic profile [54]. Further studies were developed and nowadays five molecular BC subtypes have been accepted (luminal A, luminal B, HER2-enriched, basal-like, and normal-like) [55, 56].

Considering the molecular characterization, luminal A is the most common intrinsic subtype (50% of all BC cases) and the one with the better prognosis. Luminal B has a worse prognosis compared to luminal A and accounts for around 20% of BC cases. The HER2-enriched and basal-like cases have the poorest prognosis, representing 15% of all cases in total [57]. Moreover, the normal-like group accounts for less than 5% of total cases. These specimens usually show low tumor cellularity and are predominantly composed of normal breast tissue. These facts contribute to some experts doubting the existence of this subtype, considering that this group could be a technical artifact from contamination with normal tissue [54, 55, 58, 59]. The characteristics of these five intrinsic molecular subtypes are summarized in **Table 4**.

Table 4. Summary of breast cancer intrinsic molecular subtypes characteristics.

Subtype	Positively enriched	Negatively enriched
Luminal A	High ER and PR expression Luminal-related genes	Proliferation-related genes
Luminal B	High ER expression Proliferation-related genes	Low or no PR expression Luminal-related genes
HER2-enriched	High HER2 expression Proliferation-related genes *TP53* mutations	No ER and PR expression Luminal-related genes
Basal-like	Basal myoepithelial cell genes (cytokeratin) Proliferation-related genes *BRCA1* and *TP53* mutations	No ER, PR, or HER2 expression Luminal-related genes
Normal-like	Non-epithelial cells, adipose tissue, and basal epithelial-related genes	HER2 negative Luminal-related genes Proliferation-related genes

Based on the previous findings, multigenic commercial arrays were developed and three are commonly used in clinical practice: MammaPrint, Oncotype DX, and PAM50 [60-62]. These tests allow to stratify the patient's risk of recurrence and metastatic disease and help guiding treatment choices [63]. Specifically, PAM50 comprises a 50-gene signature designed to classify the tumor intrinsic molecular subtype (luminal A, luminal B, HER2-enriched or basal-like) and predict the patient’s outcome by providing a risk of recurrence score [62].

Although molecular classification brings benefits in clinical practice, nowadays it is not fully applicable to clinics, and pathological classification remains the main factor in treatment decisions. These two classifications overlap in most cases, however in approximately 30% of the cases, the pathological subtype does not match the intrinsic subtype. Indeed, just 83% of the tumors classified as basal-like correspond to triple-negative tumors by immunohistochemistry analysis. Additionally, luminal A, luminal

B, and HER2-enriched only correspond to the pathological classification in 87%, 20%, and 51% of the cases, respectively (**Figure 3**) [59].

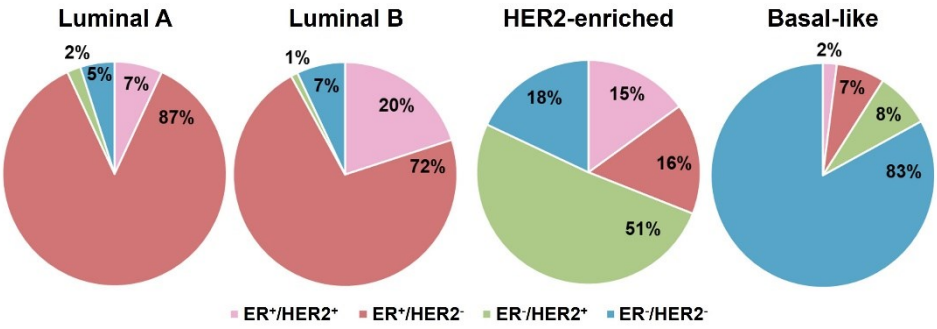

Figure 3. Distribution of $ER^+/HER2^+$, $ER^+/HER2^-$, $ER^-/HER2^+$, and $ER^-/HER2^-$ clinical groups in the five intrinsic subtype groups (Luminal A, Luminal B, HER2-enriched, and Basal-like). Adapted from Prat et *al*, 2010 [59].

1.1.5. Treatment

Treatment decisions are based on clinicopathological characteristics of the tumor, like tumor stage, grade, and subtype, as well as on the patient's features, like patient age, performance status, and menopause status. Moreover, approved gene expression signatures can also be used to determine treatment regimens [28, 64]. Considering the non-metastatic BC (stage I-III), the main goals of therapy are to eradicate the primary tumor and affected regional lymph nodes and to prevent recurrence and/or metastasis. Instead, metastatic BC (stage IV) is rarely curable, and the therapeutic goals are to minimize symptoms, extend the patient's life, and preserve the quality of life [65, 66].

Nowadays, in early-BC patients, the combination of local therapies (surgery and radiotherapy) and systemic therapies (chemotherapy, endocrine therapy, molecular targeted therapy, and immunotherapy) are

used [28]. In these cases, local therapy consists of primary tumor surgical resection and removal of affected axillary lymph nodes. Preferentially, breast-conserving surgery is performed, however, in some cases, mastectomy is recommended [67]. Sentinel lymph node sampling is also performed to determine the regional lymph node status, which remains one of the strongest prognostic markers of long-term outcome [28]. Axillary dissection should just be conducted after the sentinel lymph node examination [68]. Moreover, postoperative radiotherapy can be used after surgery to reduce the risk of recurrence [69]. In constant, in the case of metastatic setting, local therapies are only used as palliative care for quality of life [64].

Systemic therapies can be applied before surgery (neoadjuvant) and/or after surgery (adjuvant). The neoadjuvant systemic therapy purpose is to reduce the tumor burden of resectable breast tumors or to render unresectable tumors operable, improving treatment response. These therapies have as their main goal to reduce the recurrence risk and to improve long-term survival. The BC subtype guides the systemic treatment choice [70].

In the case of hormone receptor (HR)-positive tumors, that are ER and/or PR-positive, endocrine therapy is used, whereas some patients require chemotherapy as well. These drugs inhibit estrogen production or target the estrogen receptor. The most used endocrine therapeutic drugs are selective ER modulators, like tamoxifen, and aromatase inhibitors, like anastrozole, exemestane, and letrozole [71]. The standard treatment duration for HR-positive patients treated with adjuvant endocrine therapy is five years. However, treatment can be prolonged until ten years after surgery to lower recurrence risk and increase survival [72, 73]. Tamoxifen and aromatase inhibitors are used in non-metastatic BC, alone or in combination depending on menopausal status [28]. Whereas in

metastatic postmenopausal patients, the selective ER degrader fulvestrant and the tamoxifen analog toremifene are also used [64]. Moreover, cyclin-dependent kinase (CDK) 4/6-inhibitors (palbociclib, ribociclib, and abemaciclib) [74], everolimus (an mammalian target of rapamycin (mTOR) inhibitor) [75], and alpelisib (a phosphatidylinositol-4,5-bisphosphate 3-kinase (PI3K) inhibitor) [76] were recently approved for metastasis to be used in combination with endocrine therapy [64, 77].

Regarding HER2-positive tumors, HER2-based targeted therapies in combination with chemotherapy are the standard of care. Moreover, in patients with HR-positive tumors endocrine therapy is given in addition [28]. The anti-HER2 therapies can be monoclonal antibodies (like trastuzumab, pertuzumab, and margetuximab), antibody-drug conjugates (like trastuzumab-emtansine and trastuzumab-deruxtecan) or tyrosine kinase inhibitors (like lapatinib, neratinib, and tucatinib) [78]. These therapies drastically improved HER2-positive patients' prognosis. For instance, the combination of trastuzumab with chemotherapy significantly reduces recurrence and mortality in these patients [79]. In neoadjuvant treatment, a combination of trastuzumab and pertuzumab is given in addition to chemotherapy [80]. The post-neoadjuvant treatment is one year of anti-HER2 therapy (trastuzumab with/without pertuzumab) if the patients experience a pathological complete response, or trastuzumab-emtansine in the cases with reaming disease [81, 82]. The patients with initial surgery receive adjuvant trastuzumab-based therapies in combination with chemotherapy and in most cases the anti-HER2 therapy is maintained for one year [28, 79]. In addition to the HER2-based targeted therapies used in non-metastatic patients, new drugs, such as the antibody derivative of trastuzumab margetuximab [83], the antibody-drug conjugate trastuzumab-deruxtecan [84], and the tyrosine kinase

inhibitors, were developed and approved to be used in the metastatic setting [64].

For triple-negative BC patients, chemotherapy is the standard treatment due to the lack of targeted therapies. Most of these patients undergo neoadjuvant chemotherapy before surgery [28]. The chemotherapy regimens are based on the use of anthracyclines (doxorubicin (DOX), epirubicin) followed by taxanes (paclitaxel, docetaxel), being the use of platinum agents (cisplatin, carboplatin) also possible [85]. In the case of patients with residual disease for whom anthracycline administration is not possible, the use of capecitabine should be considered [86]. The programmed cell death 1 (PD-1) monoclonal antibody pembrolizumab is also approved for early-stage high-risk patients and metastatic patients in combination with chemotherapy [87, 88]. In high-risk triple-negative BC patients with *BRCA1/2* germline mutations, one year of adjuvant treatment with the like poly-ADP-ribose polymerase (PARP) inhibitor olaparib is administered [89]. In case of advanced disease, apart from these drugs, atezolizumab (anti-PD-1 antibody) [90], talazoparib (PARP inhibitor) [91], and bevacizumab (monoclonal antibody against vascular endothelial growth factor (VEGF) A) [92] can also be used [64].

Despite recent advances in triple-negative BC therapies, chemotherapy remains the standard treatment. The absence of ER and PR expression and the lack of HER2 overexpression or amplification make this subtype unsuitable for endocrine or HER2-based targeted therapies. Indeed, the number of patients who experience a relapse is still startling, leading to a shorter overall survival compared with other subtypes [9, 93]. Most of the BC therapies currently used are focused on targeting tumor cells. However, new developments in the immunology

field uncover an important role of tumor microenvironment (TME) in tumor progression and therapy resistance [94]. Hence, further advances in this scientific field are needed to improve BC patients' outcomes.

1.2. Tumor microenvironment

Tumors are composed not only of cancer cells but also of the complex surrounding ecosystem. Tumor cells interact with tumor-associated host cells embedded in an altered extracellular matrix (ECM) that form the TME. TME is constituted of immune-inflammatory cells, cancer-associated fibroblasts (CAFs), endothelial cells, adipocytes, mesenchymal stromal cells, and tissue-resident cell types (**Figure 4**) [95]. The dynamic crosstalk between cancer cells and TME cells plays a critical role from tumor initiation until metastatic outgrowth and deeply influences therapy response. Cancer cells shape the environment to support their survival, growth, and dissemination, whereas TME also modulates cancer features. Moreover, the TME cellular composition and functional state are conditioned by tumor features, and patient characteristics and are organ-dependent [96, 97].

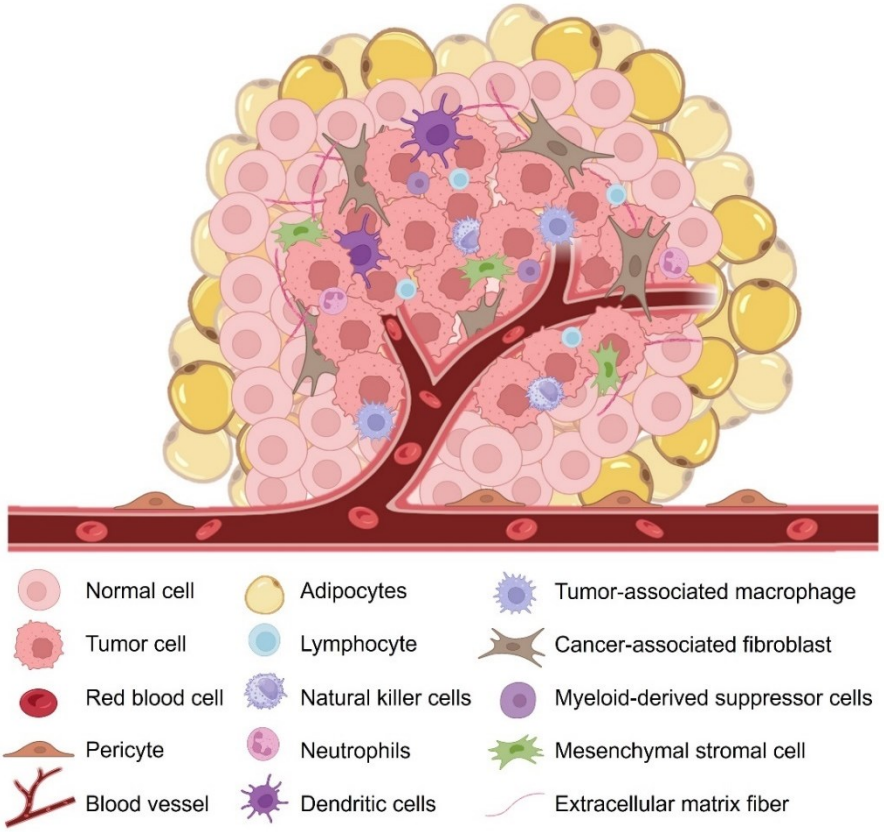

Figure 4. Cancer cells and tumor microenvironment composed of immune-inflammatory cells (myeloid-derived suppressor cells, tumor-associated macrophages, lymphocytes, natural killer cells, neutrophils, and dendritic cells), cancer-associated fibroblasts, endothelial cells, adipocytes, mesenchymal stromal cells, and tissue-resident cell.

Regarding BC TME immune components, these can be divided into adaptive (T cells, B cells, and natural killer (NK) cells) or innate immune cells (macrophages, neutrophils, and dendritic cells) [98]. Immune cells can modulate the TME by building an antitumor immune microenvironment or an immunosuppressive microenvironment that either suppresses tumor growth or promotes it, respectively [99]. On the one

hand, the antitumor immune landscape is mostly composed of cytotoxic T cells ($CD8^+$), T helper cells (proinflammatory $CD4^+$ T cells), NK cells, inflammatory M1 macrophages, N1-polarized neutrophils (tumor-suppressing neutrophils), and dendritic cells. These cells promote tumor depletion, and suppress angiogenesis, through growth factors and cytokines secretion, being associated with positive outcomes [100-103]. On the other hand, the immunosuppressive phenotype is characterized by the presence of regulatory T cells (immune-suppressive $CD4^+$ T cells), M2 tumor-associated macrophages (TAM), N2-polarized neutrophils (tumor-promoting neutrophils), and myeloid-derived suppressor cells (MDSC). This phenotype promotes tumor development and progression, leading to poor clinical outcomes [104-106].

In BC, the TME profile and structure are related to the patient's prognosis and clinical outcome [107, 108]. In this sense, the amount and type of immune cells present in the tumor predict the evolution of the disease. Some studies also revealed that a high number of MDSC, M2 macrophages, or regulatory T cells are associated with a worse prognosis in BC patients [109-111]. Moreover, TME is one of the responsible for therapy resistance in BC [112]. BC's antitumor immunity profile is vital to improve treatment response, however, many BC cases present an effective antitumor immunity that is hindered by the immunosuppressive nature of the TME. Recent studies showed that an increased number of tumor-infiltrating lymphocytes predicted a better response to neoadjuvant chemotherapy in BC patients [113]. In this sense, many pre-clinical studies demonstrated that targeting TME components in combination with tumor-directed therapies significantly reduces tumor growth, chemoresistance, and metastasis. Nonetheless, clinical trials failed to demonstrate effective results in cancer patients [114]. So, further efforts

are needed to better understand TME and to develop strategies to target tumor-TME interactions.

Considering TME stromal components, adipocytes are highly abundant in BC. These cells interact with tumor cells and other TME cells to support tumor progression. On the one hand, cancer cells stimulate adipocytes to undergo lipolysis which improves tumor metabolism. On the other hand, cancer-associated adipocytes secret enzymes, growth factors, cytokines, and hormones like leptin, that promote tumor proliferation, angiogenesis, and macrophages' recruitment [115, 116].

Other constitutive parts of the BC TME are the endothelial cells, which together with the associated pericytes, contribute to tumor angiogenic switch but also play a role in cancer growth and invasion. These cells respond to tumor angiogenic factors, such as fibroblast growth factors (FGFs) and VEGFs, present in the TME, leading to neovascularization [117, 118].

Moreover, CAFs are the most abundant cell type of the tumor stroma having a major role in facilitating crosstalk between TME and cancer cells. These cells provide a structural framework for stroma by producing most of the extracellular components, including ECM and growth factors. CAFs shape the TME by regulating tumor immunity (recruitment of immune cells), stimulating angiogenesis, promoting invasion and metastasis (ECM remodeling), and modulating chemoresistance. Due to CAFs' heterogeneity, they are often associated with poor prognosis in many cancer types, however, can serve as positive and negative regulators of tumor progression [119, 120]. The CAFs' origin, characteristics, and functions in TME and cancer will be discussed more deeply in the next section.

1.2.1. Cancer-associated fibroblasts

CAFs are the largest stromal subset in BC TME and a heterogeneous population that has a major role in tumor behavior. These cells, either by cell-to-cell communication or through soluble factors secretion, promote tumorigenic processes like tumor initiation, progression, and drug resistance. Due to these facts, CAFs become a hot topic in basic and medical research.

1.2.1.1. Origin and heterogeneity

CAFs, by definition, are all the fibroblasts present within or adjacent to the tumor, including the normal fibroblasts, the activated fibroblasts, and the tumor-recruited fibroblasts [121]. The origin of CAFs is still not fully understood, but there are several putative hypotheses. In the last decades, tissue-resident fibroblasts [122], bone marrow or adipose tissue mesenchymal stromal cells [123], mesenchymal stem cells [124], adipocytes [125], endothelial cells [126], pericytes [127], and cancer stem cells [128] were appointed as CAFs sources. Nevertheless, not all these sources have been confirmed in BC. The most widely accepted hypothesis is that CAFs are originated through the activation of the tissue-resident fibroblasts. In BC, the activation of normal fibroblasts by transforming growth factor-beta (TGF-β) receptor ligands [129], cytokines [130], and other proteins [131, 132], as well as by exosomes containing microRNAs and long non-coding RNAs [133-136] was reported. Moreover, BC CAFs can also originate from the recruitment of bone marrow or adipose tissue mesenchymal stem/stromal cells [123, 137], the activation of the TGF-β signaling pathway on mesenchymal stem cells [138-140], or the stimulation of the Wnt/β-catenin pathway on adipocytes [141] (**Figure 5**).

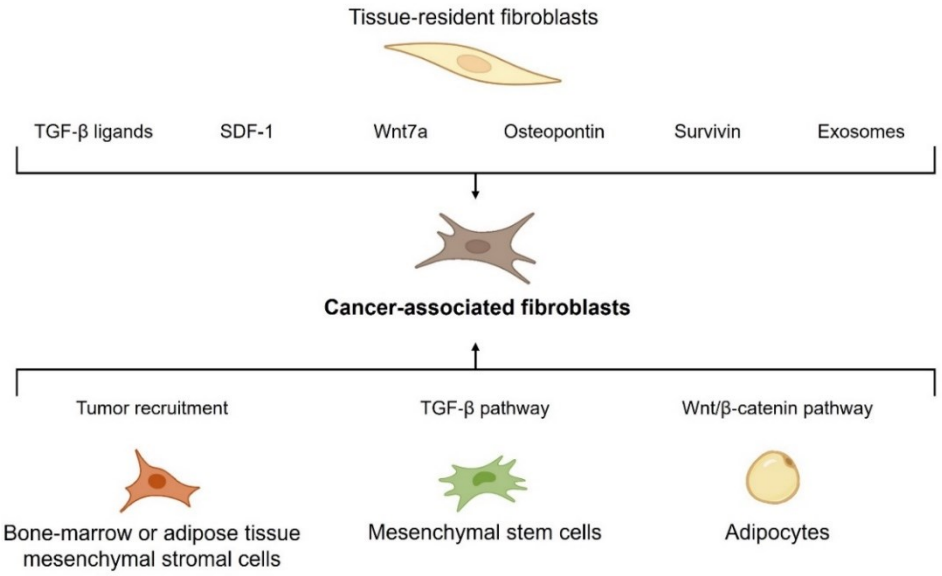

Figure 5. Cancer-associated fibroblasts origins in breast cancer. Abbreviations: SDF-1 – stromal cell-derived factor 1, TGF-β – transforming growth factor-beta.

Nowadays, due to CAFs heterogeneity, CAFs must be defined by their morphological features (elongated spindle morphology), biomarkers (negative epithelial, endothelial, and leucocyte markers and positive mesenchymal markers), and lack of genetic mutations [142]. The most used CAFs markers are fibroblast activation protein alpha (FAP-α), alpha-smooth muscle actin (α-SMA), platelet-derived growth factor receptors (PDGFR) alpha and beta, and fibroblast-specific protein 1 (FSP1) and vimentin [143]. However, none of these markers are exclusive from CAFs, and their expression level is tumor type-dependent and varies between CAFs subtypes.

On the one hand, BC CAFs heterogeneity can be attributed to different origins and intratumor spatial distributions. Single-cell RNA sequencing analysis of BC mouse models identified four different CAFs subpopulations (matrix, developmental and vascular CAFs, and the

cycling-CAFs proliferative subset) with significantly different gene expressions, that were spatially and functionally distinct, and derived from different sources. The matrix population originates from resident fibroblasts, expresses matrix-related genes, and is related to tumor invasion. The developmental CAFs are distinguished by the expression of genes involved in cellular differentiation, development, and morphogenesis, and rise from malignant cells that undergo epithelial-to-mesenchymal transition (EMT). The vascular population has a perivascular location origin and expresses genes involved in vascular development and angiogenesis [144].

In triple-negative BC, a single-cell RNA sequencing analysis revealed that the inter- and intra-tumor heterogeneity had a prognostic and therapeutic value. This study identified 3 CAFs clusters, the myofibroblast-like cluster involved in constituting the ECM and collagen production, the cluster functionally characterized by energy metabolism, and one cluster characterized by promoting proliferation and multi-drug resistance [145]. Additionally, another study identified two major CAFs populations in the same BC subtype, namely myofibroblast-like CAFs and inflammatory CAFs. The first population was characterized by myofibroblast features due to the high expression of activated fibroblast markers, like α-SMA, while the second one presented an elevated expression of growth factors and immunomodulatory molecules, like chemokine (C–X–C motif) ligand (CXCL) 12. These two populations also have distinct intratumor spatial distributions, being the myofibroblast-like CAFs located at the invasive front of tumors, and the inflammatory CAFs sited in distal areas of the tumor stroma and associated with a higher number of lymphocytes [146]. A recent study suggests that inflammatory CAFs and myofibroblast-like CAFs can originate from interlobular and lobular fibroblasts, respectively, being the latter associated with tumor-promoting properties and poor BC

survival [147]. Besides, in BC patients undergoing anti-PD-1 immunotherapy, inflammatory CAFs supported cancer cell proliferation and EMT, contributing to the establishment of an immunosuppressive microenvironment [148]. Recently was proposed that normal fibroblasts can transform into inflammatory CAFs or myofibroblast-like CAFs according to their CD26 status ($CD26^+$ and $CD26^-$ expression, respectively). Moreover, $CD26^+$ transformed fibroblasts were able to recruit myeloid cells in a stromal cell-derived factor 1 (SDF-1)-dependent manner and increase tumor cell invasion [149].

On the other hand, CAFs heterogeneity is also present between BC molecular and pathological subtypes. Several studies identified CAFs gene signatures to predict prognosis, immune features, and response to therapy in BC [150-152]. The expression of CAFs-related proteins (FAP-α, PDGFRα/β, S100 calcium-binding protein A4 (S100A4), chondroitin sulfate proteoglycan 4 (NG2), prolyl 4-hydroxylase (P4H), and podoplanin (PDPN)) in stromal cells was related to BC subtype and stromal histologic features, being the subtype that presents the higher expression of these markers the HER2-positive [153, 154]. Moreover, in this subtype significantly different CAFs with upregulation of pathways associated with cytoskeleton and integrin signaling were found [155]. Additionally, the transcriptional profile of CAFs subpopulations changes during BC progression and metastases, and according to metastatic site [156-158].

Recently, four CAFs subsets were identified in BC according to the expression of α-SMA, FAP-α, PDGFRβ, FSP1, caveolin-1 (Cav-1), and CD29. These populations accumulate differently according to BC subtype and have distinct properties and levels of activation. The markers' expression of each CAFs subset is summarized in **Table 5**. The S1 and S4 subsets, considered myofibroblastic subsets due to high α-SMA expression, were enriched in aggressive BC subtypes (HER2-positive and

triple-negative), whereas the S3 subset was significantly associated with juxta-tumors. In contrast, Luminal A tumors were enriched in CAF-S2 cells and accumulated less activated CAFs. Moreover, while the HER2-positive tumors are enriched in the S4 subset, the triple-negative subtype presented a high CAFs heterogeneity being enriched in the S1 and/or S4 subsets. The CAF-S1 fibroblasts were the ones related to immune response, once presented a strong enrichment in immune signatures. This population promotes an immunosuppressive environment by increasing the regulatory T cell capacity to inhibit T effector proliferation, contributing to resistance to immunotherapies [159]. Moreover, a later study explored in depth the CAF-S1 subset to better understand its impact on immunotherapy response [160]. Another study identified the same four CAFs subsets in BC metastatic lymph nodes. In this context, S1 and S4 populations were found in high proportion in invaded lymph nodes, whereas the S2 and S3 subsets were enriched in non-invaded axillary lymph nodes. Accordingly, the two myofibroblastic subsets were associated with BC invasion and metastasis [161].

Table 5. Markers' expression of cancer-associated fibroblasts subsets in breast cancer.

CAFs subsets	α-SMA	FAP-α	PDGFRβ	FSP1	Cav-1	CD29
CAF-S1	High	High	Med/High	Med	Low	Med
CAF-S2	Neg	Neg	Neg	Neg/Low	Neg	Low
CAF-S3	Neg/Low	Neg	Med	Med/High	Neg/Low	Med
CAF-S4	High	Neg	Low/Med	Low/Med	Low	High

Neg: negative; Med: medium

1.2.1.2. Implications in tumor microenvironment

CAFs and normal fibroblasts share some basic characteristics such as secretory phenotype and capacity to synthesize ECM, however, CAFs present a high proliferative, tumorigenicity, and invasive profile [162, 163]. Due to their plasticity and heterogeneity, CAFs can have tumor-supporting or tumor-suppressive functions.

CAFs are the major producers of ECM components and secreted soluble factors, such as cytokines, chemokines, growth factors, and proteins. Their secretome is responsible for matrix remodeling, angiogenesis driving, regulation of tumor immunity, and modulation of tumor cell behavior (**Figure 6**) [164].

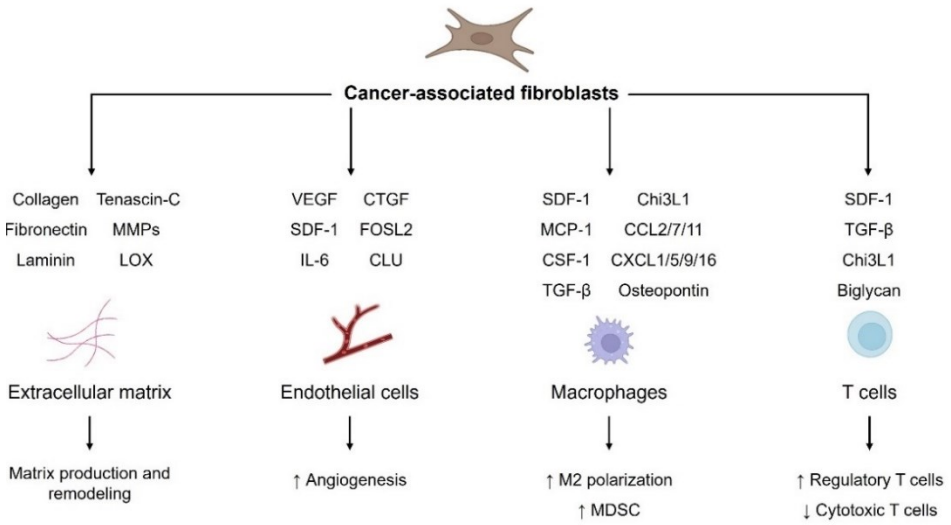

Figure 6. Effects of cancer-associated fibroblasts on extracellular matrix, endothelial cells, macrophages, and T cells on breast cancer tumor microenvironment. Abbreviations: CCL – C-C motif chemokine ligand, Chi3L1 – chitinase 3 like 1, CLU – clusterin, CSF-1 – monocyte chemotactic protein-1, CTGF – connective tissue growth factor, CXCL – CXC motif chemokine ligand, FOSL2 – FOS-like 2, IL-6 – interleukin 6, LOX – lysyl oxidase, MCP-1 – monocyte

chemotactic protein-1, MDSC – myeloid-derived suppressor cells, MMPs – matrix metalloproteinases, SDF-1 – stromal cell-derived factor 1, TGF-β – transforming growth factor-beta, VEGF – vascular endothelial growth factor.

CAFs reshape the ECM structure by synthesizing and degrading its components (like collagen, fibronectin, laminin, and tenascin-C) and producing matrix proteases (like matrix metalloproteinases (MMPs)) and matrix-crosslinking enzymes (like lysyl oxidase (LOX)) [165]. In BC, the ECM composition is associated with the patient's prognosis [166]. Moreover, matrix remodeling and its components, promote progression, invasion, and metastasis, limit the recruitment of immune cells, and contribute to tumor therapeutic resistance [167-170]. Interestingly, after cancer dissemination, fibroblasts at the metastatic niche can also produce a matrix that provides supporting signals to the cancer cells [171, 172].

Regarding angiogenesis, CAFs can promote it in a VEGF-dependent or independent manner. In BC, several studies reported the induction of angiogenesis by VEGF secreted by CAFs [173-175]. For example, it was shown that inflammatory CAFs in triple-negative patients with *BRCA1* mutation can sprout angiogenesis by interaction with endothelial cells through VEGF and CXCL, as well as induce resistance to neoadjuvant chemotherapy [176]. Moreover, VEGF-A also has an important role in promoting an angiogenic microenvironment at the metastatic niche to facilitate colonization by cancer cells [177]. Other pro-angiogenic factors released by BC CAFs are interleukin (IL) 6, connective tissue growth factor (CTGF), SDF-1, FOS-like 2 (FOSL2), and clusterin (CLU) [137, 174, 178, 179]. Interestingly, SDF-1 increases vascular permeability and expansion of leaky tumor vasculature by recruiting endothelial precursor cells and decreasing endothelial tight junction and adherence junction proteins, leading to enhanced tumor cell intravasation and formation of

distant metastasis [180]. Additionally, the mechanical force provided by CAFs also contributes to tumor-associated vasculature formation [181].

CAFs are also responsible for the modulation of the tumoral immune landscape [182, 183]. One study using a BC mouse model showed that CAFs depletion results in a shift of the immune polarization to an antitumor immune microenvironment characterized by increased expression of IL-2 and IL-7, reduction in IL-6, IL-4, and monocyte chemotactic protein-1 (CSF-1), an increased number of dendritic and $CD8^+$ T cells, and diminished recruitment of MDSC, TAM, and regulatory T cells [184]. Another study revealed the role of histone deacetylase 6 (HDAC6) in the crosstalk between CAFs and immune cells. CAFs that overexpressed HDAC6 create an immune-suppressive microenvironment, whereas its inhibition increased $CD4^+$ and $CD8^+$ T cell numbers, and reduced T-regulatory cells and macrophages with M2-phenotype [185]. Moreover, CAFs-secreted biglycan was negatively correlated with infiltrating CD8 + T cell number and poor prognostic in triple-negative BC patients [186]. On the one hand, BC CAFs recruit monocytes into M2-like macrophages through secretion of secreting SDF-1, monocyte chemotactic protein-1 (MCP-1), CXCL16, and C-C motif chemokine ligand (CCL) 2 [187-191]. Moreover, increased expression of cyclin D1 in BC CAFs enhances the recruitment of macrophages through the secretion of proinflammatory cytokines (CCL2, CCL7, CCL11, CXCL1, CXCL5, CXCL9, SDF-1), CSF-1 and osteopontin (OPN) [192]. On the other hand, inhibition of T cell infiltration and enhanced capacity of regulatory T cells can be mediated by CAFs through SDF-1 [159, 193]. Another study demonstrated the role of chitinase 3 like 1 (Chi3L1) produced by BC CAFs in the recruitment of macrophages, induction of M2-like phenotype, and inhibition of T-cell infiltration [194]. Moreover, CAF-derived TGF-β has also an immunosuppressive role by cytotoxic T cell inhibition, recruitment of M2-

like macrophages, and neutrophils' depletion [160, 195-197]. CAF-derived exosomes are other players in tumor immune suppression. These can increase programmed cell death receptor ligand 1 (PD-L1) expression in BC cells, which significantly promotes apoptosis and impaired proliferation of T cells leading to a suppressed function of tumor-infiltrated immune cells [198]. Remarkably, FAP-α-expressing CAFs subsets seem to have an immunosuppressive function by suppressing T cells proliferation, being related to immunotherapeutic efficacy in BC patients [159, 160, 199].

1.2.1.3. Implications in tumor progression and therapy resistance

CAFs are key regulators of tumor cell behavior (**Figure 7**). These cells sustain cancer cell survival and proliferation due to the secretion of growth factors and cytokines. For example, CAFs play an important role in the progression of *in situ* mammary lesions to invasive carcinoma by releasing factors like IL-6 and CXCL1 [200-202]. Like CXCL1, CAFs-derived IL-8 enhanced cell proliferation and migration in BC by binding to tumor cells' CXCR2 receptor [203, 204]. Pentraxin 3 (PTX3) is another factor secreted by signal transducer and activator of transcription (STAT) 1-expressing CAFs that promotes tumor cell viability and proliferation and influences the progression of early-stage BC [205]. Moreover, SDF-1, an important factor released by CAFs, beyond stimulating angiogenesis, also promotes BC growth through the sustenance of tumor cell stemness by direct stimulation of tumor cells through the CXCR4 receptor [178, 206]. Like SDF-1, platelet-derived growth factor (PDGF) ligands (PDGF-A and -B) secreted by malignant stromal cells also increase cell proliferation and angiogenesis in luminal BC [207]. In addition to the role of TGF-β signaling in tumor-stroma crosstalk**,** TGF-α secreted by CAFs was also implicated

in cell proliferation promotion, but not migration, by activation of epidermal growth factor receptor (EGFR), AKT serine-threonine kinase (AKT), and extracellular signal-regulated kinase (ERK) in tumor cells [208].

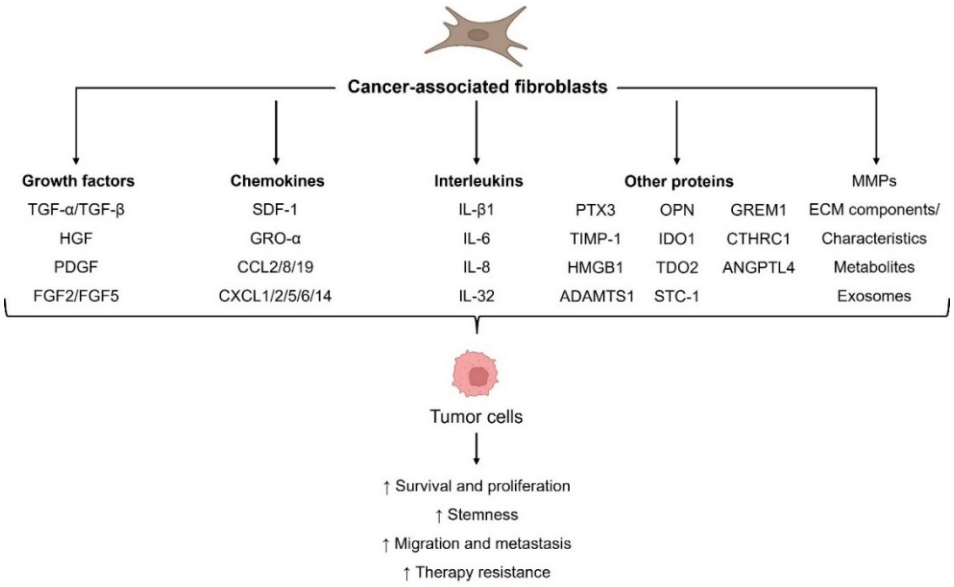

Figure 7. Effects of cancer-associated fibroblasts on cancer cell behavior (sustain cancer cell survival and proliferation, maintenance of stemness, enhance migration, invasion, distant metastasis, and therapy resistance). Abbreviations: ADAMTS1 – a disintegrin and metalloproteinase (ADAM) with thrombospondin motifs 1, ANGPTL4 – angiopoietin-like 4, CCL – C-C motif chemokine ligand, CTHRC1 – collagen triple helix repeat containing 1, CXCL – CXC motif chemokine ligand, ECM – extracellular matrix, FGF – fibroblast growth factor, GREM1 – gremlin 1, GRO-α – growth-regulated oncogene alpha, HGF – hepatocyte growth factor, HMGB1 – high mobility group box 1, IDO1 – indoleamine 2,3-dioxygenase 1, IL – interleukin, MMPs – matrix metalloproteinases, OPN – osteopontin, PDFG – platelet-derived growth factor, PTX3 – pentraxin 3, SDF-1 – stromal cell-derived factor 1, STC-1 – stanniocalcin-1, TDO1 – tryptophan 2,3-dioxygenase 2, TGF-α – transforming growth factor-

alpha, TGF-β – transforming growth factor-beta, TIMP-1 – tissue inhibitor of metalloproteinase 1.

Other growth factors secreted by CAFs, like FGF2 and hepatocyte growth factor (HGF), also stimulate the growth and progression of BC cells [209-211]. Remarkably, HGF not only has a role in tumor growth but also induces EMT and radio-resistance of BC cells through activation of the MET proto-oncogene, receptor tyrosine kinase (c-Met) signaling pathway [212, 213]. Moreover, a recent study demonstrated that osteoprotegerin upregulation in stromal fibroblasts, through BC cells in an IL-6/STAT3-dependent manner, promotes tumor growth due to the activation of adjacent fibroblasts and their pro-carcinogenic effect [214]. Therefore, STAT3 signaling is essential for the CAFs' pro-tumorigenic functions, being BC growth related to STAT3-dependent secretion of angiopoietin-like 4 (ANGPTL4), MMP13, and stanniocalcin-1 (STC-1) [215].

The induction of stemness is also related to cancer stem cell-mediated disease progression. In this context it was found that CAFs-derived CCL2 induces the stem-cell-like phenotype in BC cells and the self-renewing expansion of cancer stem cells, by activating NOTCH signaling, leading to tumor progression [216]. Additionally, cancer cells' stemness can be supported by high-mobility group box 1 (HMGB1) released by autophagic CAFs. HMGB1 activated its receptor (toll-like receptor 4, TLR4) in cancer cells, being the HMGB1-TLR4 axis associated with tumor aggressiveness and cancer progression in luminal BC patients [217].

CAFs also enhance migration, invasion, and distant metastasis through the production and release of growth factors, cytokines, and ECM proteins. In BC, different subtypes may require a distinct TME to undergo malignant progression. For example, in basal tumor cells, invasion can rely upon a reorganization of collagen fibers by fibroblasts, whereas in

luminal tumor cells, this ECM modulation does not trigger an invasive phenotype [218]. Likewise, in BC patients, specific CAFs subpopulations were correlated with the development of distant metastases. These CAFs not only promote cancer cell migration and initiation of EMT through SDF-1 and TGF-β pathways invasion but also induce cancer cell invasion via NOTCH signaling [161]. TGF-β1 and SDF-1 are important cytokines secreted by CAFs, being key mediators of the interaction between stromal and cancer cells. CAFs-derived TGF-β1 induces EMT phenotype in BC cells and promotes metastatic activity by activating the TGF-β/Smad signaling pathway [219-221], while SDF-1 derived from CAFs promotes metastasis by increasing EMT, tumor cell motility, and intravasation [180, 222, 223]. Other chemokines like CCL8, CCL11, and CXCLs also accelerate BC cell growth and metastatic process, as well as induce drug resistance [224-226].

Interleukins are other cytokines released by CAFs that are involved in tumor progression and metastasis. For example, IL-6 promotes the growth and invasion of BC cells in a STAT3-dependent manner and enhances apoptotic resistance by favoring MCL-1 expression [227, 228]. However, CAFs-derived IL-8 mediated tumor cells EMT by inhibiting the AKT pathway [229]. Besides, IL-32 promotes BC cell invasion and metastasis by specific bound to integrin β3 present in cancer cell membranes, inducing activating of downstream p38/MAPK signaling that in turn increases the expression of EMT markers [230]. In response to tissue damage, CAFs activate the NLR family pyrin domain containing 3 (NLRP3) inflammasome and pro-inflammatory IL-1β secretion that facilitates BC tumor growth and metastasis. In this sense, the CAF-derived NLRP3/IL-1β pathway modulates the TME through the recruitment of myeloid cells and upregulates the expression of adhesion molecules on endothelial cells as well as the expression of MMPs in tumor

cells [231]. Other factors secreted by CAFs, like OPN, a disintegrin and metalloproteinase (ADAM) with thrombospondin motifs 1 (ADAMTS1), tissue inhibitor of metalloproteinase 1 (TIMP-1), Gremlin 1 (GREM1), or collagen triple helix repeat containing-1 (CTHRC1) were also related to the promotion of BC cells' growth, EMT, invasion, migration, and metastasis [232-237]. Moreover, VEGF-A and tenascin-C also play a part in BC cells colonization and metastasis, once CAFs-derived VEGF-A creates an angiogenic TME at the metastatic niche and stromal tenascin-C protects tumor cells from apoptosis [177]. The polio virus receptor (PVR) secreted by CAFs in brain metastasis was also related to BC metastasis by enhancing the invasive capacity of BC cells in the brain [238].

The tumorigenic properties of CAFs are also related to their dysregulated metabolism characterized by enhanced glycolytic activity [239]. This feature can be derived by chemokines (like CCL6, CCL11, and CCL12), TGF-β1, PDGF, or hypoxia-inducible factor 1 alpha (HIF-1α) upregulation and facilitates BC progression once cancer cells use CAF-derived metabolites to fuel their metabolic activity, modifying the tumor metabolic profile and promoting tumor growth [240-243]. Metabolites like lactate, pyruvate, and ketone bodies, produced by metabolically reprogrammed CAFs, provide nutrients for cancer cells, sustain proliferation, induce stemness, and promote metastasis and drug resistance, contributing to BC progression [244-246]. One example is CAFs-derived lactate that promotes BC invasion by activating the TGF-β1/p38 MAPK/MMP2/9 signaling axis and increasing mitochondrial activity in cancer cells [247]. Additionally, exosomes released by CAFs, carrying microRNAs, proteins, or metabolites, have also been implicated in BC aggressiveness by increasing cell growth, stemness, EMT, invasive capacity, and therapy resistance [248-252].

Likewise, CAFs are also linked to therapy resistance. In BC patients, stromal gene signatures that predict prognosis and therapeutic response to chemotherapy and immunotherapy were identified [253, 254]. Likewise, in ER-positive BC tumors, the presence of CAFs with CD146 negative expression was associated with resistance to tamoxifen and worse patient outcomes. This CAFs subpopulation was able to suppress ER expression in ER-positive BC cells decreasing tumor cell sensitivity to estrogen and in turn to tamoxifen treatment [255]. Besides, in HER2-positive BC patients trastuzumab resistance was linked with a population of TGF-β-activated CAFs with FAP-α-positive expression and low IL-2 activity. The stimulation of the stromal IL-2 in unresponsive tumors restored immune infiltration and trastuzumab efficacy through NK cells activation [256].

Additionally, CAFs can promote therapy resistance by remodeling the ECM, once the characteristics of ECM, as well as interactions of tumor cells with its components, can restrict drug availability at the tumor or induce adhesion-mediated drug resistance [257, 258]. For example, CAFs-derived fibronectin can induce EMT phenotype and resistance to tamoxifen in BC cells in an integrin β1-dependent manner [259]. Moreover, docetaxel-induced collagen type IV secretion by CAFs protected BC cells from chemotherapeutic-induced cell death [260].

CAFs secretome is also connected to therapy response. In BC, CAFs secretome can drive chemoresistance by stimulating the tumor cell proliferation and tumor recovery between chemotherapy cycles [261] or drive DOX resistance by increasing tumor cells' extracellular secretion of high mobility group box 1 (HMGB1) [262]. In HR-positive patient-derived organoids (PDOs) it was observed that CAF-secreted cytokines such as growth-regulated oncogene alpha (GRO-α) and CCL19 induce resistance to endocrine therapy [263]. CAF-derived IL-6 was also related to tumor growth, radio-resistance, DOX resistance, and tumor immune

suppression through STAT3 pathway activation [264, 265]. Radio resistance was also linked to the crosstalk between delta-like canonical Notch ligand 1 (Dll1)-positive cancer stem cells and CAFs. In this context, Dll1-positive cells recruited CAFs in an IL-6-dependent manner, whereas Dll1-driven Notch signaling in recruited CAFs promoted Wnt ligand secretion, achieving stemness and metastasis [266]. Moreover, FGF5 secretion by CAFs promoted resistance to HER2-targeted therapies, by inducing FGFR2 transactivation of HER2 via c-Src. In HER2-positive patients, FGF5 expression was associated with poor outcomes and correlated with a lower pathologic complete response rate in patients treated with neoadjuvant trastuzumab [267, 268]. The secretion of indoleamine 2,3-dioxygenase 1 (IDO1) and tryptophan 2,3-dioxygenase 2 (TDO2) by PDPN-positive CAFs was also found to promote resistance to trastuzumab through inhibition of antibody-dependent NK cell-mediated cytotoxicity [269]. Additionally, CAFs can also promote an exit from therapy-induced dormancy of BC cells, resulting in therapy resistance [270].

Cancer stem cell enrichment and chemoresistance are interlocked in cancer. In BC, IL-6 and IL-8, secreted by the CD10+/GPR77+ CAFs, promote tumor formation and chemoresistance through sustaining cancer stemness [271, 272]. The expression of AUF1 in CAFs was also related to carcinogenesis (EMT and stemness) and chemoresistance in an IL-6-dependent manner, being high heterogeneous nuclear ribonucleoprotein D (AUF1) level in stromal fibroblasts a factor of poor prognosis in locally advanced BC patients [273]. Moreover, in triple-negative BC, hedgehog-activated CAFs promote chemo-resistant cancer stem cells by FGF5 secretion and ECM collagen deposition [274].

For a long time, tumor cells were the focus of anti-cancer therapies. However, important advances in research have shown that targeting the TME is a powerful tool to control tumor progression. In BC, studies reported that CAFs depletion inhibits tumor growth and metastasis [177, 180]. Due to its implication on tumor behavior, CAFs become potential targets to improve therapy outcomes. Novel therapeutic approaches targeting CAFs are being developed and various preclinical and clinical trials have highlighted the potential of CAF-targeting therapies. Nevertheless, efforts must continue to be made to improve the efficacy of these treatments.

1.3. Nanoparticles in medicine

In the last two decades, nanoparticles (NPs) emerged as important players in modern medicine. These are materials with nanoscale dimensions, normally with a diameter between one and a few hundred nanometers [275]. In medicine, NPs can be applied as diagnostic tools, in medical imaging, as drug delivery systems, and in regenerative medicine. Due to their large surface area to volume ratio, NPs present unique chemical and physical properties that can be easily modified to enhance their clinical potential [276].

Nanomedicine is a promising field in cancer therapy. Nowadays, despite only 16 NP-based cancer therapies have been approved globally, the number of clinical trials involving NPs is rising every year [277]. NPs have unique characteristics that can overcome conventional drug disadvantages, such as non-specific targeting, poor biodistribution and bioavailability, and adverse side effects [278]. Likewise, NPs can be designed to target specific tissues or cells and release their content in a controlled manner. Accordingly, the incorporation of a targeting system in

the NP surface allows active targeting and protects normal cells against side effects of cancer therapy [279]. Besides, NPs improve the stability and solubility of encapsulated cargo and the transport and delivery of poorly soluble or hydrophobic drugs into the tumor [280]. Moreover, the incorporation of specific coatings like polyethylene glycol (PEG) can decrease opsonization and avoid immune system clearance [281].

In this manner, NPs can carry chemotherapeutic agents or nucleic acids to achieve cytotoxic effects or gene therapy in tumor cells, as well they can also be used to enhance immunotherapy or reverse the tumor immunosuppressive microenvironment [282-284]. The drug delivery systems can be based on organic (such as lipid-based or polymers-based NPs) and/or inorganic supports (such as carbon nanotubes, quantum dots, gold NPs, iron oxide NPS, or silica-based NPs) (**Figure 8**) [282].

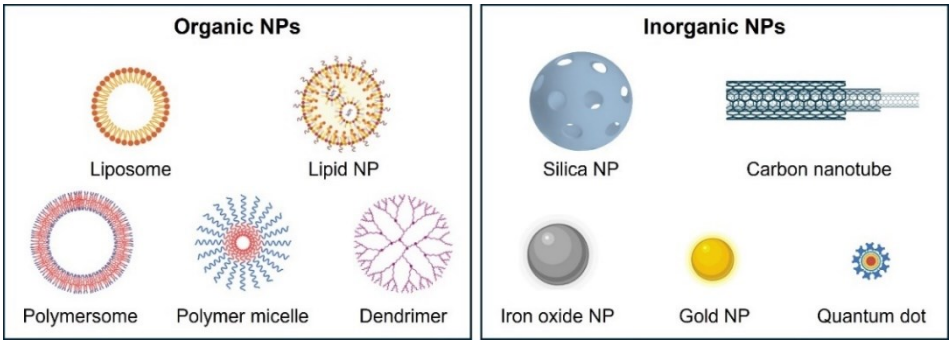

Figure 8. Examples of organic and inorganic nanoparticles applied as drug delivery systems in cancer therapy. Abbreviations: NP – nanoparticles.

On the one hand, organic NPs are based on natural or synthetic organic molecules. The most appealing feature of these NPs is their excellent biocompatibility and low cytotoxicity since the molecules used for their assembly can be degradable naturally. Moreover, organic NPs

offer a malleable synthesis, facile processability, and relatively simple routes for the encapsulation of drugs [285]. The NPs can be divided into lipid-based or polymers-based NPs. Interestingly, we can find some examples of organic NPs in nature, such as protein aggregates, lipid bodies, and viruses [286].

Lipid-based NPs are typically spherical structures with one or more lipid external layers surrounding at least one internal aqueous compartment and include liposomes, solid lipid NPs, and nanoemulsions [287]. These structures are normally composed of cationic or ionizable lipids (enable drug encapsulation), helper lipids (stabilize the lipid layer and facilitate membrane fusion), and PEGylated lipids or surfactants (improve particle stability and prevent rapid degradation *in vivo*) [288]. Compared to other NPs, lipid-based NPs offer many advantages as delivery systems, as they present high biocompatibility, and bioavailability, and easily cross the cell membrane to deliver NP's contents [289]. For these reasons, lipid-based NPs are the most common type of NPs approved [290]. For example, two liposomal DOX NPs have been approved for BC treatment with comparable efficacy and reduced cardiotoxicity [291, 292].

Polymer-based NPs can be synthesized from natural or synthetic polymers that are made up of large repeating units designated as monomers [293]. These NPs can be divided into nanocapsules (cavities surrounded by a polymeric covering) and nanospheres (solid matrix systems) and subdivided according to their architecture in polymersomes, micelles, or dendrimers, among others [294]. Polymer-based NPs drug delivery features can be enhanced by drug encapsulation in the NP core, or drug bonding to the NP surface. These NPs are generally good delivery vehicles with good biocompatibility. However, they present a high risk of

particle aggregation and toxicity [295]. Due to these facts, only a small number of polymeric NPs are currently approved [290].

On the other hand, inorganic NPs are normally made from inorganic precursors, forming a three-dimensional arrangement with linked atoms [296]. These NPs have unique material- and size-dependent physicochemical properties, such as optical, electrical, and magnetic properties. Moreover, they are usually hydrophilic, non-toxic, and biocompatible with living systems, and have the advantage of being more stable than organic NPs [285]. Some examples of inorganic NPs are gold NPs, iron oxide NPs, quantum dots, carbon nanotubes, and silica-based NPs.

Gold NPs are among the most studied inorganic NPs and have been widely used for medical applications as they are inert, non-toxic, and biocompatible [297]. Moreover, their surface can be easily functionalized to enhance delivery capabilities into the tumor [298]. In addition to targeted drug delivery and gene therapy, these NPs, as well as other metallic NPs, are commonly used in imaging and photothermal therapy due to their optical, magnetic, and photothermal properties. Some other examples of commonly used metallic NPs are silver and iron-based NPs [299].

Magnetic NPs, such as iron oxide NPs have also been widely studied in nanomedicine. These NPs are generally used in drug delivery as well as in imaging and thermal-based therapies. To enhance stability and biocompatibility, they are usually coated with organic materials like polymers and fatty acids [300]. Moreover, magnetic NPs have demonstrated high efficacy in targeting (chemotherapy and gene therapy) and imaging in BC [301-303].

Quantum dots are typically made of semiconducting materials and display a broad spectrum of absorption, and restricted emission bands. These characteristics make them optimal candidates for imaging applications. However, they are still not approved for *in vivo* diagnosis in humans [304, 305].

Carbon nanotubes are one type of carbon-based NPs. They are well-ordered carbon graphitic NPs that form single or multi-walled cylindrical tubes. Carbon nanotubes have been used for DNA delivery and drug delivery, imaging, and thermal ablation [306, 307].

Silica NPs are highly moldable, biocompatible, and stable NPs [308]. There are many different types of silica NPs, being mesoporous silica NPs (MSNs) considered one of the best options for targeted drug delivery due to their properties. These NPs have good biocompatibility, tunable pore size and volume, good drug-loading capacity, and easy functionalization [309, 310]. Moreover, MSNs have shown great potential in immunotherapy [311]. The characteristics of MSNs will be discussed more deeply in the next section.

To improve the biological and structural properties and overcome the disadvantages of both types of NPs, different NPs (including organic and inorganic components) can be combined in a single hybrid drug delivery system [312]. Some examples of these hybrid NPs are liposome-silica NPs that are formed by a silica core surrounded by a lipid bilayer, or lipid-polymer NPs that consist of an inner polymeric core enclosed by a lipidic layer. These NPs combine the high biocompatibility of lipids with the structural integrity and stability of the other components [313, 314]. Moreover, the organic or inorganic NPs can also be combined with natural biomaterials, like cell membranes, to enhance safety and treatment efficacy [315].

1.3.1. Mesoporous silica nanoparticles

MSNs are inorganic materials usually with spherical shape and an ordered tunable porous structure. These NPs normally have a diameter of around one hundred nanometers. However, due to surface modifications, their diameter can be larger. Moreover, their mesopores are cylindric channels arranged in a hexagonal pattern with a pore size typically between 2 and 5 nm [316]. These materials exhibit several excellent features. On the one hand, MSNs show good biocompatibility as well as a high level of clearance and excretion, and excellent chemical and thermal stability in addition to controllable degradability in a biological context. On the other hand, MSNs have a high drug-loading capability due to their high surface area and pore volume [317, 318]. Moreover, the high surface reactivity allows their easy functionalization, improving the solubility and pharmacodynamical profile. They can be functionalized with gatekeepers (also known as molecular gates or nanovalves) that allow the controlled release of their content at the target site in response to specific external (such as temperature, pH, light, ultrasounds, or magnetic fields) or internal (such as pH, redox environment or presence of enzymes) stimuli (**Figure 9**) [319]. MSNs surface can also be functionalized with organic groups to increase stability, biocompatibility, and cellular internalization [310, 320]. Besides, specific ligands, like antibodies, peptides, or nucleic acids, can also be included in the MSN surface to achieve active targeting of specific cells [321].

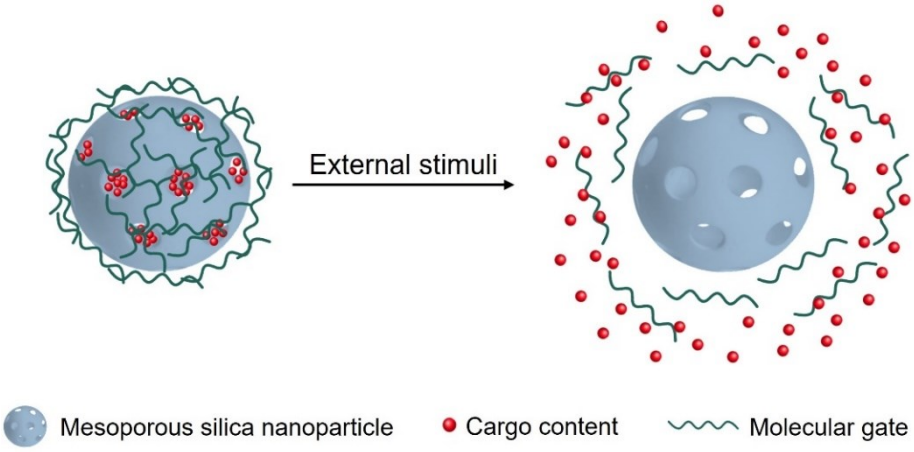

Figure 9. Representation of a mesoporous silica nanoparticle functionalized with a molecular gate (or gatekeeper) responsive to external stimuli.

Altogether, MSNs characteristics allow specific and efficient cargo release, minimizing off-target toxicity, making them excellent candidates for anticancer therapies. However, several aspects of MSNs, such as size and surface functionalization, must be considered to ensure that NPs reach the tumor [322]. First, the NPs should remain stable in the blood system until reach their target and evade renal and hepatic clearance [323]. Then, NPs should avoid reticuloendothelial system clearance (the mononuclear phagocyte system that rapidly sequestrates the NPs), to finally reach the tumor [324]. The MSNs extravasate from the bloodstream through tumors' defective vasculature and accumulate in TME by passive (due to the enhanced permeability and retention effect in the tumor areas) and active targeting (**Figure 10**) [325]. Additionally, the NPs must overcome the high interstitial fluid pressure and TME features to successfully reach the target tumor cells [326].

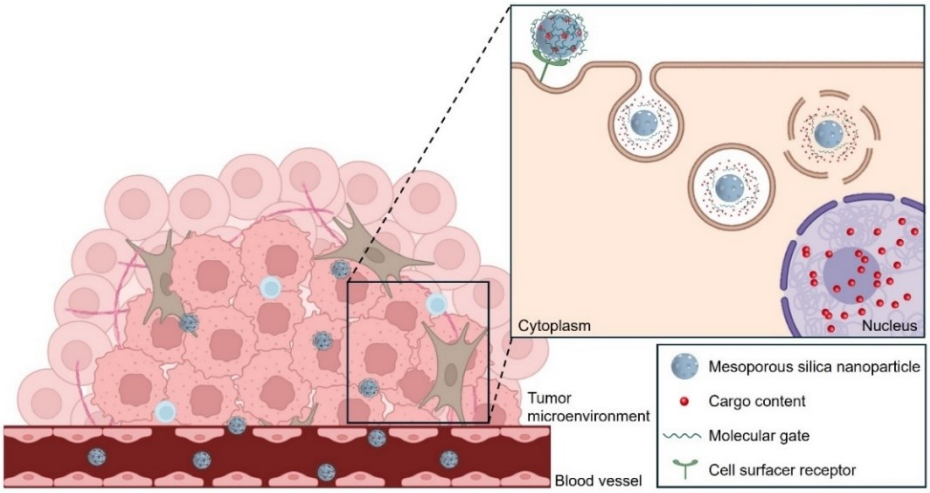

Figure 10. Mesoporous silica nanoparticles-controlled cargo delivery in tumor microenvironment. Nanoparticles in the bloodstream reach and accumulate in the tumor tissue passively (due to enhanced permeability and retention effect in tumor area) and actively (due to the interaction between ligands in the nanoparticle surface and receptors in the tumor cell membrane) targeting cancer cells. Once the nanoparticles reach the tumor, the molecular gates deliver the cargo content achieving the antitumoral effect.

Considering the MSNs as an alternative to conventional therapies, these nanodevices have been studied as promising delivery systems. Nevertheless, the transition into clinical practice remains a challenge, whereas most of the nanomaterials currently approved are organic-based NPs [327]. Despite the optimal performance of MSNs in preclinical settings, with visibly improved safety, biodistribution, pharmacokinetics, and efficacy, some nanodevices fail to enhance overall survival in clinical trials, probably due to heterogeneous tumor vasculature that decreases tumor uptake and NPs' efficacy [328].

Nowadays, the design and application of novel NP-based systems for the diagnosis and treatment of BC are arising. However, just a small

number of them are currently approved for BC [329]. Regarding diagnosis, a silica NP functionalized with PEGylated and loaded with Cy5.5 (as a fluorescent dye) and radiolabeled RGD peptides (to enhance PET imaging) are currently under clinical investigation for visualization of metastatic lymph nodes during surgery in BC patients (NCT02106598). Concerning treatment, the first nanodevice approved for BC treatment was the PEGylated liposomal DOX (Caelyx/Doxil). This treatment was able to reduce cardiotoxicity while preserving drug efficacy [291]. The combination of PEGylated liposomal DOX with other chemotherapy drugs and HER2-targeted therapy (such as trastuzumab) in advanced BC patients has shown good efficacy and low toxicity [330-333]. Moreover, another liposome-encapsulated DOX (Myocet) is also approved for BC treatment and shows the same clinical benefits [292]. In 2005, an albumin-bound paclitaxel NP (Abraxane or nab-paclitaxel) was also approved for BC treatment showing comparable or superior efficacy over paclitaxel, alone or in combination with standard chemotherapy or targeted therapy, as well as a good safety profile [334-337]. Generally, these nanodevices and the ones under clinical trials are based on standard anticancer drugs and not based on specific features of BC cells. Taking this into account, new specific BC NPs-based targeted therapies are currently being developed.

MSNs applications in gene and/or drug-delivery targeted therapies in BC have been studied. It was demonstrated that NP surface functionalization with polyethyleneimine (PEI) maximizes RNA and DNA delivery into tumor cells [338]. One example of this application is a nanodevice based on MSNs coated with PEI and hyaluronic acid (that targets the CD44 receptor in BC cells) engineered for microRNA-200c-3p delivery in BC cells. *In vivo*, these NPs showed good therapeutic efficacy by targeting genes related to proliferation, EMT, invasion, and migration,

with no signs of toxicity [339]. Moreover, a similar NP was developed for the combined delivery of DOX and microRNA-99a-5p. In this case, the MSNs demonstrated to reduce tumoral size in a triple-negative BC xenograft mice model, through inhibition of microRNA-99a-5p' targets that enhance the therapeutic effect of DOX, while decreasing the cardiotoxicity [340]. Altogether, the preclinical results highlight the potential of MSNs in cancer treatment, even if they have not been clinically implanted yet. Besides, new strategies for using nanodevices to target TME instead of targeting cancer cells directly are of interest.

1.3.2. Modulation and targeting of tumor microenvironment by nanoparticles

As discussed before, TME has a high impact on cancer progression and metastasis. Thus, several studies have been focused on using NPs to modulate and target TME instead of targeting tumor cells directly to achieve an effective treatment. In this context, two approaches have been explored.

On the one hand, strategies that use specific TME features, like acidic pH, elevated reactive oxygen species (ROS) and adenosine triphosphate (ATP) levels, high glutathione (GSH) concentration, hypoxic environment, and modified ECM, were developed using stimuli-responsive NPs (**Figure 11**) [341].

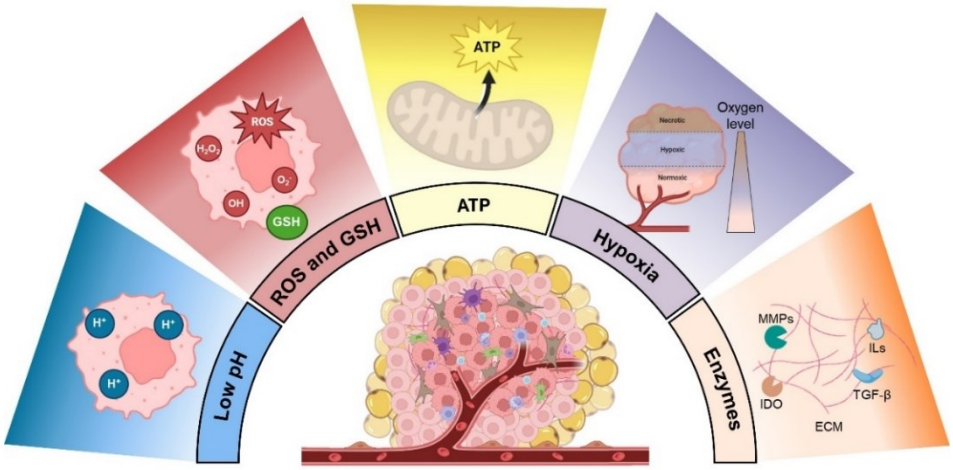

Figure 11. Tumor microenvironment features used to develop responsive nanoparticles, including low pH, elevated ROS and GSH levels, high ATP production, hypoxic environment, and overexpressed enzymes (like MMPs and IDO) and factors (like TGF-β and ILs) in the ECM. Abbreviations: ATP – adenosine triphosphate, ECM – extracellular matrix, GSH – glutathione, IDO – indoleamine 2,3-dioxygenase, ILs – interleukins, MMPs – matrix metalloproteinases, ROS – reactive oxygen species, TGF-β – transforming growth factor-beta.

One common characteristic of solid tumors is the acidic pH in the TME, due to tumor-altered metabolism and insufficient tumor irrigation [342]. In this context, pH-responsive NPs were developed to release their content under acidic conditions [343]. Besides TME's acidic pH, the low pH in intracellular lysosomal and endosomal compartments can also potentiate drug release inside tumor cells upon NP internalization [344]. Several studies developed pH-responsive drug delivery systems for BC cells [345]. Moreover, pH-responsive nanodevices can also be designed to release tumor immunity modulators and enhance immune response [346]. One example is the dual pH-responsive NPs charged with a

chemotherapeutic drug (DOX) and an antitumor immune regulator (R848). This NP released its cargo in response to TME's acidic pH, achieving synergistic effects of chemotherapy and immunotherapy in BC treatment [347].

Cancer cells produce elevated ROS levels, especially hydrogen peroxide (H_2O_2), due to genetic mutations and deregulated energy metabolism patterns. Besides, ROS accumulation results in oxidative stress and increased levels of GSH [348]. So, ROS and GSH-responsive NPs were proposed to target tumors [349, 350]. ROS-responsive NPs were developed with various aims, like enhancing drug delivery into the tumor [351], improving photodynamic therapy [352], inhibiting tumor growth by ROS amplification [353], or promoting immune checkpoint blockade response [354]. These NPs can modulate TME and improve BC therapy, for instance, liposomal NPs co-loaded with zoledronic acid and a photosensitizer infrared dye (IR780) were designed to co-target macrophages and tumor cells. The presence of H_2O_2 triggered NP's content release that reprogramed M2 to M1 macrophages and allowed photodynamic therapy application with adequate oxygen supply on tumor cells [355]. Moreover, redox-sensitive nanodevices, that trigger drug release in the presence of elevated GSH levels, were used to enhance the chemotherapeutic efficacy in BC models [356]. Additionally, these GSH-responsive NPs were also developed to reverse the immunosuppressive TME and inhibit metastasis [357, 358]. For example, an MSN responsive to high GSH levels and loaded with monocarboxylic acid transporter 4 (MCT4) inhibitors was able to reprogram macrophages' phenotype (from M2 to M1 macrophages) and restore CD8+ T cells activity, as a consequence of intracellular lactate increase and tumor cell apoptosis [359]. As well, strategies that combine both ROS and GSH-responsive NPs have also been developed. Accordingly, a ROS-

responsive NP encapsulated with GSH-activatable drugs was tested in BC models. ROS triggers NP's drug delivery inside tumor cells, whereas the endogenous GSH stimulates drug activation. Furthermore, the combined treatment with anti-PD-L1 antibody improved $CD8^+$ T cells number, and $CD8^+$ T cells/T lymphocytes ratio, and hindered tumor growth and metastasis [360].

Due to their glycolytic metabolism, tumor cells exhibit higher ATP levels in comparison with normal cells. Based on this feature, ATP-responsive NPs were designed for BC treatment [361]. These NPs can be used for specific drug delivery in TME promoting tumor growth inhibition and metastasis, being also used in tumor immune modulation [362].

Hypoxia is a distinct feature of solid tumors, caused by the rapid tumor growth followed by the formation of deficient neo-vasculature that creates a decreasing oxygen gradient from the surface to the tumor core [363]. Considering this significant difference between tumor tissue and normal tissue, many nanodevices have been proposed to target hypoxia by directly targeting hypoxia or by oxygen generation/delivery in hypoxic tumors [364, 365]. Moreover, several nano-based strategies were developed to target or restore tumor vasculature increasing drug delivery [366].

TME presents a unique enzymatic profile that can be used to design enzyme-responsive NPs [367]. In BC, the MMP2 expression proved to be remarkably important for disease progression, being correlated with lymph node metastasis and tumor staging [368]. Therefore, several studies have been focused on the use of MMP2-derived NPs for BC treatment [369, 370]. Indeed, a triple-responsive NP, that responded to MMP2, pH, and GSH sequentially, was designed for triple-negative BC immunotherapy. This NP promotes immunogenic cell death response and antitumoral immunity through controlled drug release, which amplifies the

ROS cascade and increases the formation of H_2O_2 and toxic •OH [371]. Besides, NPs that target immunosuppressive enzymes (like IDO) or soluble factors (like TGF-β and ILs) present in TME have also been studied [372, 373].

On the other hand, NPs functionalized with specific ligands were synthesized to actively target TME cells, like macrophages, dendritic cells, lymphocytes, and CAFs [374].

TAM are important immunoregulatory cells, that secret immunosuppressive cytokines as well as growth factors to promote tumor growth, angiogenesis, and metastasis [375]. NPs were developed to target TAM and reprogram TME through inhibition of TAM recruitment to the tumor, TAM depletion, or reprogramming (**Figure 12**) [376]. In a BC mouse model, a biomimetic nano red blood cell NP loaded with DOX was used to specifically target TAM via the CD163 surface receptor. This NP was able to kill M2 macrophages in the tumor and decrease their recruitment by alleviating the tumor hypoxia, which restored an antitumoral immune environment [377]. Additionally, other strategies were developed to target TAM, like NPs charged with DOX and modified with mannose (whose receptor is overexpressed in TAM), or NPs loaded with the macrophage-depleting colony-stimulating factor-1 receptor (CSF-1R) inhibitor (pexidartinib). In both cases, NPs led to TAM depletion and enhanced antitumoral immunity [378, 379]. Moreover, some studies were focused on the use of NP to reprogram TAM. These NPs target the anti-inflammatory M2 macrophages and re-educate them to pro-inflammatory M1 phenotype [380].

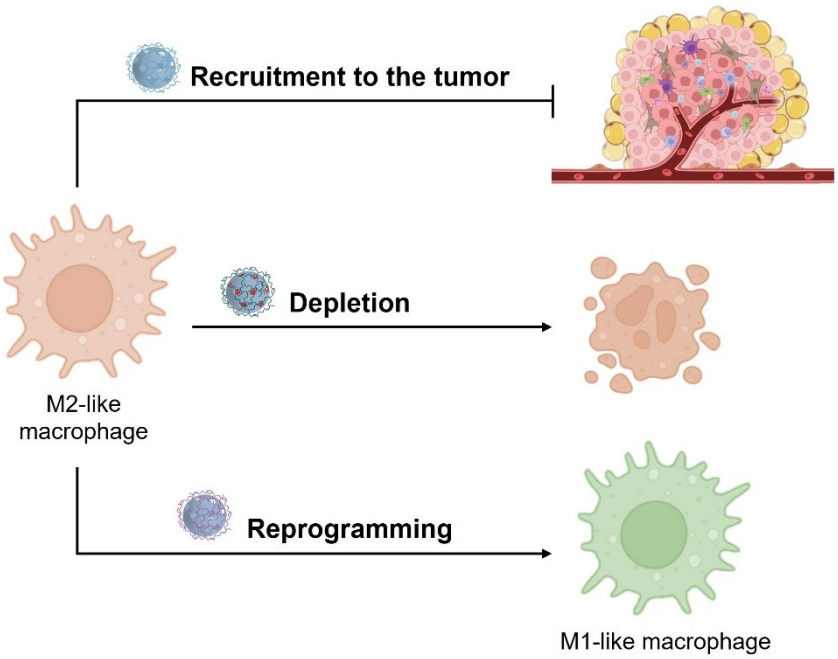

Figure 12. Nanomedicines targeting tumor-associated macrophages (TAM) and reprogramming tumor microenvironment through inhibition of TAM recruitment to the tumor, TAM depletion, or TAM reprogramming from an M2-like pro-tumoral phenotype into M1-like macrophages with antitumor functions.

Dendritic cells are antigen-presenting cells that stimulate and activate the T cells, promoting the antitumoral immune response [381]. NPs are being developed to target and reprogram these cells (**Figure 13**). For example, a NP loaded with the immunosuppressive rapamycin and modified to target the CD209 present in the dendritic cells surface showed to modulate dendritic cells to a maturation-resistant phenotype [382]. Besides, dendritic cells vaccines loaded with tumor antigens have also been studied for the activation of immune T cells and immune response [383]. NPs loaded with tumor antigens have also demonstrated potential for enhancing antigen presentation efficiency and remodeling the

immunosuppressive TME [384, 385]. Moreover, nanodevices were also used for the development of artificial antigen presentation cells, which deliver stimulatory signals to cytotoxic lymphocytes, increasing antigen-specific T cell proliferation [386].

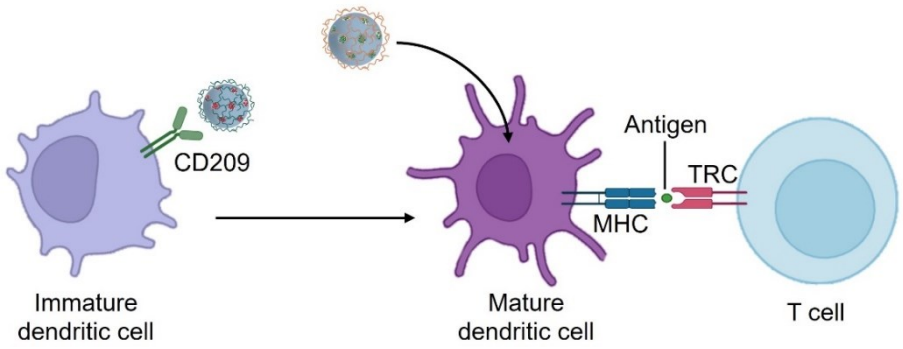

Figure 13. Nanomedicines targeting dendritic cells to promote a mature phenotype and improve antigen presentation to T cells, simulating their activation and enhancing the antitumoral immune response. Abbreviations: MHC – major histocompatibility complex, TRC – T-cell receptor.

T cells have a special relevance in tumor immunity. On the one hand, the cytotoxic T cells are responsible for eliminating cancer cells in the adaptive immune system. However, these cells are often ineffectively activated in tumors, contributing to tumor evasion of immune surveillance [387]. On the other hand, helper T cells are crucial organizers of cell-mediated immunity, being involved in developing and sustaining effective antitumor immunity [388]. Thus, NP-based strategies are focused on improving the reactivity and specificity of these cells against the tumor (**Figure 14**) [389]. Besides, regulatory T cells negatively regulate the immune response. In turn, NPs' antitumoral strategies are based on the

elimination of these cells or the blockage of their immunosuppressive functions (**Figure 14**) [390]. In BC, the use of NPs to block or inhibit negative regulators of immune response, like the PD-1 or cytotoxic T-lymphocyte antigen 4 (CTLA-4) expression in T cells, as well as the PD-L1 expression in cancer cells, resulted in an increase of cytotoxicity of T cells in the tumor and a reduction of immunosuppressive cells [391, 392]. Moreover, an MMP2-responsive NP was developed to deliver neuropilin-1 monoclonal antibodies in TME that bind to regulatory T cells' surface, blocking their immunosuppression activity [393]. Additionally, another NP was constructed with a homodimer of oxaliplatin and IDO inhibitor to improve antitumoral immune response in two forms. First, the homodimer of oxaliplatin promotes intra-tumoral accumulation of cytotoxic T cells by triggering immunological cell death in TME. Second, the IDO inhibitor downregulates IDO-mediated immunosuppression and suppresses regulatory T cells [394].

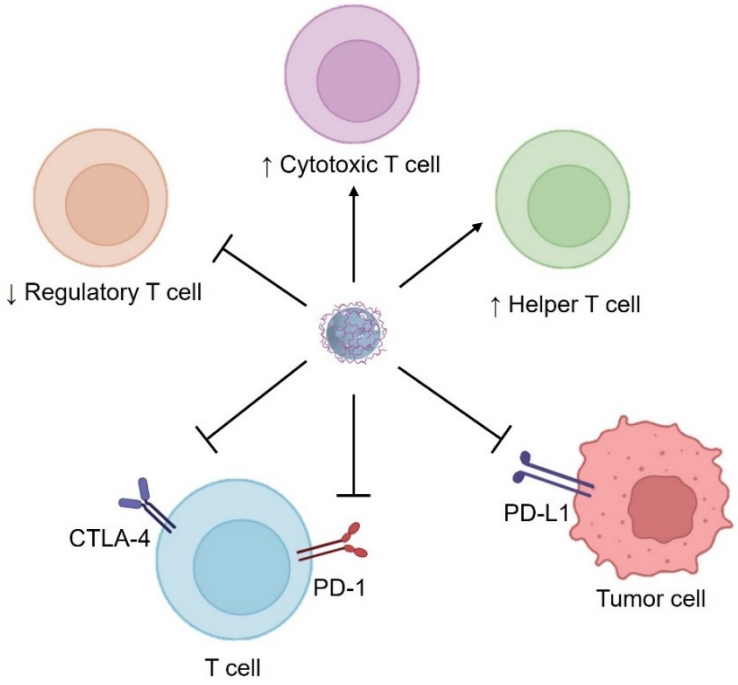

Figure 14. Nanomedicines targeting T cells and reprogramming tumor microenvironment through improving the reactivity and specificity of cytotoxic and helper T cells against the tumor, elimination of regulatory T cells or the blockage of their immunosuppressive functions, and inhibition of negative regulators of the immune response, like PD-1, PD-L1, and CTLA-4.

As commented in Section 1.2.1, CAFs are key regulators of cancer progression, being involved in tumor growth, metastasis, and drug resistance. Considering their role in TME, CAFs have emerged as potential therapeutic targets. In the next section, the nano-based strategies currently developed to target CAFs will be highlighted.

1.3.2.1. Nanoparticles targeting cancer-associated fibroblasts

Several studies have been conducted to prove the role of CAFs in BC growth, metastasis, therapy resistance, and immunosuppression. Therefore, new strategies to target CAFs have been developed, and promising drugs are currently under investigation in clinical trials of BC [395, 396]. Besides, CAF-based nanotherapeutic strategies have also been studied. The CAFs-targeting strategies include direct depletion, blocking CAF activation, and reprogramming CAFs into quiescent fibroblasts (**Figure 15**).

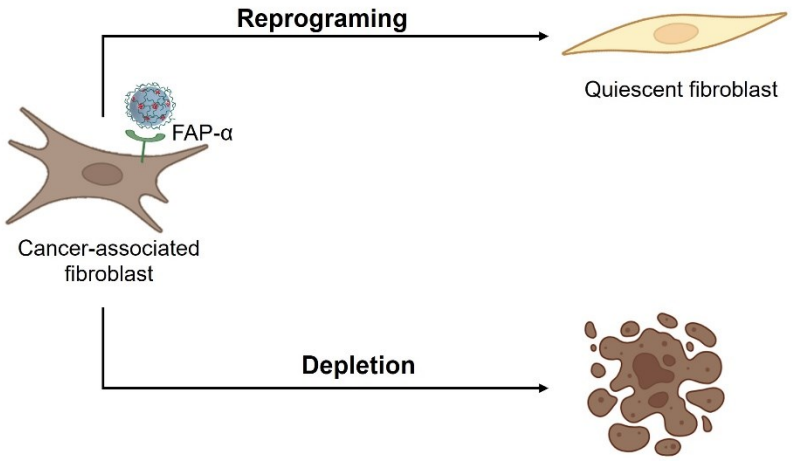

Figure 15. Nanomedicines targeting cancer-associated fibroblasts (CAFs) and reprogramming tumor microenvironment through reprogramming CAFs into quiescent fibroblasts, or direct CAFs depletion by targeting CAFs markers, like FAP-α.

On the one hand, some studies developed strategies to revert the activated CAFs into a quiescent state. Likewise, a multi-functional NP

responsive to MMP2 and GSH in TME was able to reprogram the activated CAFs into quiescent fibroblasts through downregulation of FAP-α and α-SMA expression. CAFs' reprogramming results in a reduction of tumor intercellular pressure and enhanced NPs' penetration, contributing to the antitumoral effect in HER2-positive BC models [397]. Moreover, salvianolic acid B loaded into a silica NP demonstrated an inhibitory effect on activated fibroblasts and inhibited the migration and invasion of BC cells, as well as lung metastasis in a BC mouse model [398]. Another study constructed a NP containing a plasmid encoding relaxin, a potent anti-fibrotic that suppresses fibroblast activation. The treatment with this NP reversed aberrantly activated CAFs, reshaped the tumor stromal microenvironment, and decreased the immunosuppressive cell infiltration in the tumor, leading to tumor growth inhibition in a BC mouse model [399].

On the other hand, most of the CAFs-targeting strategies are focused on direct depletion. These approaches use CAFs markers, like FAP-α, as targets. FAP-α is the most common tumor-targeting CAF antigen. It is a surface marker overexpressed on activated stromal fibroblasts in tumors, including BC [400]. One common approach is the use of nanodevices conjugated with a single-chain variable fragment of anti-FAP-α antibody. These NPs efficiently eliminated CAFs in BC tumors, reversed the tumor immunosuppressive microenvironment, and improved antitumoral therapy [401, 402]. Another strategy centers on the use of FAP-α-responsive peptides. For example, a nanodevice based on a FAP-α-responsive cleavable amphiphilic peptide was designed as a nano-based drug delivery system. The nanodevice releases its cargo (taxol) upon FAP-α cleavage in TME, resulting in CAFs depletion and tumor growth inhibition on BC xenograft models [403]. Moreover, FAP-based vaccines were also developed to target CAFs. The use of these vaccines demonstrated good results in tumor growth inhibition, enhanced tumor

drug uptake, and activation of antitumoral immune response in BC models [184, 404, 405].

Altogether, it is important to highlight the implications of TME in cancer development and therapy resistance and to study CAFs as key therapeutic targets. Besides, the potential use of nanodevices as treatment options to improve BC patients' outcomes must be considered.

CHAPTER 2 |

OBJECTIVES

Most of the BC therapies currently used in clinical practice are focused on targeting tumor cells. However, new developments in the immunology field uncovered an important role of TME, specifically CAFs, in tumor progression and therapy resistance. Hence, this project hypothesized that nanodevices targeting CAFs could be a potential therapeutic strategy for BC treatment.

Thus, this Ph.D. thesis intends to develop a nanodevice based on mesoporous silica loaded with DOX targeting CAFs and to evaluate its potential for BC treatment.

Accordingly, the specific objectives for the project are:

1. Design, synthesis, and characterization of NPs containing a CAFs-specific ligand on its surface and loaded with DOX.
2. Evaluation of the NPs' *in vitro* efficacy in BC cell lines, CAFs, and PDOs.
3. Evaluation of the NPs' *in vivo* efficacy in a triple-negative BC mouse model.

CHAPTER 3 |

MATERIALS AND METHODS

3.1. Cell culture

3.1.1. Commercial cell lines

One non-tumorigenic breast cell line (MCF-10A), three triple-negative BC cell lines (MDA-MB-231, MDA-MB-436, and MDA-MB-468), and one BC cell line originally derived from a spontaneously arising carcinoma in the mammary gland tissue of a mouse BALB/c strain (4T1) were obtained from American Type Culture Collection (ATCC, USA). The cells were maintained in DMEM/F-12 (Biowest, France) supplemented with 10% heat-inactivated fetal bovine serum (FBS, GIBCO, USA), 1% L-glutamine 100X 200 mM (Biowest), and 1% sterile filtered penicillin/streptomycin (P/S, Biowest) at 37 °C and 5% CO_2 in a humidified chamber.

During culture, the culture media was changed 3 days a week, and the cells were passed when reached 70-90% confluence. For that, the cells were washed with Phosphate-Buffered Saline (PBS, Biowest) and trypsinized through incubation at 37 °C with trypsin-EDTA 1X (Biowest). Then, the trypsinized cells were collected in supplemented culture media and centrifuged at 1,500 rpm for 5 minutes. To perform the *in vitro* experiments, the cells were counted using a Neubauer's chamber to determine the number of cells per mL, and the accurate number of cells was seeded.

3.1.2. Cancer-associated fibroblasts

CAFs were obtained from triple-negative BC patients' tumor biopsies at the Hospital Clínico Universitario de Valencia (Spain). Primary tumor biopsies were taken before any patients' treatment and were analyzed by an expert pathologist to ensure > 20% tumor infiltration and to confirm the BC subtype by immunohistochemical analysis. This study was approved

by the Biomedical Research Institute INCLIVA (Spain) (2024-VSC-PEA-0075), and all patients signed the informed consent.

Firstly, the biopsy was washed with 10% P/S diluted in PBS for 10 minutes at room temperature, following mechanical disaggregation. Then, the sample was digested with 300 U/mL of collagenase (Gibco) and 100 U/mL of hyaluronidase (Sigma-Aldrich, USA) resuspended in Advanced-DMEM (Biowest) with 1% P/S for 1 hour at 37 °C with shaking. After tissue digestion, the cells were centrifuged at 300 xg for 5 minutes at room temperature. Then, to eliminate the erythrocytes, the cells' pellet was incubated for 3 minutes at room temperature with ammonia-chloride-potassium (ACK) lysis buffer (Gibco). Supplemented culture media was added to inactivate the reaction and the sample was centrifuged at 300 xg for 5 minutes at room temperature. Then, the cells were resuspended in supplemented media and filtered using a 200 µm cell strainer (PluriSelect, USA) and centrifuged at 300 xg for 5 minutes at room temperature. Finally, the cells were resuspended in DMEM/F-12 supplemented with 10% FBS, 1% L-glutamine, and 1% P/S and maintained at 37 °C and 5% CO_2 in a humidified chamber.

The CAFs were allowed to grow and maintained as described for the commercial cell lines. All experiments were performed with CAFs that have been cultured between passages 3 and 10. Before *in vitro* experiments, the CAFs' phenotype was confirmed by flow cytometry. For that, cells were resuspended in eBioscience™ Flow Cytometry staining buffer (FACS buffer, Invitrogen, USA) and incubated with an antibody cocktail containing anti-CD326-Brilliant Violet 421 (324220, BioLegend, USA), anti-CD31-APC-Vio® 770 (130-110-672, Miltenyi Biotec, Germany), anti-CD45-Vio® Bright R720 (130-127-376, Miltenyi Biotec) and anti-CD90-APC (130-114-861, Miltenyi Biotec) for 30 minutes at room temperature. Flow cytometry analysis was performed on the LSR

FORTESSA X-20 analyzer (BD Biosciences, USA), and data analysis was performed using FlowJo version 9.8.1 (LLC, USA).

3.1.3. Patient-derived organoids

The BC PDOs were obtained from triple-negative BC patients' tumor biopsies at the Biomedical Research Institute INCLIVA (Spain) (2024-VSC-PEA-0075) after ethical approval and signing of the informed consent.

First, the primary tumor biopsies taken before performing patients' treatment were implanted in the mammary fat pad of 6- to 8-week-old NOD/SCID female mice purchased from Charles River Laboratories (USA) and maintained at Animal Facilities from the Universitat de Valencia (Valencia, Spain). The tumors were allowed to grow until reached the institutional euthanasia criteria for tumor size. Then, the tumors were collected and the PDOs were processed following the same protocol described for obtaining CAFs.

Briefly, the tumor was washed, followed by mechanical and chemical digestion. After that, erythrocytes were eliminated, the reaction was stopped using PDO culture media (**Table 6**), and the sample was centrifuged at 300 xg for 5 minutes at room temperature. The cells were then resuspended in PDO culture media and filtered through a 100 µm cell strainer before centrifuging at 300 xg for 5 minutes. Finally, 200,000 cells were seeded in a dome of 200 µL of 75% Matrigel Growth Factor Reduced Basement (Corning, USA) in a tissue-treated 6-well plate. After incubating for 15 minutes at 37 °C, 5 mL of PDOs' culture media were added.

Table 6. Triple-negative breast cancer patient-derived organoids' culture media composition.

	Final concentration
Advanced-DMEM (Biowest)	N/A
Heat-inactivated fetal bovine serum (Gibco)	5% (v/v)
L-glutamine (Biowest)	1% (v/v)
HEPES (Gibco)	10 µM
Gentamicin (Gibco)	50 µg/mL
Human EGF (Merck)	10 ng/mL
Hydrocortisone (MedChemExpress)	1 µg/mL
Y-27632 (Stemcell Technologies)	10 µM

For PDOs maintenance, the culture media was changed twice a week, and the organoids were passed every 7-14 days. For that, PDOs' culture media was discarded, cold PBS was used to disrupt the Matrigel dome, and the organoids were centrifuged at 300 xg for 5 minutes at room temperature. Then, the pellet was incubated with 2 mL of TrypLE™ Express Enzyme 1X (Gibco) supplemented with 2 µL of Y-27632 (Stemcell Technologies, Canada) for 15 minutes at 37 °C. The trypsinized cells were resuspended in PDOs' culture media and centrifuged at 300 xg for 5 minutes. After counting the cells in a Neubauer's chamber, the number of cells per mL was determined, and, in a tissue-treated 6-well plate, a new dome of 200 µL of 75% Matrigel containing 200,000 cells was formed. The Matrigel was allowed to solidify, 5 mL of PDOs' culture media was added, and the PDOs were maintained at 37 °C and 5% CO_2 in a humidified chamber.

Before *in vitro* experiments, the PDOs' ER, PR, HER2, and Ki67 protein expression was evaluated by immunocytochemistry. For that, the matrigel dome containing organoids was disaggregated using cold PBS, and the organoids were centrifuged at 300 xg for 5 minutes at room temperature. The organoids were washed with PBS and fixated with 4%

paraformaldehyde (VWR BDH Chemicals, USA) for 1 hour at room temperature. Then, the organoids were embedded into HistoGel™ (Thermo Fisher Scientific, USA) and FFPE. Hematoxylin and eosin (H&E), ER, PR, HER2, and Ki67 automated immunohistochemical staining were performed in 4 µm thick sections, and representative photographs were taken in Leica DM 2500 LED microscope (Leica Microsystems, Germany) with a digital camera MC170 HD at 20X magnification at the Central Medicine Research Unit of Universitat de Valencia (UCIM-UV).

3.2. Gene expression studies

RNA extraction was performed using the Trizol reagent method. The samples were resuspended in Trizol (Invitrogen) and incubated for 5 minutes at 4 ºC. Then, chloroform (Sigma-Aldrich) was added, and the samples were vortexed and incubated for 3 minutes at 4 ºC. After centrifuging the samples at 13,200 rpm for 15 minutes at 4 °C, the aqueous phase containing the RNA was transferred to a new tube, and isopropanol (AppliChem, Italy) was added. The RNA was allowed to precipitate overnight at -20 °C. On the next day, the samples were centrifuged at 13,200 rpm for 15 minutes at 4 °C, and the RNA pellets were washed by adding 75% ethanol (Sigma-Aldrich). A final centrifuging at 13,200 rpm for 15 minutes at 4 °C was performed and the pellets were allowed to dry. Finally, RNA pellets were eluted in RNase-free water and the RNA concentration and purity ratio were determined using the NanoDrop 2000 spectrophotometer (Thermo Fisher Scientific).

Reverse transcription was performed from 1,000 ng of RNA using High-Capacity cDNA Reverse Transcription Kit (Applied Biosystems, USA), according to the manufacturer's indications.

Real-time quantitative polymerase chain reaction (RT-qPCR) was performed in a QuantStudio 5 Real-Time PCR System (Thermo Fisher Scientific) using 2 µL of resulting complementary DNA (cDNA), 5 µL of TaqMan® Universal Master Mix (Applied Biosystems), 0.5 µL of TaqMan® 20x assays (human *FAP-α*: Hs00990791_m1, human *GAPDH*: Hs03929097_g1, mouse *FAP-α*: Mm01329177_m1, mouse *GAPDH*: Mm99999915_g1, mouse *MKI67*: Mm01278617_m1, mouse *MYH7*: Mm00600555_m1; Applied Biosystems), and 2.5 µL of RNase-free water, according to the manufacturer's instructions. *FAP-α* and *MKI67* transcript levels were evaluated using the $2^{-\Delta Ct}$ method, and *GAPDH* was used as a reference gene to normalize results ($\Delta Ct = Ct_{(Gene\ of\ interest)} - Ct_{(Reference\ gene)}$). All the samples were run in triplicates.

3.3. Western blot

Total protein was extracted from cells using Pierce® RIPA buffer (Thermo Fisher Scientific) supplemented with protease and phosphatase inhibitor cocktail (Thermo Fisher Scientific) and sonication was performed by the Sonics Vibra Cell VC 505 (Sonics & Materials, USA) (10 seconds at 40% pulse). After centrifuging at 13,200 rpm for 30 minutes at 4 °C, the supernatant containing the proteins was collected in a new tube. Then, the protein concentration was determined using the Pierce™ BCA Protein Assay Kit (Thermo Fisher Scientific), according to the manufacturer's procedures.

30 µg of total protein were boiled for 5 minutes at 95 °C with Laemmli loading buffer 2X (Sigma-Aldrich) for protein denaturalization. Then, the proteins were separated by 10% polyacrylamide gel by sodium dodecyl sulfate-polyacrylamide gel electrophoresis (SDS-PAGE) and transferred into an immunoblot nitrocellulose membrane (Bio-Rad, USA) in a 25 mM

Tris-base/glycine buffer using a Trans-Blot Turbo Transfer system (Bio-Rad). Membranes were blocked with 5 % bovine serum albumin (BSA) in Tris-Buffered Saline/0.1% Tween20 (TBS/T) for 1 hour at room temperature. Then, the membranes were incubated overnight at 4 °C with specific primary antibodies for FAP-α (ab53066, dilution 1:500, Abcam, UK) and loading control GAPDH (#MA5-15738, dilution 1:100 Thermo Fisher Scientific). After incubation, the membranes were washed in TBS/T and incubated with the secondary antibody (anti-rabbit #7074 or anti-mouse #7076, dilution 1:2000, Cell Signaling, USA) for 1 hour at room temperature. After washing with TBS/T, the proteins were detected by chemiluminescence using Pierce ECL Western Blotting Substrate (Thermo Fisher Scientific) according to the manufacturer's using the ImageQuant™ LAS 4000 system (GE Healthcare, USA).

3.4. Nanoparticles' synthesis

To synthesize NPs, 1 g of the structure-directing agent N-cetyltrimethylammonium bromide (CTABr, Sigma-Aldrich) was dissolved in 480 mL of deionized water, and the solution was magnetically stirred. Then, 3.5 mL of sodium hydroxide (NaOH, 2 M, Sigma-Aldrich) was added to increase the pH, followed by a temperature adjustment to 80 °C. After that, 5 mL of tetraethyl orthosilicate (TEOS, 2.57×10^{-2} mol, Sigma-Aldrich) were added dropwise to the solution and the mixture was stirred for 2 hours allowing the formation of a white precipitate (as-synthesized NPs). The precipitate was isolated and collected by centrifugation, washed with deionized water, and dried at 70 °C. Finally, the solid was calcined for 5 hours at 550 °C to remove the template phase, obtaining the final MSNs.

To prepare the NP-CTR-DOX and NP-FAP-DOX, 100 mg of NPs was dispersed in 6 mL of anhydrous acetonitrile (ACN) and reacted with 98 mL of (3-mercaptopropyl)-trimethoxy silane for 5.5 hours. Then, 112 mg of 4,4′-dipyridyl disulfide were added to the mixture, and the reaction was magnetically stirred for 24 hours. The thiolated solid was washed with ACN, ethanol and PBS, and stirred 24 hours after adding 98 mg of DOX in 8 mL of PBS. The solid was then isolated by centrifugation, resuspended in 8 mL of ACN, and 195 mg of SH-PEG_{12}-COOH was added, keeping the mixture stirred overnight to form the molecular gate. To attach the peptide, first the NPs were washed with ACN, ethanol and PBS, and after that, were resuspended in 8 mL of PBS pH 6, where 50 mg of *N*-Ethyl-*N*′-(3-dimethylaminopropyl)carbodiimide hydrochloride (EDC) and 50 mg of *N*-Hydroxysuccinimide (NHS) were added to activate the carboxylic group of the molecular gate. The mixture was stirred for 2 hours. Then, the activated NPs were collected by centrifugation and resuspended in 8 mL of water pH 7. To this suspension, 100 mg of a control peptide (CTR peptide sequence: Gly-Gly-Gly-Gly-Gly-Gly-Gly-Ala-Thr-Lys-Asp-Ala-Thr-Gly-Asp-Lys-Thr-Ala) or a FAP-α ligand peptide with a high affinity for FAP-α (FAP-α peptide sequence: Gly-Gly-Gly-Gly-Gly-Gly-Gly-Ala-Thr-Lys-Asp-Ala-Thr-Gly-Pro-Ala-Lys-Thr-Ala) were added and the mixture was stirred overnight. The final solids (NP-CTR-DOX and NP-FAP-DOX) were washed with water and dried at 37 ºC.

The control nanodevices without DOX (NP-CTR and NP-FAP) were prepared following the same procedure without the drug-loading process.

3.5. Nanoparticles' characterization

Transmission electron microscopy (TEM) images were taken using a JEOL TEM-2100F electron microscope (JEOL Europe SAS, France).

Elemental mapping was conducted using scanning transmission electron microscopy coupled with electronic energy-dispersive X-ray spectroscopy (STEM-EDX) using a JEM 2100F instrument. Thermogravimetric analysis (TGA) was performed with a TA Instruments SDTQ600 apparatus (Mettler Toledo, Inc., Switzerland) in an oxidizing atmosphere (air, 80 mL minutes^{-1}). The loss of weight was registered within a dynamic step with a heating program consisting of a heating rate of 10 °C/minute from 25 °C to 100 °C, an isothermal heating step at 100 °C for 60 minutes, a heating rate of 10 °C/minute 100 °C to 1000 °C, and an isothermal heating step at this final temperature for 30 minutes. Fourier transform infrared spectroscopy (FTIR) measurements were performed in a Tensor 27 instrument (Bruker, Germany). Dynamic light scattering (DLS), and ζ potential evaluations were carried out using a Zetasizer Nano ZS (Malvern Panalytical, UK). UV−visible measurements were performed with a JASCO V-650 spectrophotometer (Jasco, USA). Fluorescence measurements were carried out in a JASCO FP-8500 spectrophotometer.

3.6. Control release studies

For *in vitro* cargo-controlled release studies, 2 mg of NP-CTR-DOX and NP-FAP-DOX were suspended in 1 mL of 10 mM PBS pH 7.5 and separated into two fractions. Then, 1 mL of PBS or GSH (final concentration of 10 mM) was added, and the suspensions were incubated for 3 hours on a shaker (PCMT Thermo-shaker HC24N, Grant Instruments, UK) at 37 ºC. At successive times (5, 15, 30, 60, 180, 210 minutes), the mixtures were centrifugated (5 minutes, 12,500 rpm) to remove solids and the fluorescence emission of DOX released to the medium was measured (λ_{exc} = 470 nm, λ_{em} = 555 nm).

To determine the total amount of DOX contained in the NPs, forced release assays were performed. For that purpose, 1 mg of the corresponding NPs was suspended in 1 mL of dimethyl sulfoxide (DMSO) and stirred for 24 hours in the dark. The suspensions were then centrifuged, and the absorbance of the supernatant was measured (λ_{abs} = 495 nm) in a JASCO FP-8300 spectrophotometer. DOX concentration was calculated by Lambert-Beer's law ($A = \varepsilon \cdot c \cdot l$). Where A is absorbance, c is the molar concentration (M), l is the optical length path (cm) and ε is the molar absorption coefficient of DOX (9250 $M^{-1}cm^{-1}$).

3.7. Hemolysis assay

Blood from BALB/C mice was collected in EDTA tubes and red blood cells were isolated after centrifuging at 500 xg for 5 minutes. The cells were washed three times with PBS and diluted in the same buffer (1:50). Then, 180 µL of the red blood cells suspension were incubated at 37 °C with 20 µL of NPs (NP-CTR, NP-FAP, NP-CTR-DOX, and NP-FAP-DOX) at different concentrations (final concentrations of 10, 25, 50, 100, 250, 500, 750, and 1000 µg/mL). PBS and 1% Triton X-100 in PBS were used as negative and positive controls, respectively. After 1 hour, the samples were centrifuged at 500 xg for 5 minutes, and the hemoglobin release was determined by measuring the supernatant absorbance at 540 nm in a microplate reader Spectra Max Plus (Thermo Fisher Scientific). The percentage of hemolysis was calculated as [(sample absorbance − negative control) / (positive control − negative control) × 100].

3.8. Cellular uptake and targeting efficacy

3.8.1. 2D culture models

The MCF-10A and MDA-MB-436 cell lines (40,000 cells/well), and the CAFs (15,000 cells/well) were seeded in an 8-well chambered coverslip (Ibidi GmbH, Germany) and incubated at 37 °C. On the following day, the cells were incubated for 15 minutes or 3 hours with 25 µg/mL of NP-CTR-DOX and NP-FAP-DOX. Then, cells were washed with PBS (Gibco) and fixed with a solution of 4% paraformaldehyde (VWR BDH Chemicals), for 10 minutes. Nuclei were stained with 4',6-diamidino-2-phenylindole (DAPI, 5 µg/ml, Merck, Germany). The DOX and DAPI fluorescence were analyzed by fluorescence microscopy using the Leica DMi8 inverted fluorescence microscope (Leica Microsystems) with a PE4000 LED light source and DFC9000GT camera at 40X magnification at the UCIM-UV. 5 pictures per well were taken with an excitation of 365 nm and 550 nm, and an emission of 435-485 nm and 590 nm for DAPI and DOX, respectively. The DOX mean fluorescence intensity per cell was quantified using Image J Software (version 1.51h, NIH). For each condition, a minimum of 200 cells were analyzed, and the fluorescence intensity of NP-FAP-DOX was normalized for NP-CTR-DOX.

3.8.2. 3D culture models

The BC PDOs were used as 3D models. For that, the matrigel dome containing organoids was desegregated using cold PBS, and the organoids were centrifuged at 300 xg for 5 minutes at room temperature. The organoids were resuspended in PDOs' culture media and counted using 2 µL of the sample in a Neubauer's chamber without a cover slide. 3,000 aggregates were seeded in a dome of 30 µL of 75% Matrigel Growth Factor Reduced Basement (Corning) in an 8-well chambered coverslip

(Ibidi GmbH). After incubating for 15 minutes at 37 °C, 300 µL of PDOs' culture media were added. After 72 hours, the organoids were incubated with 25 µg/mL of NP-CTR-DOX and NP-FAP-DOX for 24 hours. Then, nuclei were stained with Hoechst 33342 (Invitrogen) for 4 hours. The NP penetration was analyzed by confocal microscopy using the Leica TCS SP8 X White Light Laser Confocal Microscope (Leica Microsystems) with an HC PL APO CS2 20x/0.75 IMM objective at the UCIM-UV. 5 pictures per well were taken in sequential order with an excitation of 405 nm and 546 nm, and an emission of 380-547 nm and 584-637 nm for Hoechst and DOX, respectively. The DOX mean fluorescence intensity per organoid was quantified using Image J Software (version 1.51h, NIH). For each condition, a minimum of 30 organoids were analyzed, and the fluorescence intensity of NP-FAP-DOX was normalized to NP-CTR-DOX.

3.9. Cellular cytotoxicity

3.9.1. 2D culture models

The MDA-MB-436 cells (8,000 cells/well) and the CAFs (3,000 cells/well) were plated into 96-well plates and incubated overnight. On the following day, the cells were treated with NP-CTR, NP-CTR-DOX, NP-FAP, or NP-FAP-DOX at different concentrations (0, 1, 5, 10, 25, and 50 µg/mL). After 72 hours, cell viability was evaluated by Colorimetric Cell Viability Kit II (WST-1) (Deltaclon, Spain) according to the manufacturer's instructions. Briefly, the cells were incubated for 2 hours at 37 °C with 100 µL of 7% WST-1 reagent in phenol red-free media. Spectrophotometric analysis was measured at 450 nm (reference wavelength: 650 nm) in a microplate reader Spectra Max Plus (Thermo Fisher Scientific).

3.9.2. 3D culture models

The BC PDOs were seeded in 96-well plates as single cells. For that, the matrigel dome containing grown organoids was desegregated using cold PBS, and the organoids were centrifuged at 300 xg for 5 minutes at room temperature. To obtain single cells, the pellet was incubated with 2 mL of TrypLE™ Express Enzyme 1X (Gibco) supplemented with 2 µL of Y-27632 for 15 minutes at 37 °C. The cells were resuspended in PDOs' culture media, centrifuged at 300 xg for 5 minutes, and counted in a Neubauer chamber. 10,000 cells/well were seeded in 50% matrigel, and the plate was incubated for 15 minutes at 37 °C. After that, 100 µL of PDOs' culture media were added and the organoids were allowed to form. When the organoids were formed, the PDOs were treated with NP-CTR, NP-CTR-DOX, NP-FAP, or NP-FAP-DOX at different concentrations (0, 1, 5, 10, 25, and 50 µg/mL), and the 0 hours control plate without treatment was measured by using CellTiter-Glo® 3D Cell Viability Assay (Promega, USA), according to the manufacturer's instructions. Briefly, the CellTiter-Glo® 3D Cell Viability Assay was added to each well in a 1:4 ratio and incubated for 25 minutes in the dark at room temperature. For luminescence reading, the content of the wells was transferred to a black 96-well plate and measured in the luminometer Promega™ GloMax® Plate Reader (Promega). After 72 hours of treatment, the organoids' viability was determined by luminescence following the same protocol. The luminescence values obtained for 72 hours were normalized for the 0-hour time point.

3.10. *In vivo* studies

3.10.1. *In vivo* model

The *in vivo* experiments were performed in 6- to 8-week-old BALB/C female mice purchased from Charles River Laboratories and maintained at the animal facilities of UCIM-UV. All experiments were approved by the Institutional Review Board of INCLIVA (2023/VSC/PEA/0287).

To generate the *in vivo* tumor model, 250,000 4T1 cells were injected into the mammary fat pad of BALB/C mice and the tumors were allowed to grow. Once tumors were palpable, mice were randomly divided into 5 groups of 12 animals and treated separately with PBS or 50 mg/kg of NPs (NP-CTR, NP-FAP, NP-CTR-DOX, and NP-FAP-DOX) four times per week for fifteen days. Additionally, another group of 12 animals was treated with 3.75 mg/kg of free DOX for eight days. All treatments were administered intravenously (via tail) and prepared in free-serum DMEM-F12 media every day before administration. The NPs suspension was slightly sonicated for 30 minutes to avoid NPs aggregates. Tumors were measured four times per week and tumor volume was calculated using the formula $(Dxd^2)/2$, based on the longest (D) and the shortest (d) tumor diameters. Body weight was registered four times per week, and mice were observed continuously for normal health conditions and behavior. Three days after the last treatment, or when the institutional euthanasia criteria for tumor size or overall health condition were reached, the mice were sacrificed.

After mice sacrifice, tumors were dissected for flow cytometry and histological and molecular analyses. Hearts were dissected for histological and molecular analysis. The liver, spleen, and kidneys were also collected for morphological and histological analysis. For histological analysis, the tissues were fixed in 4% paraformaldehyde and embedded

in paraffin. H&E staining was performed in 4 µm thick sections of FFPE tissue samples of the heart to evaluate cardiotoxicity. Representative photographs were taken in Leica DM 2500 LED microscope (Leica Microsystems) with a digital camera MC170 HD at 4x and 20X magnification at the UCIM-UV.

3.10.2. Doxorubicin penetration

FFPE tumor 4 µm thickness sections were deparaffinized and rehydrated. Then, the samples were incubated for 15 minutes at room temperature with Triton X-100 0.25% in PBS for cell permeabilization. Nuclear staining was performed by incubating with DAPI (5 µg/ml, Merck) for 10 minutes at room temperature. Following, the slides were mounted using 50% glycerol in PBS. DOX intensity was analyzed by confocal microscopy using the Leica TCS SP8 X White Light Laser Confocal Microscope (Leica Microsystems) with an HC PL APO CS2 20x/0.75 IMM objective at the UCIM-UV. Pictures were taken in sequential order with an excitation of 405 nm and 546 nm, and an emission of 410-500 nm and 584-637 nm for DAPI and DOX, respectively.

3.10.3. Masson’s trichrome staining

Masson’s trichrome staining was performed to evaluate the extracellular matrix content by selective staining the collagen fibers, muscle, and connective tissue. For that, 4 µm thick sections of FFPE tumor samples were used. Automated staining was performed using the Dako Artisan Link Pro (Dako, Denmark) with Masson's Trichrome Stain Kit (AR173, Dako). Representative photographs were taken in Leica DM 2500 LED microscope (Leica Microsystems) with a digital camera MC170 HD at 20X magnification at the UCIM-UV.

3.10.4. Immunofluorescence

FFPE tumor sections of 4 μm thickness were pretreated in the DAKO PT Link Pretreatment module (#PT100/PT101, Dako) and antigen retrieval was performed with Dako High Retrieval Solution (EDTA buffer) for 30 minutes. Then, the samples were incubated for 15 minutes at room temperature with Triton X-100 0.25% in PBS for cell permeabilization. After that, the samples were blocked with 5% BSA in PBS for 1 hour at room temperature, and incubated with α-SMA-Alexa Fluor® 488 antibody (ab184675, dilution 1:100, Abcam) or cleaved caspase-3 (#9661, dilution 1:200, Cell Signaling) diluted in 2.5% BSA in 1x PBS, overnight at 4 °C. On the following day, the samples stained with cleaved caspase-3 were incubated with anti-rabbit-Alexa Fluor® 488 secondary antibody (#A11034, dilution 1:500, Invitrogen) for 1 hour at room temperature. Finally, the samples were stained with DAPI (5 μg/ml, Merck) for 10 minutes at room temperature, and the slides were mounted using 50% glycerol in PBS. Immunofluorescence staining was analyzed by confocal microscopy using the Leica TCS SP8 X White Light Laser Confocal Microscope (Leica Microsystems) with an HC PL APO CS2 20x/0.75 IMM objective at the UCIM-UV. Pictures were taken in sequential order with an excitation of 405 nm and an emission of 410-500 nm for DAPI, or with an excitation of 448 nm and an emission of 505-544 nm for α-SMA or cleaved caspase-3.

3.10.5. Flow cytometry

For flow cytometry analysis, tumor samples were disaggregated using scalpels and digested with a digestion solution (0.015 g collagenase and 0.001 g hyaluronidase in 10 mL PBS) for 45 minutes at 37 °C in agitation. To help digestion, the tissue was dissociated with a mechanic pistol and RNase-free DNase I (Qiagen, Germany) was added. After 10 more

minutes of incubation, the digestion was stopped by adding 10% FBS in PBS, and the samples were centrifuged at 800 rpm for 6 minutes at 4 °C. Then, red blood cells were eliminated by using ACK lysis buffer (Gibco). After 3 minutes of incubation, 10% FBS in PBS was added, and the mixture was filtered through 100 µm strainers. Then, the samples were centrifuged at 800 rpm for 4 minutes at 4 °C, and the pellet was resuspended in PBS for further staining.

First, the samples were stained with Zombie Aqua™ (BioLegend) diluted 1:4 in DMSO for 30 minutes in the dark at room temperature. The samples were washed with PBS and centrifuged at 2,000 rpm for 5 minutes. For surface staining, the cells were resuspended in FACS buffer, and incubated with the surface antibodies (**Table 7**) for 30 minutes in the dark at 4 °C. After incubation, the samples were fixed with 4% paraformaldehyde for 10 minutes at room temperature, washed with PBS and centrifuged at 2,000 rpm for 5 minutes. Then, the samples were resuspended in FACS buffer and stored at 4 °C in the dark until analysis.

Table 7. Antibody panel for characterization of immune cells in tumor microenvironment by flow cytometry.

Flow cytometry panel	
Anti-CD326 (EpCAM), VioBlue®	130-117-759, Miltenyi Biotec
Anti-CD31, BV421	562939, BD Biosciences
Anti-CD45, FITC	130-110-658, Miltenyi Biotec
Anti-CD3ε, APC-Vio® 770	130-117-676, Miltenyi Biotec
Anti-CD8a, PE-Vio® 770	130-118-946, Miltenyi Biotec
Anti-CD4, PE-Vio® 615	130-118-316, Miltenyi Biotec
Anti-NK1.1, APC	130-120-507, Miltenyi Biotec
Anti-F4/80, PE	130-116-499, Miltenyi Biotec
Anti-CD86, Vio® Bright R720	130-128-565, Miltenyi Biotec
Anti-CD206, BUV395	568817, BD Biosciences

Flow cytometry analysis was performed on the LSR FORTESSA X-20 analyzer (BD Biosciences), and data analysis was performed using FlowJo version 9.8.1 (LLC).

3.11. Statistical analysis

Statistical analysis was performed using the GraphPad Prism 8.0.1 software (GraphPad Software Inc., La Jolla, USA). Shapiro-Wilks' test was used to confirm if the sample data fitted a normal distribution. Two-tailed t-Student test or non-parametric Mann-Whitney U test was used to compare between groups. The results were represented as mean ± standard deviation (SD) or mean ± standard error of the mean (SEM). All experiments were performed at least in biological and technical triplicates. P-values were considered statistically significant when inferior to 0.05. Significance is shown vs. the respective control and depicted as follows: *$p < 0.05$, **$p < 0.01$, ***$p < 0.001$, and ****$p < 0.0001$.

CHAPTER 4 |

RESULTS

4.1. Synthesis and characterization of nanoparticles targeting cancer-associated fibroblasts

A nanodevice based on mesoporous silica loaded with DOX to target CAFs was designed to improve BC treatment. CAFs are characterized by the high expression of FAP-α in their cellular membranes. FAP-α is a transmembrane protein commonly overexpressed in several tumors and is associated with tumor progression and metastasis [400]. Furthermore, recent studies also reported an increased FAP-α expression in tumor cells and TAM [406, 407]. Taking this into account, FAP-α was chosen as a therapeutic target.

After careful literature revision, a described FAP-α ligand peptide with a high affinity for FAP-α was selected to be anchored on the NPs' surface [403]. NPs were synthesized using mesoporous silica as support. First, the surface of MSNs was modified with (3-mercaptopropyl)trimethoxysilane, which was reacted with 2,2-dipyridyl disulfide. DOX was then loaded onto the mesoporous network and the pore was blocked by adding SH-PEG_{12}-COOH, which allowed the construction of a redox-sensitive molecular gate (S-S-PEG-COOH). Finally, the FAP-α peptide was attached to the acid group of PEG ligand, through an amide bond, obtaining NP-FAP-DOX (**Figure 16**). In addition, NPs coated with a control peptide with a similar sequence of the FAP-α ligand peptide but lacking FAP-α specificity were also synthesized (NP-CTR-DOX) [403]. Additionally, the same materials without the presence of DOX were used as controls (NP-FAP and NP-CTR).

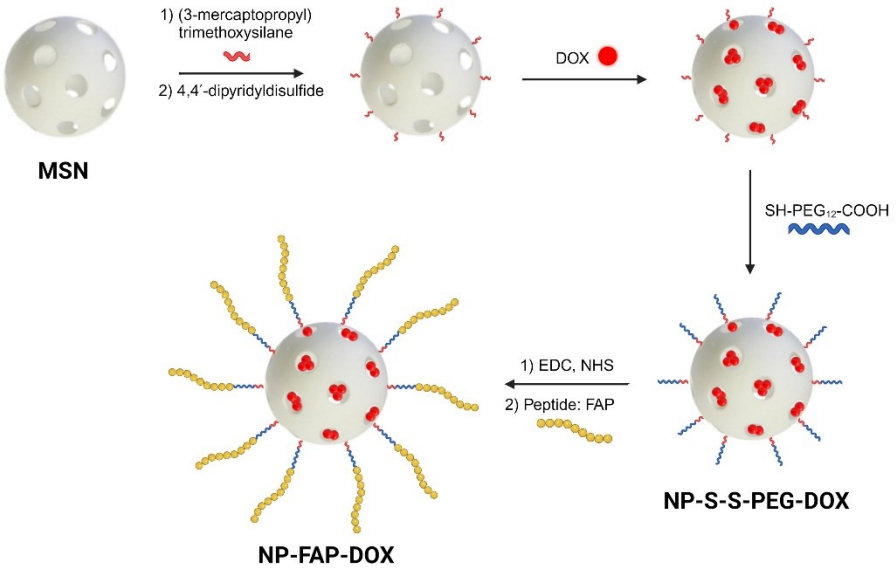

Figure 16. Schematic synthesis of NP-FAP-DOX. The pores *of* MSN were loaded with DOX and their surfaces were coated *with* a redox-sensitive molecular gate formed by a disulfide bond attached to PEG and a peptide selective for FAP-α. Abbreviations: DOX – doxorubicin, EDC – *N*-Ethyl-*N*′-(3-dimethylaminopropyl)carbodiimide hydrochloride, MSN – mesoporous silica nanoparticle, NHS – *N*-Hydroxysuccinimide, NP – nanoparticles, PEG – polyethylene glycol.

After the synthesis of the NPs, the structure and functionalization were studied by standard characterization methods. The NPs' mesoporous structure, morphology, and size were assessed by TEM. The MSN scaffold showed an ordered mesoporous structure and a spherical morphology with a diameter of 102 ± 22 nm (**Figure 17A-B**). The synthesized NP-FAP was also monitored by STEM-EDX, showing the presence of Si (green) and O (red) atoms, which confirmed the composition of the MSN scaffold. In addition, S atoms (green), assigned to the redox-sensitive molecular gate (S-S ligand), and N atoms (purple),

attributed to the FAP-α peptide, were mapped (**Figure 17C**). This demonstrates the correct functionalization of the NPs.

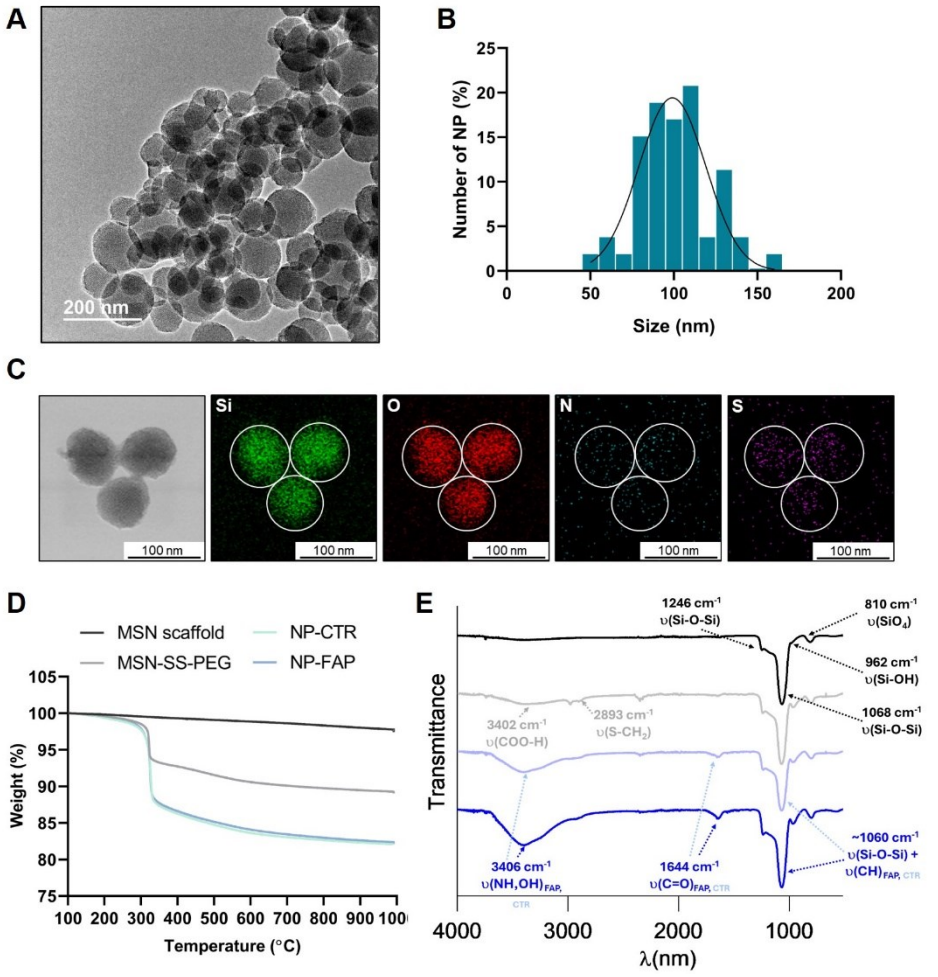

Figure 17. Mesoporous silica nanoparticles characterization. (A) Transmission electron microscopy images of MSNs scaffold. Scale bar: 200 nm. **(B)** Histogram representing the size (diameter) distribution of MSNs determined by quantifying the dimensions of 50 NPs by transmission electron microscopy. **(C)** Electronic energy-dispersive X-ray spectroscopy atomic mapping of Si (green), O (red), N (blue), and S (purple) atoms in NP-FAP. Wt% composition was calculated in 52.8% of O_2, 46.7% of Si, and 0.6% of S. **(D)** Fourier transform

infrared spectroscopy spectrum and **(E)** thermogravimetric analysis of MSN scaffold (black), MSN-SS-PEG (grey), NP-CTR (light blue), and NP-FAP (dark blue). Abbreviations: MSNs – mesoporous silica nanoparticles, NP – nanoparticles, PEG – polyethylene glycol.

Moreover, the correct functionalization of NP-FAP and NP-CTR was further confirmed by FTIR (**Figure 17D).** All the nanomaterials showed the typical bands attributed to stretching vibrations of Si-O-Si bonds at 1068 and 1246 cm^{-1} (shoulder), Si-OH groups at 962 cm^{-1}, and SiO_4 tetrahedrons at 810 cm^{-1} [408]. Both NP-FAP and NP-CTR spectra stated the amide I absorption band at 1644 cm^{-1} and stretching vibrations of OH and NH groups at 3400 cm^{-1}, corresponding to FAP-α and CTR peptides. Additionally, the organic content was confirmed by the TGA (**Figure 17E, Table 8)**. The thermal decomposition of the organic content in the different steps of synthesis allowed the quantification of the -S-S-PEG-COOH ligand in 15 µg, as well as FAP-α and CTR peptides, calculated in 68.7 and 71.5 µg respectively, per mg of NPs.

Table 8. Percentage in weight of organic content, SS-PEG, and peptide in nanoparticles obtained by thermogravimetry analysis.

Nanoparticle	Total organic content (µg mg^{-1} solid)	SS-PEG-COOH (µg mg^{-1} solid)	Peptide (µg mg^{-1} solid)
MSN scaffold	262	--	--
MSN-SS-PEG	109.6	83.4	--
NP-CTR	181.1	154.9	71.5
NP-FAP	178.3	152.1	68.7

MSN – mesoporous silica nanoparticle, NP – nanoparticle, PEG – polyethylene glycol

Finally, the NPs were also studied by DLS. The hydrodynamic diameter increased from 180 ± 2 nm for the MSNs to 276 ± 3 nm (NP-CTR) and 268 ± 3 nm (NP-FAP), after the functionalization with SH-PEG-COOH and the corresponding peptides (**Table 9**). A similar size was found for the DOX-loaded NPs (NP-CTR-DOX and NP-FAP-DOX). Moreover, the ζ potential showed the typical negative surface charge in mesoporous silica due to the presence of silanol groups (-34.9 mV), which slightly decreased after the functionalization with the -S-S-PEG-COOH (-39.7 mV). In DOX loading process the charge augmented (-18.9 mV) due to DOX positive charge. However, the ζ-potential value decreased again in the final nanoparticles NP-FAP-DOX and NP-CTR-DOX (-32.8 and -30.6 mV) due to the attachment of peptides (**Table 10**). Similar values were also obtained for the unloading NPs (**Table 10**).

Table 9. Nanoparticles' hydrodynamic size distribution obtained by dynamic light scattering measurements and polydispersity index.

Nanoparticle	Size (nm) ± SD	PDI I ± SD
MSN scaffold	180 ± 2	0.242 ± 0.008
NP-CTR	276 ± 3	0.315 ± 0.026
NP-FAP	268 ± 3	0.400 ± 0.014
NP-CTR-DOX	246 ± 1	0.316 ± 0.010
NP-FAP-DOX	247 ± 9	0.369 ± 0.024

DOX – doxorubicin, MSN – mesoporous silica nanoparticle, NP – nanoparticle, PDI – poly dispersion index, SD – standard deviation of 3 measurements

Table 10. Nanoparticles' ζ potential.

Nanoparticle	ζ potential (mV) ± SD
MSN scaffold	-34.9 ± 0.404
MSN-SS-PEG	-39.7 ± 0.808
MSN-SS-PEG-DOX	-18.9 ± 1.970
NP-CTR	-34.1 ± 0.709
NP-FAP	-37.3 ± 0.513
NP-CTR-DOX	-30.6 ± 0.586
NP-FAP-DOX	-32.8 ± 0.794

DOX – doxorubicin, MSN – mesoporous silica nanoparticle, NP – nanoparticle, PEG – polyethylene glycol, SD – standard deviation of 3 measurements

Once the NPs characterization was demonstrated, their capacity to deliver drugs in a controlled manner was evaluated. The NPs were designed to deliver DOX only in the presence of GSH, which is known to reduce the dithiol bonds of the gatekeeper, resulting in the delivery of the cargo. GSH is known to be intracellularly at high concentrations (10 mM in cancer cells) (**Figure 18**) [409].

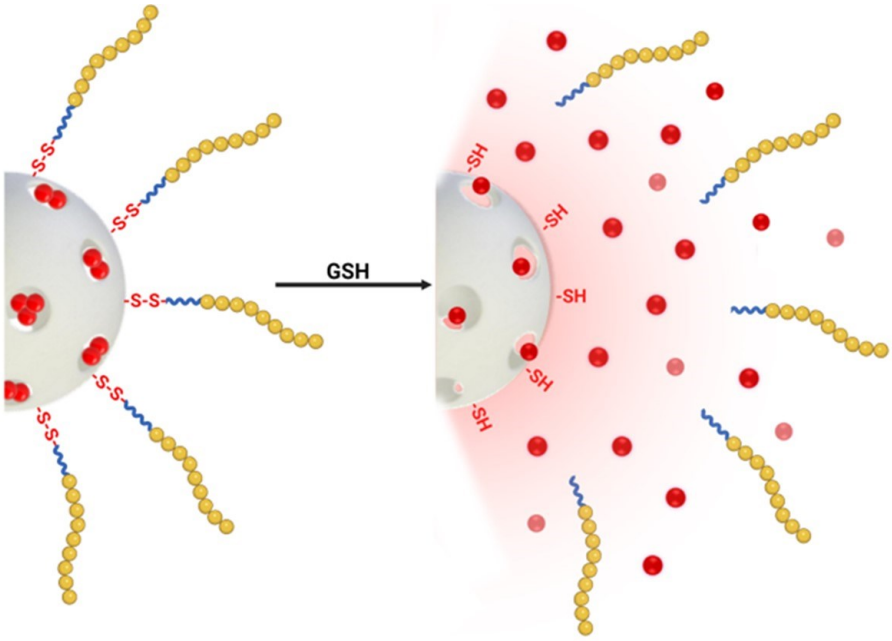

Figure 18. Schematic illustration of glutathione-mediated DOX release of NP-FAP-DOX. The NP-FAP-DOX actively targets FAP-α positive cells, and the molecular gate opens in the presence of glutathione (GSH) when the nanoparticles are internalized ensuring controlled cargo release.

To confirm the capacity of NPs to deliver their content in a controlled manner, *in vitro* cargo release studies were performed using GSH or PBS. NP-FAP-DOX and NP-CTR-DOX showed controlled DOX delivery only in the presence of GSH, confirming the molecular gate opening mechanism. In contrast, in PBS condition, both NPs remained capped, and the delivery of DOX was negligible (less than 10% of the total DOX released after 210 minutes) (**Figure 19**). This result confirms that the content of the NPs will remain inside the pores until they are internalized by cells avoiding unspecific DOX delivery.

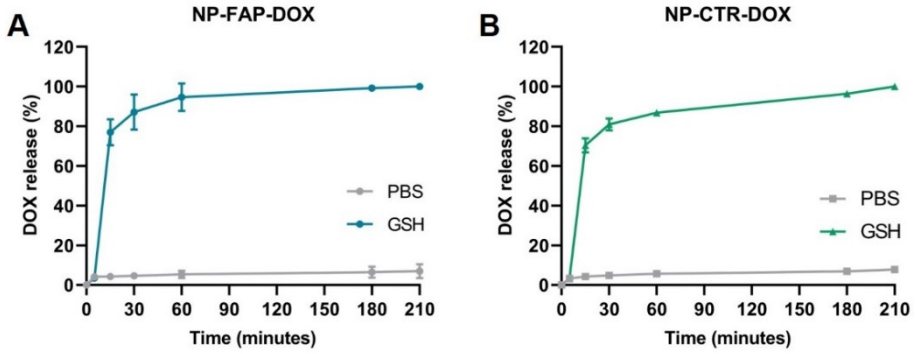

Figure 19. Mesoporous silica nanoparticles' doxorubicin release. Cargo release study of the **(A)** NP-FAP-DOX and **(B)** NP-CTR-DOX. Doxorubicin (DOX) release in PBS or glutamine (GSH) after incubation at 37 °C for 210 minutes. The DOX fluorescence emission band was measured at the indicated time points at 557 nm (λ_{exc} = 480 nm) in a JASCO FP-8300 spectrophotometer, to determine cargo release. Mean ± SD.

In addition, the total DOX content in NP-FAP-DOX and NP-CTR-DOX was calculated, resulting in 82.7 ± 2.5 µg and 81.6 ± 2.2 µg (mean ± SD) *per* mg of solid, respectively.

Besides, the biocompatibility of the NPs was evaluated by hemolysis experiments. The interactions between the NPs and the red blood cells did not induce hemoglobin release even at the higher concentrations (**Figure 20** and **Figure S1**), demonstrating the nontoxic profile of the NPs.

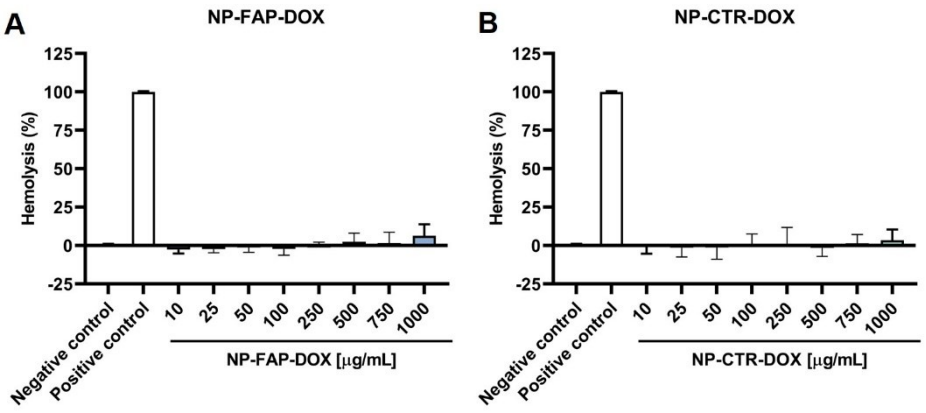

Figure 20. Mesoporous silica nanoparticles biocompatibility. Hemolytic activity of the **(A)** NP-FAP-DOX and **(B)** NP-CTR-DOX. Red blood cells were incubated with PBS (negative control), 1% Triton X-100 (positive control), or NPs at different concentrations for 1 hour at 37 °C. Mean ± SD.

4.2. FAP-α expression in breast cancer cells, cancer-associated fibroblasts, and patient-derived organoids

Considering the NPs' design to target FAP-α, the expression levels of this marker were first evaluated in BC cell lines, CAFs-enriched primary cultures, and PDOs from triple-negative BC patients.

On the one hand, the FAP-α basal expression levels were evaluated in three triple-negative BC cell lines (MDA-MB-231, MDA-MB-436, and MDA-MB-468), as well as in one non-tumorigenic breast cell line (MCF-10A), by RT-qPCR and Western blot. The results showed that the MCF-10A cell line did not express FAP-α at mRNA or protein levels. In contrast, MDA-MB-436 was the cell line with higher FAP-α levels in both mRNA and protein (**Figure 21**). Taking this into account, the MCF-10A and MDA-MB-436 cell lines were selected as negative and positive controls for NPs' targeting studies, respectively.

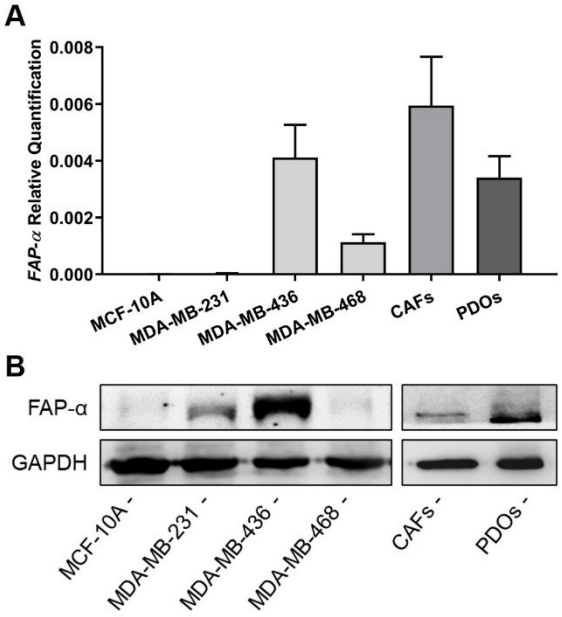

Figure 21. FAP-α expression. Characterization of FAP-α mRNA and protein expression in one normal breast cell line (MCF-10A), three triple-negative breast cancer cell lines (MDA-MB-231, MDA-MB-436, and MDA-MB-468), cancer-associated fibroblast cells (CAFs) derived from triple-negative breast cancer biopsies, and triple-negative breast cancer patient-derived organoids (PDOs) by RT-qPCR and Western blot, respectively. Mean ± SD.

On the other hand, CAFs-enriched primary cultures and PDOs were established from triple-negative BC patients' biopsies, and FAP-α basal expression levels were also evaluated in these models. First, the CAFs-enriched primary cultures were characterized by flow cytometry. The results showed that approximately 98% of the cells were $CD45^-$, $CD31^-$, $EpCAM^-$, and $CD90^+$, confirming a CAF phenotype (**Figure 22**). Besides, the PDOs were characterized by immunohistochemistry to verify if the organoids maintained the patient's features. The results confirmed that the organoids remain negative for the hormonal receptors (ER and PR)

and HER2 and presented a Ki67 of approximately 90% (**Figure 23**, immunohistochemistry positive controls in **Figure S2**). Moreover, both CAFs and PDOs showed a high FAP-α expression (**Figure 21**), representing good models to evaluate the targeting efficacy of the NPs.

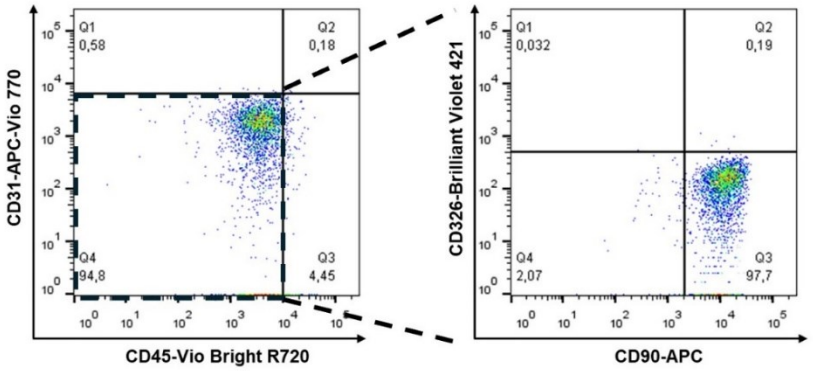

Figure 22. Cancer-associated fibroblasts characterization. Representative gating of cancer-associated fibroblasts-enriched primary cultures: $CD45^-$ and $CD31^-$, and $EpCAM^-$ and $CD90^+$.

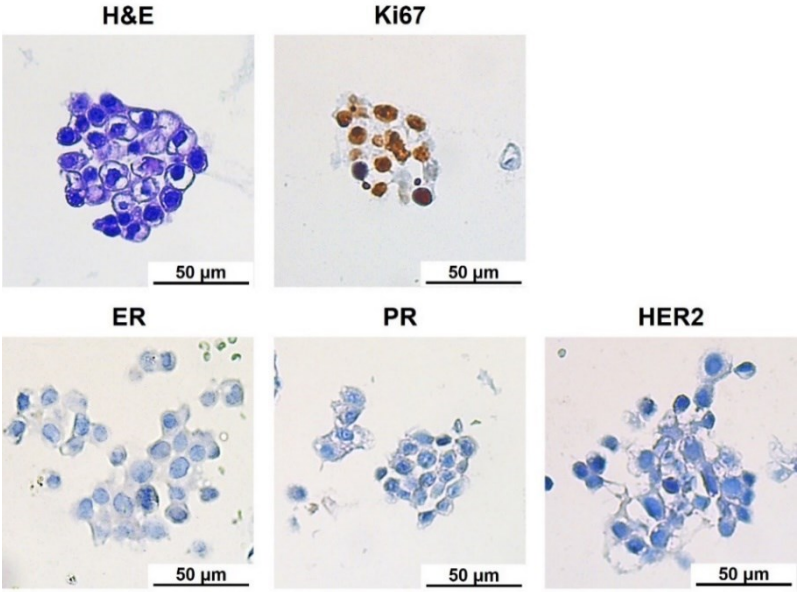

Figure 23. Patient-derived organoids characterization. Representative images of hematoxylin and eosin (H&E) staining, and immunocytochemistry staining of Ki67, estrogen receptor (ER), progesterone receptor (PR), and human epidermal growth factor receptor 2 (HER2) of triple-negative breast cancer patient-derived organoids. Scale bar: 50 µm.

4.3. Nanoparticles' targeting efficacy in breast cancer cells, cancer-associated fibroblasts, and patient-derived organoids

The FAP-α targeting capacity of the designed NPs was assessed in BC cells with positive FAP-α expression (MDA-MB-436 cell line) and in CAFs and PDOs from triple-negative BC patients' biopsies by fluorescence microscopy.

First, the cellular uptake of the NP-FAP-DOX was compared between the positive and negative FAP-α cell lines (MDA-MB-436 and MCF-10A, respectively). After incubation with NP-FAP-DOX for 15 minutes or 3

hours, the FAP-α positive cells (MDA-MB-436) showed effective internalization of the NPs, whereas the uptake by MCF-10A cells was significantly lower (approximately 47% and 67% compared with MDA-MB-436, respectively) (**Figure 24**).

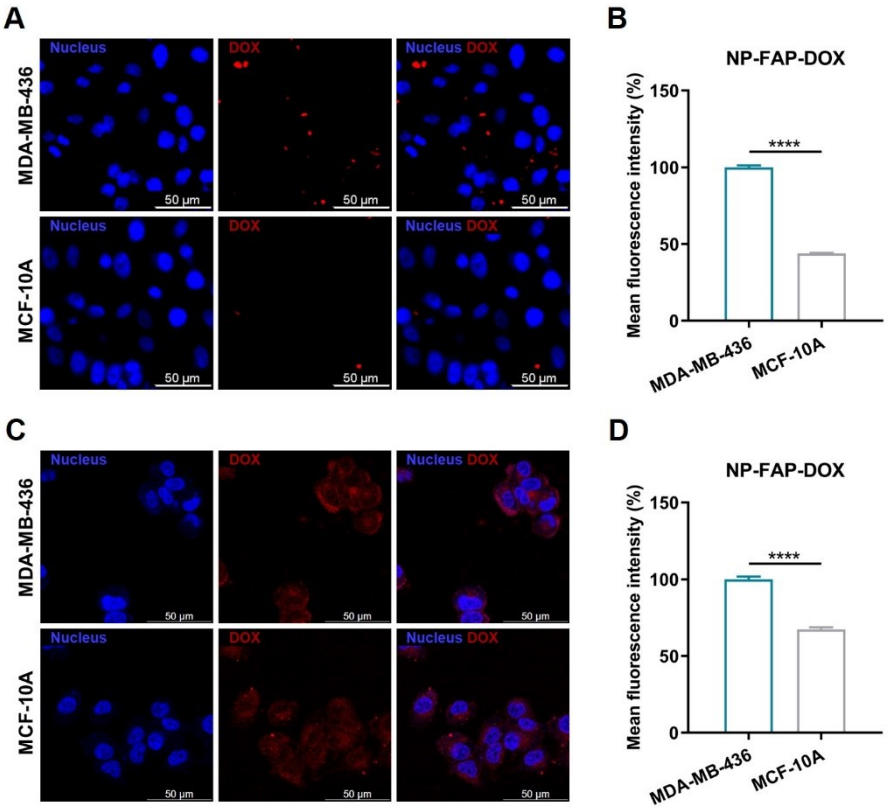

Figure 24. NP-FAP-DOX nanoparticles targeting efficacy. Fluorescence microscopy images of internalized doxorubicin (DOX) in MDA-MB-436 and MCF-10A cell lines treated with 25 µg/mL of NP-FAP-DOX for **(A)** 15 minutes or **(C)** 3 hours. Blue: Nucleus, Red: DOX. Scale bar: 50 µm. **(B, D)** DOX fluorescence intensity quantification. The fluorescence intensity of MCF-10A was normalized for MDA-MB-436. Mean ± SEM, ****$p < 0.0001$.

Then, the targeting efficacy of the NP functionalized with FAP-α ligand peptide (NP-FAP-DOX) was also evaluated in comparison with the one functionalized with the control peptide (NP-CTR-DOX) in the MCF-10A and MDA-MB-436 cell lines. In the FAP-α negative cells (MCF-10A) no differences were observed between the two NPs (**Figure 25**). In contrast, in FAP-α positive cells (MDA-MB-436) a statistically significant stronger DOX intensity was observed in NP-FAP-DOX condition compared to NP-CTR-DOX after 15 minutes and 3 hours of incubation (approximately 142% and 172% compared with control, respectively) (**Figure 26**). Thus, it has been verified that the NPs with a FAP-α ligand peptide efficiently target and are preferentially internalized by cells with FAP-α positive expression.

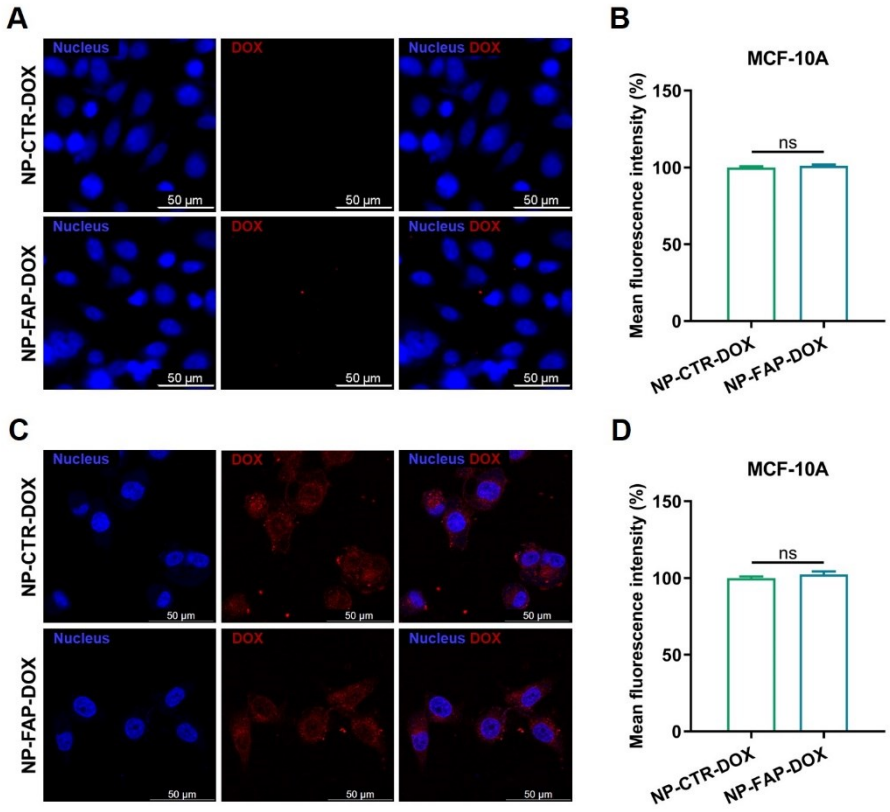

Figure 25. Mesoporous silica nanoparticles targeting efficacy in non-tumorigenic breast cell line. Fluorescence microscopy images of internalized doxorubicin (DOX) in MCF-10A cells treated with 25 µg/mL of NP-CTR-DOX or NP-FAP-DOX for **(A)** 15 minutes or **(C)** 3 hours. Blue: Nucleus, Red: DOX. Scale bar: 50 µm. **(B, D)** DOX fluorescence intensity quantification. For each cell line, the fluorescence intensity of NP-FAP-DOX was normalized for NP-CTR-DOX. Mean ± SEM.

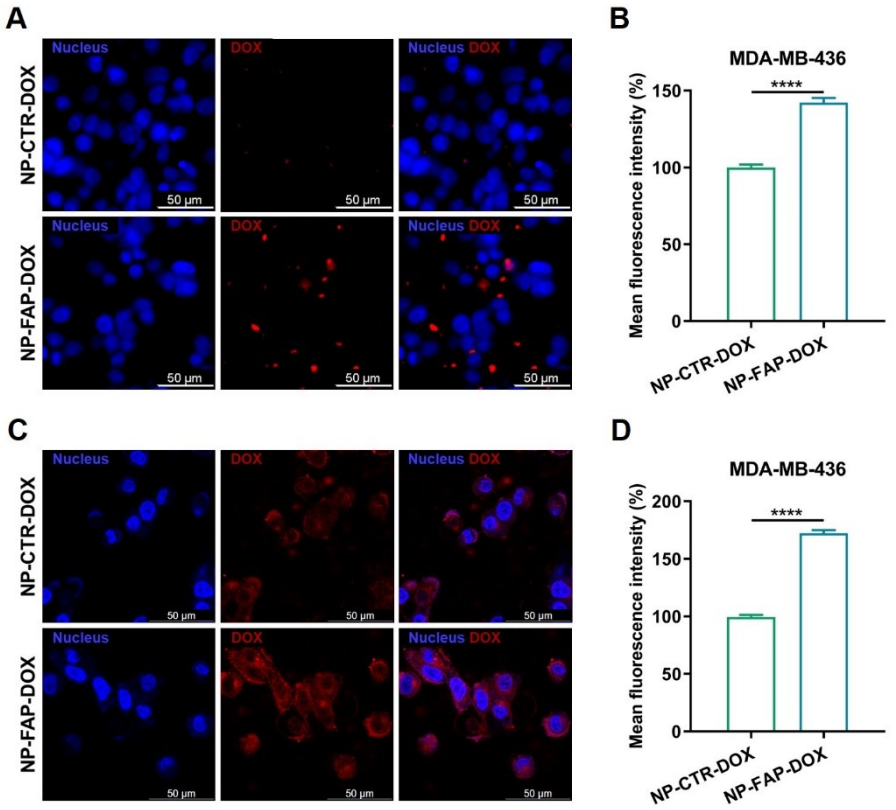

Figure 26. Mesoporous silica nanoparticles targeting efficacy in breast cancer cell line. Fluorescence microscopy images of internalized doxorubicin (DOX) in MDA-MB-436 cells treated with 25 µg/mL of NP-CTR-DOX or NP-FAP-DOX for **(A)** 15 minutes or **(C)** 3 hours. Blue: Nucleus, Red: DOX. Scale bar: 50 µm. **(B, D)** DOX fluorescence intensity quantification. For each cell line, the fluorescence intensity of NP-FAP-DOX was normalized for NP-CTR-DOX. Mean ± SEM, ****$p < 0.0001$.

Additionally, the NP-FAP-DOX's cellular uptake and targeting efficacy were also evaluated in CAFs. When incubated with NP-CTR-DOX and NP-FAP-DOX for 15 minutes or 3 hours, the CAFs presented a significantly higher internalization of the NPs containing the FAP-α ligand peptide compared to NP-CTR-DOX (approximately 133% and 182%

compared with control, respectively) (**Figure 27**). These results confirmed the capacity of NP-FAP-DOX to target CAFs.

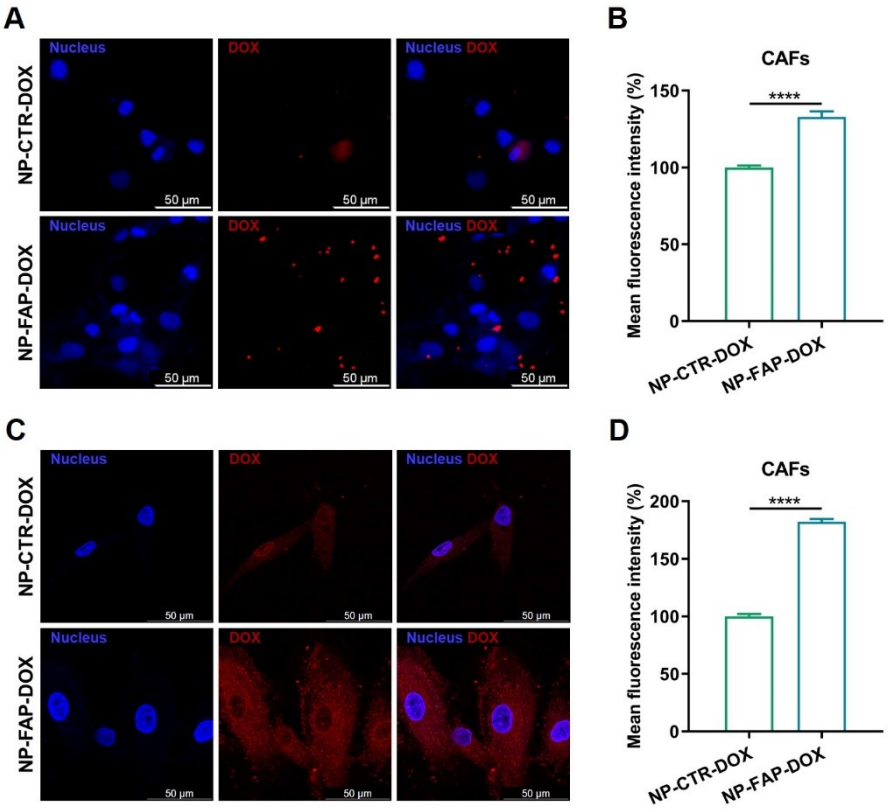

Figure 27. Mesoporous silica nanoparticles targeting efficacy in cancer-associated fibroblasts. Fluorescence microscopy images of internalized doxorubicin (DOX) in CAFs treated with 25 µg/mL of NP-CTR-DOX or NP-FAP-DOX **(A)** 15 minutes or **(C)** 3 hours. Blue: Nucleus, Red: DOX. Scale bar: 50 µm. **(B, D)** DOX fluorescence intensity quantification. The fluorescence intensity of NP-FAP-DOX was normalized for NP-CTR-DOX. Mean ± SEM, ****$p < 0.0001$.

Finally, PDOs were used to evaluate NPs' tumor penetration. The PDOs were incubated with NPs for 24 hours, and the DOX fluorescence

intensity was evaluated by confocal microscopy. The images showed that the DOX intensity inside the organoids was significantly higher when treated with NP-FAP-DOX (approximately 144% compared to NP-CTR-DOX) (**Figure 28**). Therefore, the NP-FAP-DOX not only demonstrated a good DOX delivery but also maintained the targeting effect in PDOs.

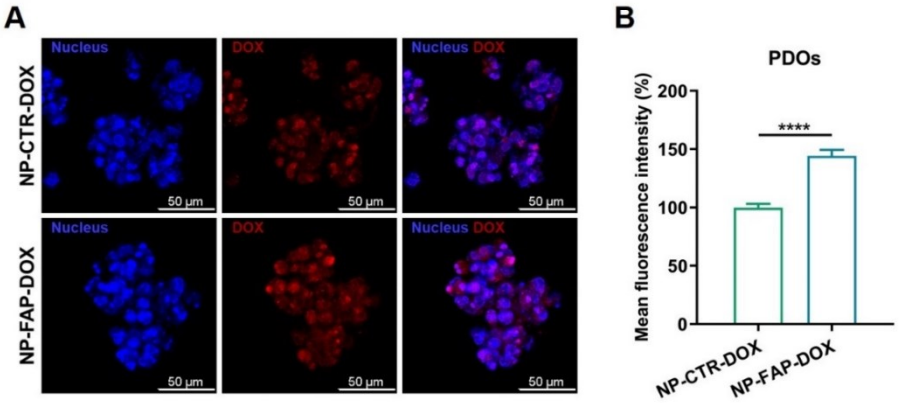

Figure 28. Mesoporous silica nanoparticles targeting efficacy and tumor penetration in patient-derived organoids. (A) Confocal microscopy images of internalized doxorubicin (DOX) in PDOs treated with 25 µg/mL of NP-CTR-DOX or NP-FAP-DOX for 24 hours. Blue: Nucleus, Red: DOX. Scale bar: 50 µm. **(B)** DOX fluorescence intensity quantification. The fluorescence intensity of NP-FAP-DOX was normalized for NP-CTR-DOX. Mean ± SEM, ****$p < 0.0001$.

4.4. Nanoparticles' cytotoxic efficacy in breast cancer cells, cancer-associated fibroblasts, and patient-derived organoids

NPs' cellular cytotoxicity was evaluated in the BC cell line MDA-MB-436 and CAFs using the Colorimetric Cell Viability Kit II (WST-1). In both cases, the unloaded NPs (NP-FAP and NP-CTR) showed only mild

toxicity at the highest concentration. By contrast, the NPs loaded with DOX (NP-FAP-DOX and NP-CTR-DOX) showed a good cytotoxic effect, where the highest concentration led to a decrease of around 85% in cell viability (**Figure 29** and **Figure S3A-B**).

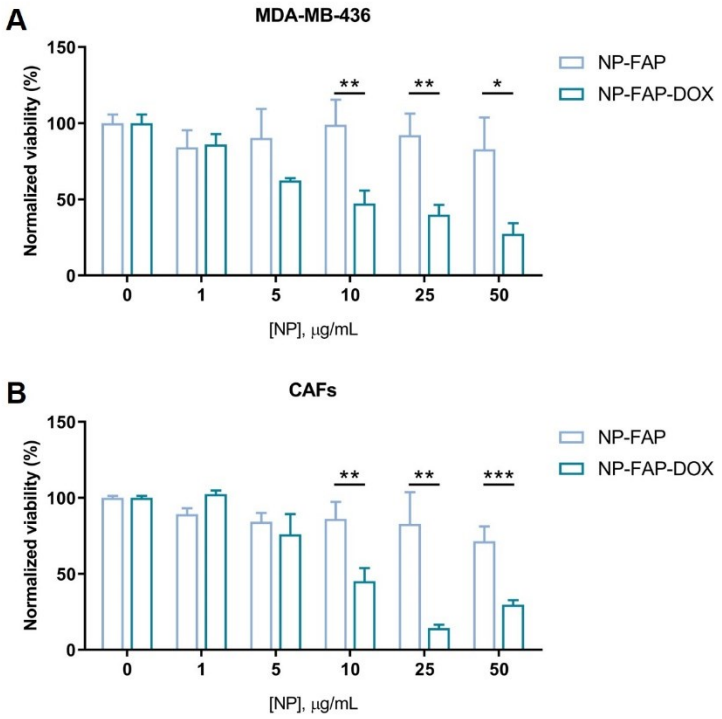

Figure 29. NP-FAP-DOX cytotoxic effect on breast cancer FAP-α positive cells and cancer-associated fibroblasts. Cellular cytotoxicity of NP-FAP and NP-FAP-DOX in **(A)** MDA-MB-436 cell line and **(B)** CAFs. Cells were treated with 0, 1, 5, 10, 25, and 50 µg/mL for 72 hours and viability was determined. Mean ± SD, *$p < 0.05$, **$p < 0.01$, ***$p < 0.001$.

Moreover, NPs' cellular cytotoxicity was also evaluated in 3D models by CellTiter-Glo® 3D Cell Viability Assay. In PDOs, the NPs loaded with DOX (NP-FAP-DOX and NP-CTR-DOX) also decreased cell viability up

to approximately 80%, whereas the unloaded NPs (NP-FAP and NP-CTR) remained nontoxic at the highest concentration (**Figure 30** and **Figure S3C**).

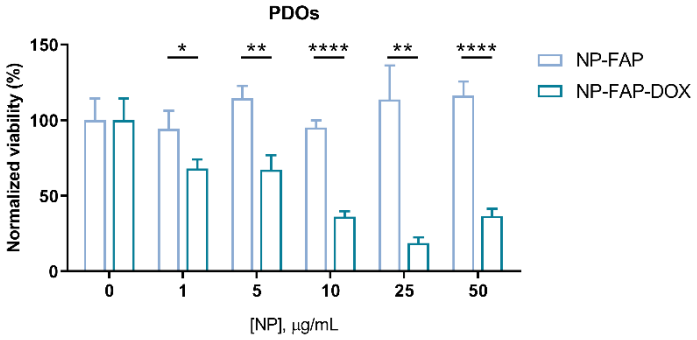

Figure 30. NP-FAP-DOX cytotoxic effect on patient-derived organoids. Cellular cytotoxicity of NP-FAP and NP-FAP-DOX in PDOs. Cells were treated with 0, 1, 5, 10, 25, and 50 µg/mL for 72 hours and viability was determined. Mean ± SD, *$p < 0.05$, **$p < 0.01$, ****$p < 0.0001$.

4.5. Nanoparticles' *in vivo* antitumoral efficacy in a triple-negative breast cancer mouse model

The NP-FAP-DOX's *in vivo* antitumoral efficacy was evaluated in a murine triple-negative BC orthotopic allograft model. The tumor-bearing mice were treated with PBS (vehicle), NP-CTR, NP-FAP, NP-CTR-DOX, or NP-FAP-DOX for fifteen days. After eight days, treatment with the equivalent dose free of DOX was ended due to severe toxic effects observed on the mice. The mice were sacrificed three days after the last treatment, and the tumors and organs were collected **(Figure 31**).

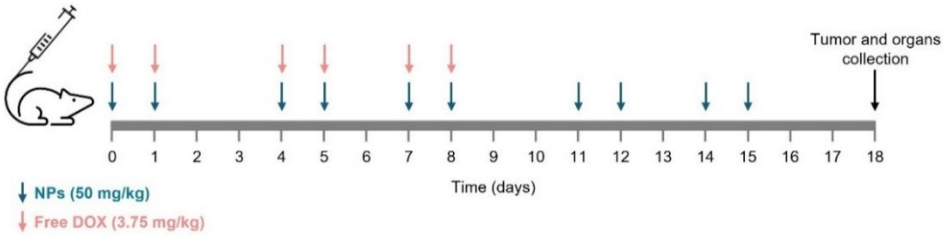

Figure 31. Schematic representation of *in vivo* study. 4T1 cells were injected into the mammary fat pad of BALB/C mice. The tumors, with an initial size of approximately 50 mm^3 were intravenously treated with PBS (vehicle) or 50 mg/kg of nanoparticles (NPs: NP-CTR, NP-FAP, NP-CTR-DOX, or NP-FAP-DOX) four times per week for fifteen days (n = 12 per group). Free doxorubicin (DOX, 3.75 mg/kg) was intravenously administrated for eight days (n = 12). The mice were sacrificed three days after the last treatment, and the tumor and organs were collected.

The NP-FAP-DOX inhibited tumor growth in comparison with the vehicle (PBS) and control NPs (NP-CTR, NP-FAP, and NP-CTR-DOX) (**Figure 32A**). At the treatment endpoint, the NP-FAP-DOX significantly reduced tumor volume by approximately 30%, whereas no statistical differences were observed between the PBS-treated animals and the control NPs (**Figure 32B**). These results were consistent with confocal microscopy images of the tumors that showed a higher accumulation of DOX in the NP-FAP-DOX-treated tumors compared to the other treatment groups, demonstrating a tumor-targeting ability and effective drug delivery to the tumors (**Figure 32C** and **Figure S4A**). Besides, the antitumoral effect of NP-FAP-DOX was also confirmed by the high number of apoptotic cells in the treated tumors, showed by cleaved-caspase 3 immunofluorescence staining (**Figure 32D** and **Figure S4B**). Additionally, the NP-FAP-DOX ability to reduce tumor cells' proliferation was also demonstrated by the significant decrease in *MKI67* mRNA expression in

the NP-FAP-DOX-treated tumors compared to the other groups (**Figure 32E**). Nevertheless, despite the equivalent free DOX dose having also presented an antitumoral effect, the treatment was discontinued after eight days due to severe toxicity. Moreover, regardless of the decrease in tumor growth, the number of apoptotic cells present in the tumors was comparable to the NP-FAP-DOX treatment, whereas the proliferation marker *MKI67* mRNA expression did not show significant differences with the PBS group (**Figure 32**).

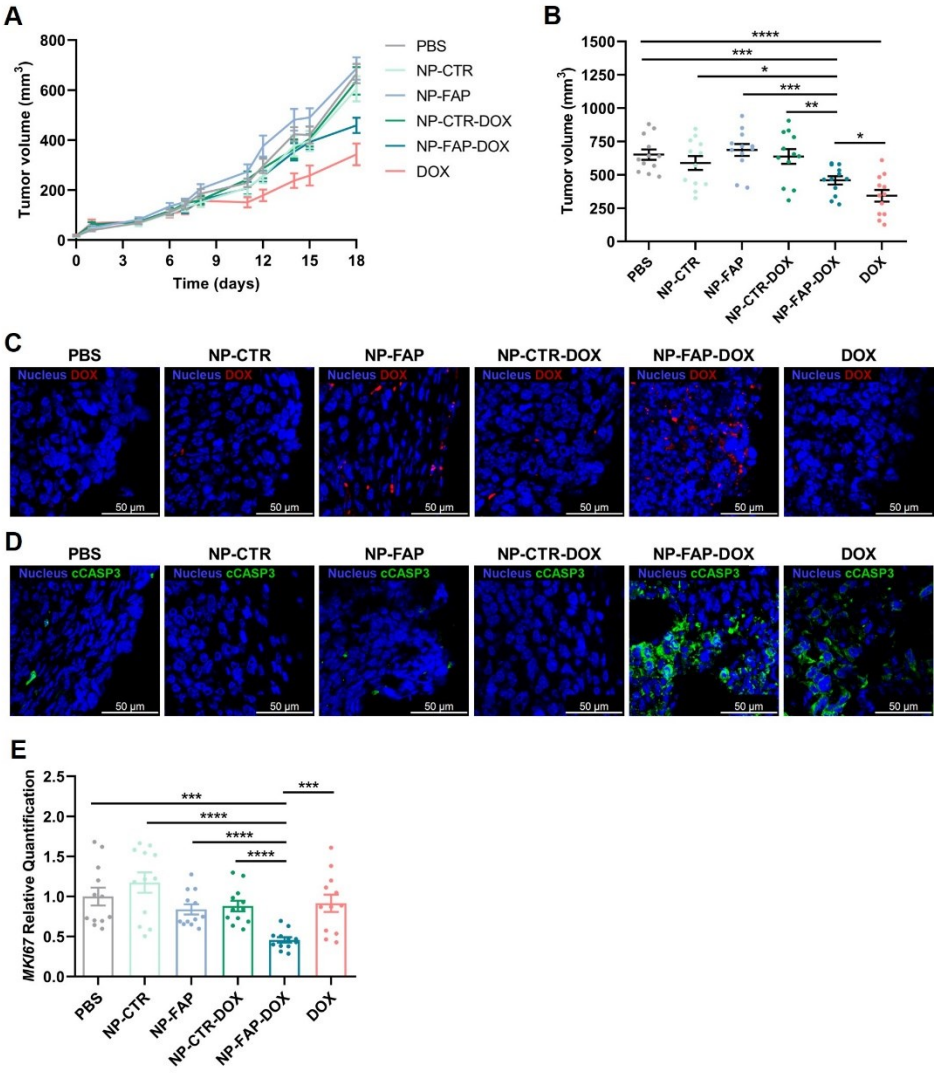

Figure 32. NP-FAP-DOX's *in vivo* antitumoral efficacy. (A) Tumor growth curve mice treated with PBS (vehicle), NP-CTR, NP-FAP, NP-CTR-DOX, NP-FAP-DOX, or free doxorubicin (DOX) (n = 12 per group). **(B)** Tumor volume at the treatment endpoint. **(C)** Representative images of internalized DOX in paraffin-embedded tumor sections at the treatment endpoint. Blue: Nucleus, Red: DOX. Scale bar: 50 µm. **(D)** Representative images of immunofluorescence staining of cleaved-caspase 3 (cCASP3) in paraffin-embedded tumor sections at the treatment endpoint. Blue: Nucleus, Green: cCASP3. Scale bar: 50 µm. **(E)** *MKI67*

expression in tumors at the treatment endpoint determined by RT-qPCR normalized to PBS (n = 12 per group). Mean ± SEM, *$p < 0.05$, **$p < 0.01$, ***$p < 0.001$, ****$p < 0.0001$.

4.6. Nanoparticles' *in vivo* targeting of cancer-associated fibroblasts

After the antitumoral efficacy and the tumor-targeting ability of the NP-FAP-DOX had been confirmed, the nanodevice capacity to target CAFs was assessed. On the one hand, the number of CAFs present in the tumor was evaluated by the α-SMA immunofluorescence staining (**Figure 33A** and **Figure S5**) and *FAP-α* mRNA expression (**Figure 33B**), which are CAFs markers. The NP-FAP-DOX treatment reduced the number of α-SMA positive cells and significantly decreased the *FAP-α* mRNA expression in the tumors in comparison with the PBS and NP-CTR-DOX groups, and also compared to the tumors treated with free DOX. On the other hand, CAFs' depletion was indirectly evaluated through Masson's trichrome staining which showed a decrease in the contents of collagen in the tumor ECM evaluated in the NP-FAP-DOX-treated tumors (**Figure 33C**). These results indicate that the NP-FAP-DOX not only efficiently targeted tumor CAFs but also induced collagen degradation contributing to ECM hemostasis balance and a most effective antitumoral therapy.

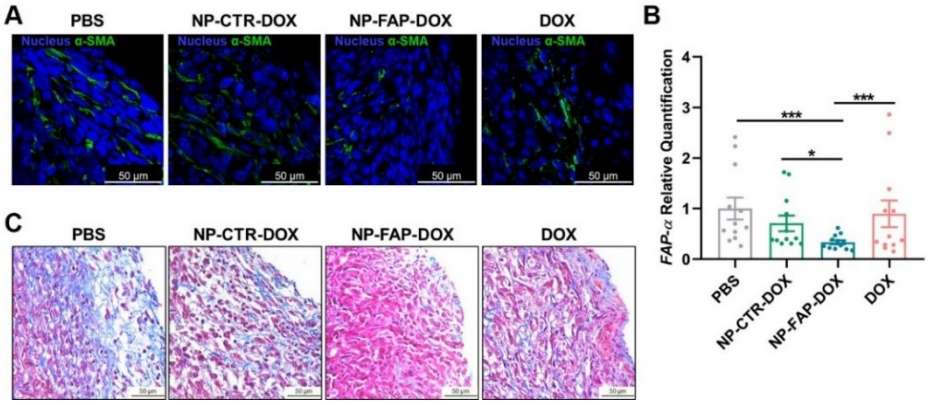

Figure 33. NP-FAP-DOX's *in vivo* targeting of cancer-associated fibroblasts. **(A)** Representative images of immunofluorescence staining of α-SMA in paraffin-embedded tumor sections at the treatment endpoint. Blue: Nucleus, Green: α-SMA. Scale bar: 50 µm. **(B)** *FAP-α* expression in tumors at the treatment endpoint determined by RT-qPCR normalized to PBS (n = 12 per group). Mean ± SEM, **p* < 0.05, ****p* < 0.001. **(C)** Representative images of Masson's trichrome staining in paraffin-embedded tumor sections at the treatment endpoint. Blue: Collagen, Pink: Fibrin, Red: Muscle fibers, Black: Nucleus. Scale bar: 50 µm.

4.7. Nanoparticles' *in vivo* tumor microenvironment modulation

Regarding the major role of CAFs in shaping the TME, the potential of NP-FAP-DOX treatment to re-modulate the immune components and to trigger tumor immune activation was studied. A flow cytometry panel was developed to analyze T lymphocytes ($CD45^+/CD3\varepsilon^+$), cytotoxic T cells ($CD45^+/CD3\varepsilon^+/CD8a^+$), helper T cells ($CD45^+/CD3\varepsilon^+/CD4^+$), NK cells ($CD45^+/NK1.1^+$), M1-like macrophages ($CD45^+/F4/80^+/CD86^+$), and M2-like macrophages ($CD45^+/F4/80^+/CD206^+$) in the treated tumor (**Figure S6**).

The NP-FAP-DOX's treatment increased tumor lymphocyte infiltration. Specifically, this treatment significantly increased the percentage of T lymphocytes, cytotoxic T cells, and also helper T cells (about 1.8, 1.5, and 1.7 times more than in the PBS group, respectively) (**Figure 34A-C** and **Figure S7A-C**). Remarkably, the only alteration observed in these immune cells in the other treatments was a similar increase in helper T cells in the NP-CTR-DOX group (about 1.7 times more than in the PBS group), whereas the free DOX did not induce alterations in T cells tumor infiltration. Moreover, the percentage of NK cells also duplicated after NP-FAP-DOX's treatment compared to the other groups (**Figure 34D** and **Figure S7D**). Regarding the TAM, no significant difference in the percentage of M1-like macrophages of NP-FAP-DOX-treated mice tumor tissues was observed (**Figure 34E** and **Figure S7E**). However, the infiltration of M2-like macrophages was significantly decreased after NP-FAP-DOX's treatment (a decrease of approximately 27% compared to untreated mice) (**Figure 34F** and **Figure S7F**), increasing significantly the M1/M2 ratio (about 1.5 times more in comparison with the other groups) (**Figure 34G**). No alterations were found in the NP-CTR-DOX group related to TAM, although the free DOX treatment induced a significant decrease in both M1 and M2-like macrophages, leading to no changes in the M1/M2 ratio compared to the untreated group. Altogether, these results showed that NP-FAP-DOX re-modulated the TME and reversed the immunosuppressive environment of the tumors.

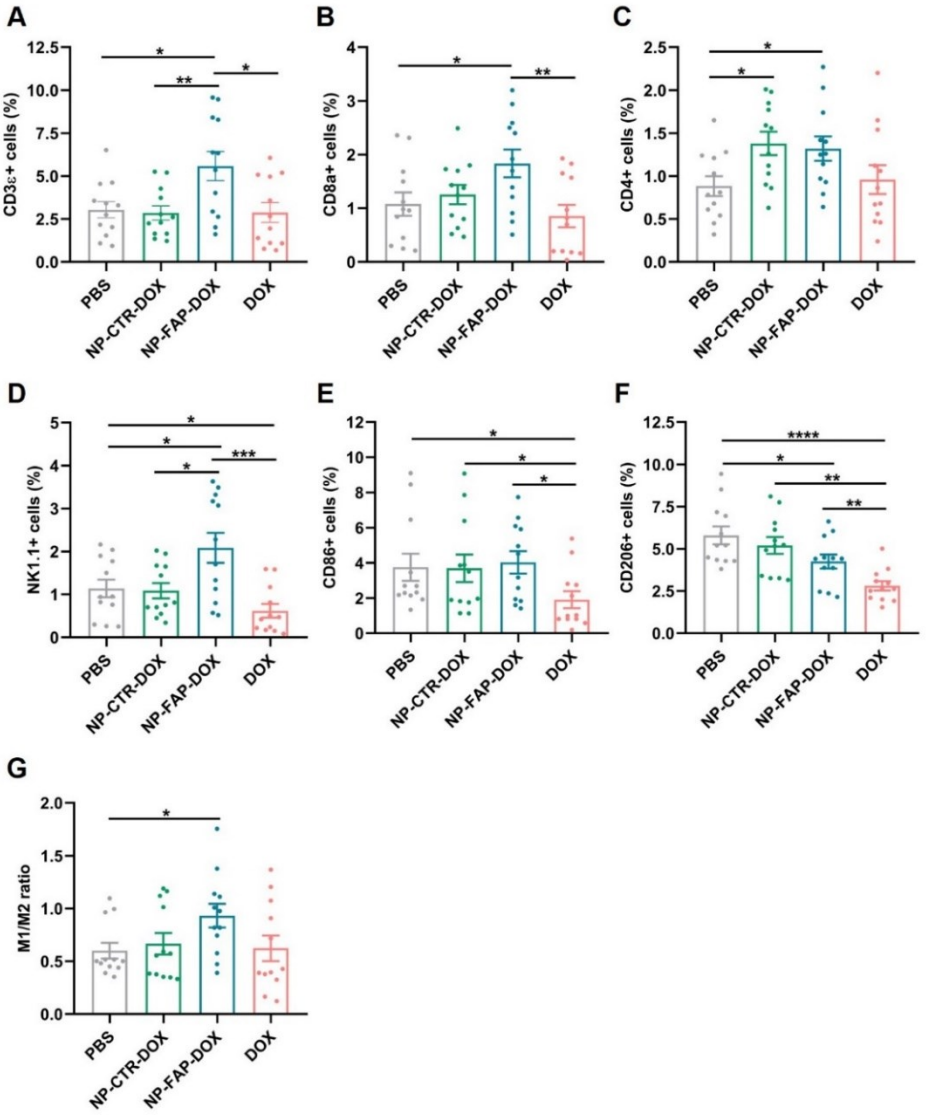

Figure 34. NP-FAP-DOX's *in vivo* tumor microenvironment modulation. Percentage of **(A)** T lymphocytes ($CD45^+/CD3\varepsilon^+$), **(B)** cytotoxic T cells ($CD45^+/CD3\varepsilon^+/CD8a^+$), **(C)** helper T cells ($CD45^+/CD3\varepsilon^+/CD4^+$), **(D)** natural killer cells ($CD45^+/NK1.1^+$), **(E)** M1-like macrophages ($CD45^+/F4/80^+/CD86^+$), and **(F)** M2-like macrophages ($CD45^+/F4/80^+/CD206^+$) in xenograft tumors analyzed by flow cytometry at the treatment endpoint (n = 12 per group). **(G)** Ratios of M1 to M2 (M1/M2) were calculated as the percentage of M1-like macrophages divided

by the percentage of M2-like macrophages on xenograft tumors analyzed by flow cytometry at the treatment endpoint (n = 12 per group). Mean ± SEM, *$p < 0.05$, **$p < 0.01$, ***$p < 0.001$, ****$p < 0.0001$.

4.8. Nanoparticles' *in vivo* biocompatibility and safety

The NP-FAP-DOX's safety profile was confirmed by the absence of alterations in mice's body weight during treatments. In contrast, the free DOX-treated mice presented a rapid decline in body weight, ruffled fur, and hunching at the early stage of treatment, leading to its early cessation (**Figure 35A**). These results suggest that free DOX dose could be causing systemic toxicity, like cardiac, hepatic, renal, and gastrointestinal toxicity, that contributes to the decline of global health in the mice, whereas the NP-FAP-DOX treatment showed to be well tolerated by the animals.

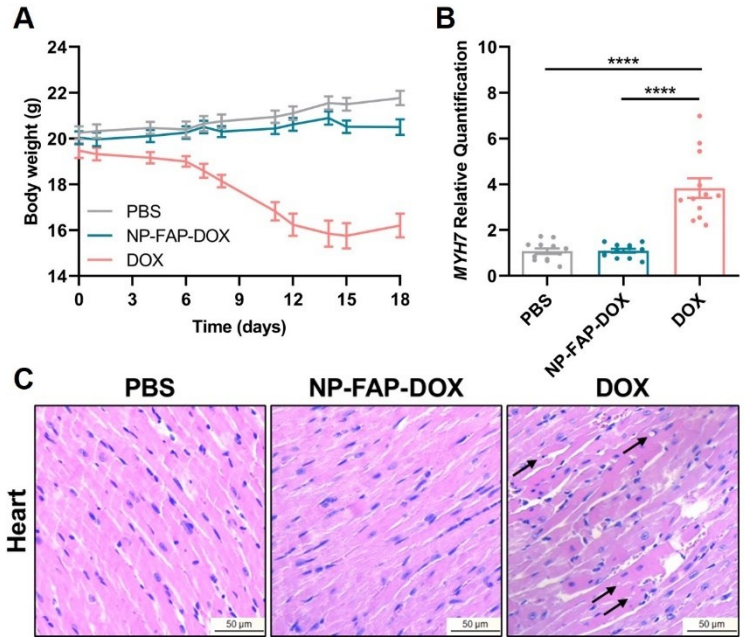

Figure 35. NP-FAP-DOX's safety and cardiotoxicity evaluation. (A) Body weight changes in tumor-bearing mice during treatment with PBS (vehicle), NP-FAP-DOX, or free doxorubicin (DOX) (n = 12 per group). **(B)** *MYH7* expression in heart tissue at the treatment endpoint determined by RT-qPCR normalized to PBS (n = 12 per group). Mean ± SEM, ****$p < 0.0001$. **(C)** Representative images of H&E staining in paraffin-embedded heart tissue sections at the treatment endpoint. Arrows indicate cytoplasmic lysosomes. Scale bar: 50 µm.

The NP-FAP-DOX's potential to protect from DOX-induced cardiotoxicity was investigated. The results confirmed that, in contrast to free DOX, NP-FAP-DOX treatment did not induce cardiotoxicity, evidenced by the normal levels of the marker of cardiac *atrophy myosin heavy chain β* (*MHC-β*, *MYH7*) (**Figure 35B**) and the absence of cytoplasmic vacuoles in NP-FAP-DOX-treated mice heart tissues (**Figure 35C**).

Moreover, the NP-FAP-DOX's treatment effect on hepatic, splenic, and renal toxicity was also evaluated. Compared with free DOX-treated mice that evidence tissue damage in the liver, kidneys, and spleen, the organs of the NP-FAP-DOX-treated mice remained clear of toxicity signs, without observed morphological changes (**Figure 36**). The morphological analysis of liver and spleen revealed severe atrophy after free DOX treatment, whereas no evidence of organs degeneration was observed in NP-FAP-DOX-treated mice compared to PBS group **(Figure 36A-B)**. Likewise, in free DOX-treated mice's tissues degeneration of hepatocytes, reduction of spleen white pulp, and deterioration of the kidney structures, like aberrant Bowman's space, tubule dilations, and cellular infiltrations were observed (**Figure 36C**). Neither of these alterations appeared in NP-FAP-DOX-treated mice organs nor in control group.

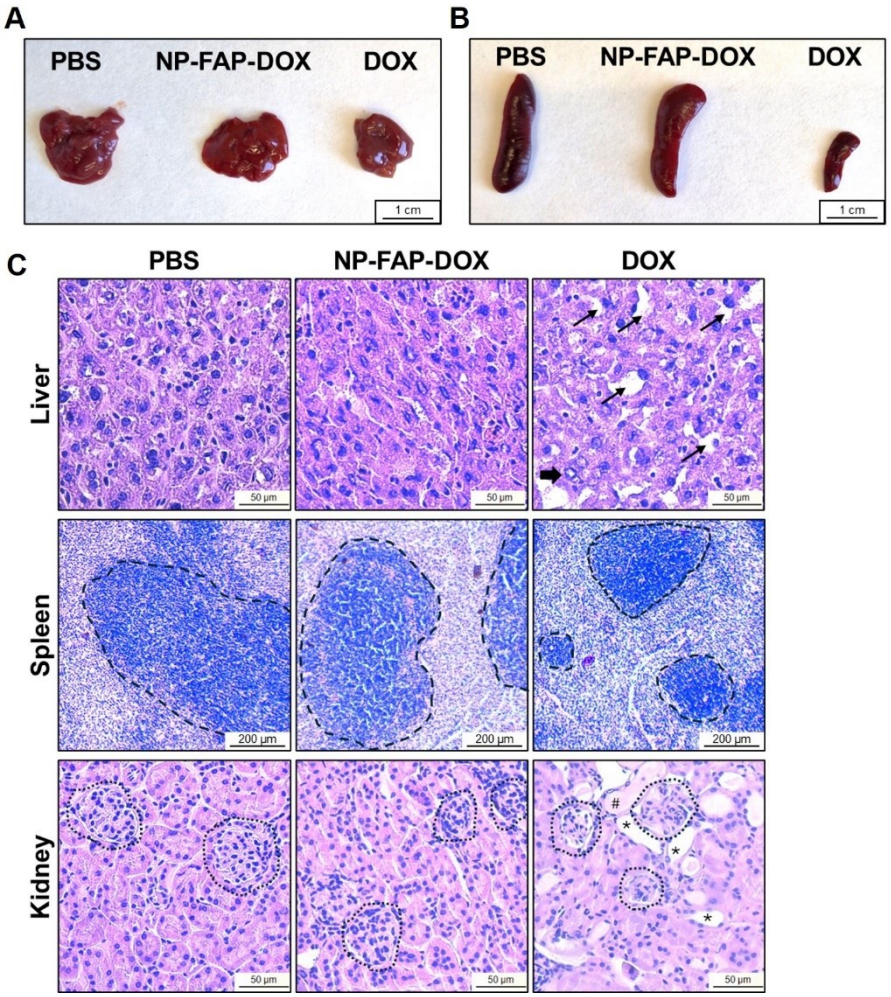

Figure 36. NP-FAP-DOX's systemic toxicity assessment. Representative **(A)** liver and **(B)** spleen morphology and size of tumor-bearing mice treated with PBS (vehicle), NP-FAP-DOX, or free doxorubicin (DOX). **(C)** Representative images of H&E staining in paraffin-embedded liver, spleen, and kidney tissue sections at the treatment endpoint. Thin and thick arrows indicate degeneration or apoptosis of hepatocytes, respectively. Dashed areas in the spleen represent the white pulp. Dotted areas in the kidney represent the glomerular capsule, the asterisk represents tubule dilations, and the hash sign represents cellular infiltrations. Scale bar: 50 µm (liver and kidney) or 200 µm (spleen).

Overall, these results demonstrated the potential of the designed nanodevice as a safe and biocompatible new targeted drug delivery system for BC treatment. The NP-FAP-DOX improved drug delivery efficacy, overcame adverse DOX side effects, and enhanced therapy efficacy through the modulation of TME.

CHAPTER 5 |

DISCUSSION

Nowadays, despite recent advances in BC therapies, the number of patients who experience a relapse is still startling. Especially in triple-negative BC patients for which no targeted therapy is available and chemotherapy remains the standard treatment, leading to a shorter overall survival compared with other subtypes [9, 93]. Most of the BC therapies currently used in clinical practice are focused on targeting tumor cells. Nevertheless, new advances in the immunology field uncover an important role of the TME in tumor modulation [94, 95]. The dynamic crosstalk between cancer cells and TME plays a critical role from tumor initiation until metastatic outgrowth and deeply influences therapy response [96, 97]. Specifically, CAFs play an important role in tumor behavior and drug resistance, by shaping the ECM, tumor immunity, and angiogenesis [119, 163]. In BC, studies reported that CAFs depletion inhibits tumor growth and metastasis [177, 180]. Therefore, CAFs become potential targets to improve therapy outcomes.

In the last decades, NPs emerged as important players in cancer therapy [276, 277]. Their unique characteristics can overcome conventional drug disadvantages, such as non-specific targeting and adverse side effects to improve BC patients' outcomes [278, 279]. Hence, this work proposes the design of a nanodevice targeting CAFs as a new therapeutic strategy for BC treatment.

In the present study, MSNs were chosen as support. Among the different types of NPs, these show good biocompatibility and stability, as well as a high level of clearance and excretion [410]. Moreover, MSNs present a high drug-loading capacity and can be easily functionalized, allowing specific and efficient cargo release, and minimizing off-target toxicity [309, 317]. The MSNs were loaded with DOX, a cytotoxic drug widely used in BC treatment, and functionalized with PEG that decrease opsonization and avoid immune system clearance [281]. Besides, FAP-α,

the most common tumor-targeting CAF antigen, was chosen as a therapeutic target. This surface marker is overexpressed on activated stromal fibroblasts in tumors, including BC, and is associated with tumor progression and metastasis [400]. Furthermore, recent studies also reported an increased FAP-α expression in tumor cells and TAM [406, 407]. Thus, the NP-FAP-DOX was synthesized using MSNs as support, loaded with DOX, and functionalized with PEG and a FAP-α ligand peptide with a high affinity for FAP-α [403].

The NP-FAP-DOX's characterization showed a hydrodynamic size of 247 ± 9 nm, which allows NPs to passively target the tumor, in addition to the active targeting. Passive targeting occurs due to the enhanced permeability and retention effect in the tumor areas, which allow small-sized NPs to extravasate from the bloodstream through tumors' defective vasculature and accumulate in TME [326]. Moreover, *in vitro* cargo release studies verified a controlled cargo delivery only in the presence of GSH, which reduces dithiol bonds that anchor PEG to the NP's surface, resulting in cargo delivery [411]. Moreover, *in vitro* biocompatibility studies showed a nontoxic profile for the NPs. Together, these results suggest that the content of the NP-FAP-DOX would remain inside the pores until it reaches the tumor and is internalized by cells, thus avoiding unspecific DOX delivery and adverse side effects.

The NP-FAP-DOX specific targeting of FAP-α was demonstrated in BC cells with FAP-α positive expression as well as in CAFs derived from triple-negative BC patient biopsies. Moreover, the cytotoxic effect of DOX-containing NPs was also confirmed. Remarkably, the NP-FAP-DOX also presented good penetration efficiency in PDOs, maintaining the targeting and cytotoxic effect in this 3D model. These *in vitro* studies revealed the potential of NP-FAP-DOX for *in vivo* tumor targeting and effective drug delivery.

The NP-FAP-DOX potential as a new therapeutic strategy for BC treatment was tested in a murine triple-negative BC model. The NP-FAP-DOX showed the capacity to target, accumulate, and deliver its DOX content in the tumor. The designed nanodevice efficiently inhibited tumor growth by decreasing the proliferation of tumoral cells and increasing apoptosis. In addition to the NP-FAP-DOX antitumoral effect, this treatment efficiently targeted and depleted CAFs, leading to tumoral collagen degradation. It is known that CAFs reshape the ECM structure contributing to tumor therapeutic resistance [165, 169]. Moreover, tumor stroma is considered a prognostic marker for triple-negative BC patients, being a high tumor-stroma ratio associated with a higher relapse rate and worse overall survival [412]. Several studies have proven that the use of NPs for CAFs depletion therapy promotes ECM hemostasis balance to a most effective antitumoral effect [397, 403]. The reduction of the stromal component in the tumor results in a reduction of tumor intercellular pressure and enhanced NPs penetration [397]. However, not always anti-stromal activity of the NPs leads to a direct effect on tumor cells. For example, docetaxel-conjugate NPs were described to reduce α-SMA-positive stroma population and, as a consequence, the matrix deposition and the tumor interstitial fluid pressure, without significant changes in the tumoral cells population [413]. Thus, based on our results, it has been proven that the NP-FAP-DOX effect is not only based on tumoral stroma remodeling but also on a strong antitumoral effect.

Additionally, CAFs are also responsible for the modulation of the tumoral immune landscape [182, 183]. In BC patients, a FAP-α-positive CAFs subset was associated with an immunosuppressive function by suppressing T cells proliferation and reducing immunotherapeutic efficacy [159, 160, 199]. Indeed, CAFs depletion, by FAP-based vaccines, was associated with an activation of anti-tumoral immune response in BC

models. The shift to an antitumor immune microenvironment was characterized by an increased number of dendritic and cytotoxic T cells, and diminished recruitment of MDSC, TAM, and regulatory T cells [184, 404, 405]. Moreover, the use of NPs that target CAFs in BC models showed similar results by increasing the cytotoxic T cells infiltration in the tumor [399, 401, 402]. In our study, the NP-FAP-DOX also led to tumor microenvironment re-modulation and activation of tumor immune response. Specifically, this treatment not only promoted tumor lymphocyte infiltration by increasing the percentage of T lymphocytes, cytotoxic T cells, and helper T cells but also increased the percentage of NK cells in the tumor. Additionally, in contrast with the previously reported NPs studies, our nanodevice was also able to decrease the M2-like macrophages leading to an increase in the M1/M2 ratio. This result can be possibly attributed to high FAP-α expression in TAM, which would also make them a target of NP-FAP-DOX [407].

The DOX-induced cardiotoxicity, as well as its toxic effect in other organs (like kidneys or liver), is a well-known side effect of this chemotherapeutic agent [414]. Over the last years, two liposomal DOX NPs were approved for BC treatment to reduce cardiotoxicity with comparable drug efficacy [291, 292]. In our study, comparing the NP-FAP-DOX with the equivalent free DOX dose in mice revealed a clear improvement in the therapeutic and safety profile of the free drug, preventing DOX-induced cardio and systemic toxicity. Despite the free DOX treatment also presented an antitumoral effect, no differences were observed in the tumor cells proliferation or apoptosis, nor in tumoral CAFs content, compared with PBS control. More importantly, the free DOX-treated mice presented a rapid decline in body weight, ruffled fur, and hunching at the early stage of treatment, leading to its early cessation. All these signs are associated with high free DOX doses that cause cardio

and systemic toxicity, which leads to the decline of global health in mice [415]. Thus, our results evidence that the NP-FAP-DOX can improve drug delivery efficacy and enhance the therapeutic effect of the free DOX, overcoming the adverse side effects.

For a long time, tumor cells were the focus of anti-cancer therapies. However, it is important to highlight the implications of TME in cancer development and therapy resistance and to study CAFs as key therapeutic targets to improve BC patients' outcomes. Nevertheless, efforts must continue to be made to improve the efficacy of current therapies, like the implementation of nanodevices in clinical practice. Overall, these data demonstrated the potential of the designed nanodevice as a new targeted drug delivery system for BC treatment. The NP-FAP-DOX can improve drug delivery to specific cell populations in a controlled manner, overcome adverse side effects, and enhance therapy efficacy through the modulation of the TME (**Figure 37**).

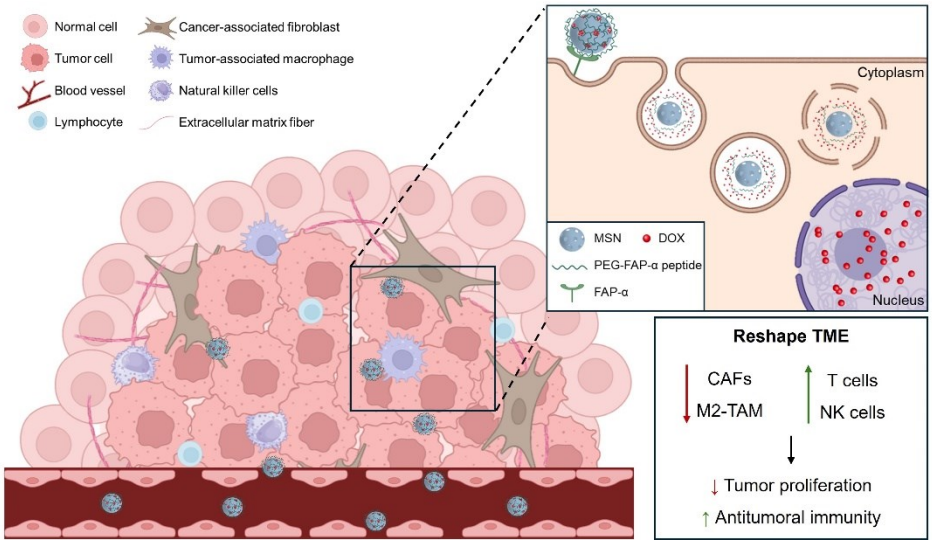

Figure 37. The antitumoral and tumor microenvironment remodeling effect of NP-FAP-DOX. The NP-FAP-DOX accumulates in the tumor passively by enhanced permeability and retention effect. In the TME, the nanodevice actively targets the FAP-α positive cells, namely the CAFs, through the FAP-α peptide on its surface, and delivers its DOX cargo content. The NP-FAP-DOX therapy reshapes the TME by decreasing the CAFs and the M2-like macrophages, whereas increases the T cells infiltration and NK cells in the tumor, leading to an antitumoral effect and activation of tumor immune response. Abbreviations: CAFs – cancer-associated fibroblasts, DOX – doxorubicin, MSN – mesoporous silica nanoparticles, NK – natural killer, PEG – polyethylene glycol, TAM – tumor-associated macrophages, TME – tumor microenvironment.

CHAPTER 6 |

CONCLUSIONS

Considering the results presented in this Ph.D. thesis, the conclusions from the study are the following:

1. The MSNs loaded with DOX and functionalized with the FAP-α ligand peptide (NP-FAP-DOX) showed controlled cargo release and an *in vitro* nontoxic profile.
2. The NP-FAP-DOX efficiently targeted and produced a preferent cytotoxic effect in BC cells with FAP-α positive expression and CAFs.
3. The NP-FAP-DOX demonstrated good penetration efficiency in the PDOs, while maintaining their FAP-α targeting ability and cytotoxic effect in this 3D model.
4. The NP-FAP-DOX showed a tumor-targeting ability and effective drug delivery, resulting in an antitumoral effect in an *in vivo* triple-negative BC mouse model.
5. The NP-FAP-DOX *in vivo* treatment efficiently targeted and depleted CAFs, leading to TME re-modulation and activation of tumor immune response.
6. The NP-FAP-DOX improved the therapeutic and safety profile of the free drug, preventing DOX-induced cardio and systemic toxicity.

CHAPTER 7 |

BIBLIOGRAPHY

1. Bray, F., et al., *The ever-increasing importance of cancer as a leading cause of premature death worldwide.* Cancer, 2021. **127**(16): p. 3029-3030.
2. Bray, F., et al., *Global cancer statistics 2022: GLOBOCAN estimates of incidence and mortality worldwide for 36 cancers in 185 countries.* CA Cancer J Clin, 2024. **74**(3): p. 229-263.
3. Korde, L.A., et al., *Multidisciplinary meeting on male breast cancer: summary and research recommendations.* J Clin Oncol, 2010. **28**(12): p. 2114-22.
4. Momenimovahed, Z. and H. Salehiniya, *Epidemiological characteristics of and risk factors for breast cancer in the world.* Breast Cancer (Dove Med Press), 2019. **11**: p. 151-164.
5. Huang, J., et al., *Global incidence and mortality of breast cancer: a trend analysis.* Aging (Albany NY), 2021. **13**(4): p. 5748-5803.
6. Soerjomataram, I. and F. Bray, *Planning for tomorrow: global cancer incidence and the role of prevention 2020-2070.* Nat Rev Clin Oncol, 2021. **18**(10): p. 663-672.
7. Miao, H., et al., *Incidence and outcome of male breast cancer: an international population-based study.* J Clin Oncol, 2011. **29**(33): p. 4381-6.
8. Key, T.J., et al., *Sex hormones and risk of breast cancer in premenopausal women: a collaborative reanalysis of individual participant data from seven prospective studies.* Lancet Oncol, 2013. **14**(10): p. 1009-19.
9. Giaquinto, A.N., et al., *Breast Cancer Statistics, 2022.* CA Cancer J Clin, 2022. **72**(6): p. 524-541.
10. Azim, H.A., Jr., et al., *Elucidating prognosis and biology of breast cancer arising in young women using gene expression profiling.* Clin Cancer Res, 2012. **18**(5): p. 1341-51.

11. Fakhri, N., et al., *Risk factors for breast cancer in women: an update review.* Med Oncol, 2022. **39**(12): p. 197.
12. Ng, A.K. and L.B. Travis, *Radiation therapy and breast cancer risk.* J Natl Compr Canc Netw, 2009. **7**(10): p. 1121-8.
13. Schacht, D.V., et al., *Importance of a personal history of breast cancer as a risk factor for the development of subsequent breast cancer: results from screening breast MRI.* AJR Am J Roentgenol, 2014. **202**(2): p. 289-92.
14. Dyrstad, S.W., et al., *Breast cancer risk associated with benign breast disease: systematic review and meta-analysis.* Breast Cancer Res Treat, 2015. **149**(3): p. 569-75.
15. *Menarche, menopause, and breast cancer risk: individual participant meta-analysis, including 118 964 women with breast cancer from 117 epidemiological studies.* Lancet Oncol, 2012. **13**(11): p. 1141-51.
16. Kanadys, W., et al., *Use of Oral Contraceptives as a Potential Risk Factor for Breast Cancer: A Systematic Review and Meta-Analysis of Case-Control Studies Up to 2010.* Int J Environ Res Public Health, 2021. **18**(9): p. 4638.
17. Zhang, G.Q., et al., *Menopausal hormone therapy and women's health: An umbrella review.* PLoS Med, 2021. **18**(8): p. e1003731.
18. Albrektsen, G., et al., *Breast cancer risk by age at birth, time since birth and time intervals between births: exploring interaction effects.* Br J Cancer, 2005. **92**(1): p. 167-75.
19. Unar-Munguía, M., et al., *Breastfeeding Mode and Risk of Breast Cancer: A Dose-Response Meta-Analysis.* J Hum Lact, 2017. **33**(2): p. 422-434.
20. Larsen, M.J., et al., *Hereditary breast cancer: clinical, pathological and molecular characteristics.* Breast Cancer (Auckl), 2014. **8**: p. 145-55.

21. Liu, L., et al., *Correlation between family history and characteristics of breast cancer.* Sci Rep, 2021. **11**(1): p. 6360.
22. Haber, G., N.U. Ahmed, and V. Pekovic, *Family history of cancer and its association with breast cancer risk perception and repeat mammography.* Am J Public Health, 2012. **102**(12): p. 2322-9.
23. Çelik, A., et al., *Relationship of breast cancer with ovarian cancer.* Concise Rev. Mol. Pathol. Breast Cancer, 2015. **32**(3): p. 87-202.
24. Brewer, H.R., et al., *Family history and risk of breast cancer: an analysis accounting for family structure.* Breast Cancer Res Treat, 2017. **165**(1): p. 193-200.
25. Kuchenbaecker, K.B., et al., *Risks of Breast, Ovarian, and Contralateral Breast Cancer for BRCA1 and BRCA2 Mutation Carriers.* Jama, 2017. **317**(23): p. 2402-2416.
26. Daly, M.B., et al., *The association between age at breast cancer diagnosis and prevalence of pathogenic variants.* Breast Cancer Res Treat, 2023. **199**(3): p. 617-626.
27. Shiovitz, S. and L.A. Korde, *Genetics of breast cancer: a topic in evolution.* Ann Oncol, 2015. **26**(7): p. 1291-9.
28. Loibl, S., et al., *Early breast cancer: ESMO Clinical Practice Guideline for diagnosis, treatment and follow-up.* Ann Oncol, 2024. **35**(2): p. 159-182.
29. Sessa, C., et al., *Risk reduction and screening of cancer in hereditary breast-ovarian cancer syndromes: ESMO Clinical Practice Guideline.* Ann Oncol, 2023. **34**(1): p. 33-47.
30. Duffy, S.W., et al., *Mammography screening reduces rates of advanced and fatal breast cancers: Results in 549,091 women.* Cancer, 2020. **126**(13): p. 2971-2979.
31. Canelo-Aybar, C., et al., *Benefits and harms of breast cancer mammography screening for women at average risk of breast cancer: A systematic review for the European Commission*

Initiative on Breast Cancer. J Med Screen, 2021. **28**(4): p. 389-404.

32. Nelson, H.D., et al., *Harms of Breast Cancer Screening: Systematic Review to Update the 2009 U.S. Preventive Services Task Force Recommendation.* Ann Intern Med, 2016. **164**(4): p. 256-67.
33. Bulliard, J.L., et al., *Breast cancer screening and overdiagnosis.* Int J Cancer, 2021. **149**(4): p. 846-853.
34. Gegios, A.R., M.S. Peterson, and A.M. Fowler, *Breast Cancer Screening and Diagnosis: Recent Advances in Imaging and Current Limitations.* PET Clin, 2023. **18**(4): p. 459-471.
35. Perry, N., et al., *European guidelines for quality assurance in breast cancer screening and diagnosis. Fourth edition--summary document.* Ann Oncol, 2008. **19**(4): p. 614-22.
36. McDonald, E.S., et al., *Clinical Diagnosis and Management of Breast Cancer.* J Nucl Med, 2016. **57**(Suppl 1): p. 9s-16s.
37. Tan, P.H., et al., *The 2019 World Health Organization classification of tumours of the breast.* Histopathology, 2020. **77**(2): p. 181-185.
38. Cserni, G., *Histological type and typing of breast carcinomas and the WHO classification changes over time.* Pathologica, 2020. **112**(1): p. 25-41.
39. Li, C.I., et al., *Trends in incidence rates of invasive lobular and ductal breast carcinoma.* Jama, 2003. **289**(11): p. 1421-4.
40. Malhotra, G.K., et al., *Histological, molecular and functional subtypes of breast cancers.* Cancer Biol Ther, 2010. **10**(10): p. 955-60.
41. Cserni, G., et al., *The new TNM-based staging of breast cancer.* Virchows Arch, 2018. **472**(5): p. 697-703.

42. Giuliano, A.E., et al., *Breast Cancer-Major changes in the American Joint Committee on Cancer eighth edition cancer staging manual.* CA Cancer J Clin, 2017. **67**(4): p. 290-303.
43. Edge, S.B., G.N. Hortobagyi, and A.E. Giuliano, *New and important changes in breast cancer TNM: incorporation of biologic factors into staging.* Expert Rev Anticancer Ther, 2019. **19**(4): p. 309-318.
44. Rakha, E.A., et al., *Prognostic significance of Nottingham histologic grade in invasive breast carcinoma.* J Clin Oncol, 2008. **26**(19): p. 3153-8.
45. Rakha, E.A., et al., *Breast cancer prognostic classification in the molecular era: the role of histological grade.* Breast Cancer Res, 2010. **12**(4): p. 207.
46. Jaroensri, R., et al., *Deep learning models for histologic grading of breast cancer and association with disease prognosis.* NPJ Breast Cancer, 2022. **8**(1): p. 113.
47. Allison, K.H., et al., *Estrogen and Progesterone Receptor Testing in Breast Cancer: American Society of Clinical Oncology/College of American Pathologists Guideline Update.* Arch Pathol Lab Med, 2020. **144**(5): p. 545-563.
48. Wolff, A.C., et al., *Human Epidermal Growth Factor Receptor 2 Testing in Breast Cancer: American Society of Clinical Oncology/College of American Pathologists Clinical Practice Guideline Focused Update.* J Clin Oncol, 2018. **36**(20): p. 2105-2122.
49. Nielsen, T.O., et al., *Assessment of Ki67 in Breast Cancer: Updated Recommendations From the International Ki67 in Breast Cancer Working Group.* J Natl Cancer Inst, 2021. **113**(7): p. 808-819.

50. Curigliano, G., et al., *Understanding breast cancer complexity to improve patient outcomes: The St Gallen International Consensus Conference for the Primary Therapy of Individuals with Early Breast Cancer 2023.* Ann Oncol, 2023. **34**(11): p. 970-986.
51. Harbeck, N., et al., *Breast cancer.* Nat Rev Dis Primers, 2019. **5**(1): p. 66.
52. Orrantia-Borunda, E., et al., *Subtypes of Breast Cancer*, in *Breast Cancer*, H.N. Mayrovitz, Editor. 2022, Breast Cancer. Brisbane (AU): Exon Publication.
53. Prat, A., et al., *Clinical implications of the intrinsic molecular subtypes of breast cancer.* Breast, 2015. **24**(Suppl 2): p. S26-35.
54. Perou, C.M., et al., *Molecular portraits of human breast tumours.* Nature, 2000. **406**(6797): p. 747-52.
55. Sørlie, T., et al., *Gene expression patterns of breast carcinomas distinguish tumor subclasses with clinical implications.* Proc Natl Acad Sci U S A, 2001. **98**(19): p. 10869-74.
56. Sorlie, T., et al., *Repeated observation of breast tumor subtypes in independent gene expression data sets.* Proc Natl Acad Sci U S A, 2003. **100**(14): p. 8418-23.
57. Eliyatkın, N., et al., *Molecular Classification of Breast Carcinoma: From Traditional, Old-Fashioned Way to A New Age, and A New Way.* J Breast Health, 2015. **11**(2): p. 59-66.
58. Yersal, O. and S. Barutca, *Biological subtypes of breast cancer: Prognostic and therapeutic implications.* World J Clin Oncol, 2014. **5**(3): p. 412-24.
59. Prat, A. and C.M. Perou, *Deconstructing the molecular portraits of breast cancer.* Mol Oncol, 2011. **5**(1): p. 5-23.
60. van de Vijver, M.J., et al., *A gene-expression signature as a predictor of survival in breast cancer.* N Engl J Med, 2002. **347**(25): p. 1999-2009.

61. Paik, S., et al., *A multigene assay to predict recurrence of tamoxifen-treated, node-negative breast cancer.* N Engl J Med, 2004. **351**(27): p. 2817-26.
62. Parker, J.S., et al., *Supervised risk predictor of breast cancer based on intrinsic subtypes.* J Clin Oncol, 2009. **27**(8): p. 1160-7.
63. Greenwalt, I., et al., *Precision Medicine and Targeted Therapies in Breast Cancer.* Surg Oncol Clin N Am, 2020. **29**(1): p. 51-62.
64. Gennari, A., et al., *ESMO Clinical Practice Guideline for the diagnosis, staging and treatment of patients with metastatic breast cancer.* Ann Oncol, 2021. **32**(12): p. 1475-1495.
65. Waks, A.G. and E.P. Winer, *Breast Cancer Treatment: A Review.* Jama, 2019. **321**(3): p. 288-300.
66. Trayes, K.P. and S.E.H. Cokenakes, *Breast Cancer Treatment.* Am Fam Physician, 2021. **104**(2): p. 171-178.
67. Curigliano, G., et al., *De-escalating and escalating treatments for early-stage breast cancer: the St. Gallen International Expert Consensus Conference on the Primary Therapy of Early Breast Cancer 2017.* Ann Oncol, 2017. **28**(8): p. 1700-1712.
68. Veronesi, U., et al., *Sentinel lymph node biopsy in breast cancer: ten-year results of a randomized controlled study.* Ann Surg, 2010. **251**(4): p. 595-600.
69. Bartelink, H., et al., *Whole-breast irradiation with or without a boost for patients treated with breast-conserving surgery for early breast cancer: 20-year follow-up of a randomised phase 3 trial.* Lancet Oncol, 2015. **16**(1): p. 47-56.
70. Kerr, A.J., et al., *Adjuvant and neoadjuvant breast cancer treatments: A systematic review of their effects on mortality.* Cancer Treat Rev, 2022. **105**: p. 102375.

71. Nicholson, R.I. and S.R. Johnston, *Endocrine therapy--current benefits and limitations.* Breast Cancer Res Treat, 2005. **93**(Suppl 1): p. S3-10.
72. Goss, P.E., et al., *Extending Aromatase-Inhibitor Adjuvant Therapy to 10 Years.* N Engl J Med, 2016. **375**(3): p. 209-19.
73. Davies, C., et al., *Long-term effects of continuing adjuvant tamoxifen to 10 years versus stopping at 5 years after diagnosis of oestrogen receptor-positive breast cancer: ATLAS, a randomised trial.* Lancet, 2013. **381**(9869): p. 805-16.
74. Grinshpun, A., et al., *The dilemma of selecting a first line CDK4/6 inhibitor for hormone receptor-positive/HER2-negative metastatic breast cancer.* NPJ Breast Cancer, 2023. **9**(1): p. 15.
75. Baselga, J., et al., *Everolimus in postmenopausal hormone-receptor-positive advanced breast cancer.* N Engl J Med, 2012. **366**(6): p. 520-9.
76. André, F., et al., *Alpelisib for PIK3CA-Mutated, Hormone Receptor-Positive Advanced Breast Cancer.* N Engl J Med, 2019. **380**(20): p. 1929-1940.
77. Cardoso, F., et al., *5th ESO-ESMO international consensus guidelines for advanced breast cancer (ABC 5).* Ann Oncol, 2020. **31**(12): p. 1623-1649.
78. Wynn, C.S. and S.C. Tang, *Anti-HER2 therapy in metastatic breast cancer: many choices and future directions.* Cancer Metastasis Rev, 2022. **41**(1): p. 193-209.
79. *Trastuzumab for early-stage, HER2-positive breast cancer: a meta-analysis of 13 864 women in seven randomised trials.* Lancet Oncol, 2021. **22**(8): p. 1139-1150.
80. Gianni, L., et al., *5-year analysis of neoadjuvant pertuzumab and trastuzumab in patients with locally advanced, inflammatory, or early-stage HER2-positive breast cancer (NeoSphere): a*

multicentre, open-label, phase 2 randomised trial. Lancet Oncol, 2016. **17**(6): p. 791-800.

81. Nitz, U., et al., *De-escalated neoadjuvant pertuzumab plus trastuzumab therapy with or without weekly paclitaxel in HER2-positive, hormone receptor-negative, early breast cancer (WSG-ADAPT-HER2+/HR-): survival outcomes from a multicentre, open-label, randomised, phase 2 trial.* Lancet Oncol, 2022. **23**(5): p. 625-635.
82. Loibl, S., et al., *Adjuvant trastuzumab emtansine in HER2-positive breast cancer patients with HER2-negative residual invasive disease in KATHERINE.* NPJ Breast Cancer, 2022. **8**(1): p. 106.
83. Rugo, H.S., et al., *Efficacy of Margetuximab vs Trastuzumab in Patients With Pretreated ERBB2-Positive Advanced Breast Cancer: A Phase 3 Randomized Clinical Trial.* JAMA Oncol, 2021. **7**(4): p. 573-584.
84. Modi, S., et al., *Trastuzumab Deruxtecan in Previously Treated HER2-Positive Breast Cancer.* N Engl J Med, 2020. **382**(7): p. 610-621.
85. Bianchini, G., et al., *Treatment landscape of triple-negative breast cancer - expanded options, evolving needs.* Nat Rev Clin Oncol, 2022. **19**(2): p. 91-113.
86. Masuda, N., et al., *Adjuvant Capecitabine for Breast Cancer after Preoperative Chemotherapy.* N Engl J Med, 2017. **376**(22): p. 2147-2159.
87. Schmid, P., et al., *Event-free Survival with Pembrolizumab in Early Triple-Negative Breast Cancer.* N Engl J Med, 2022. **386**(6): p. 556-567.
88. Cortes, J., et al., *Pembrolizumab plus chemotherapy versus placebo plus chemotherapy for previously untreated locally recurrent inoperable or metastatic triple-negative breast cancer*

(KEYNOTE-355): a randomised, placebo-controlled, double-blind, phase 3 clinical trial. Lancet, 2020. **396**(10265): p. 1817-1828.

89. Tutt, A.N.J., et al., *Adjuvant Olaparib for Patients with BRCA1- or BRCA2-Mutated Breast Cancer.* N Engl J Med, 2021. **384**(25): p. 2394-2405.
90. Schmid, P., et al., *Atezolizumab plus nab-paclitaxel as first-line treatment for unresectable, locally advanced or metastatic triple-negative breast cancer (IMpassion130): updated efficacy results from a randomised, double-blind, placebo-controlled, phase 3 trial.* Lancet Oncol, 2020. **21**(1): p. 44-59.
91. Litton, J.K., et al., *Talazoparib in Patients with Advanced Breast Cancer and a Germline BRCA Mutation.* N Engl J Med, 2018. **379**(8): p. 753-763.
92. Miles, D.W., et al., *First-line bevacizumab in combination with chemotherapy for HER2-negative metastatic breast cancer: pooled and subgroup analyses of data from 2447 patients.* Ann Oncol, 2013. **24**(11): p. 2773-80.
93. Dent, R., et al., *Triple-negative breast cancer: clinical features and patterns of recurrence.* Clin Cancer Res, 2007. **13**(15 Pt 1): p. 4429-34.
94. Bahrami, A., et al., *The Therapeutic Potential of Targeting Tumor Microenvironment in Breast Cancer: Rational Strategies and Recent Progress.* J Cell Biochem, 2018. **119**(1): p. 111-122.
95. Anderson, N.M. and M.C. Simon, *The tumor microenvironment.* Curr Biol, 2020. **30**(16): p. R921-r925.
96. de Visser, K.E. and J.A. Joyce, *The evolving tumor microenvironment: From cancer initiation to metastatic outgrowth.* Cancer Cell, 2023. **41**(3): p. 374-403.
97. Krausgruber, T., et al., *Structural cells are key regulators of organ-specific immune responses.* Nature, 2020. **583**(7815): p. 296-302.

98. Lu, C., et al., *The role of innate immune cells in the tumor microenvironment and research progress in anti-tumor therapy.* Front Immunol, 2022. **13**: p. 1039260.

99. Lei, X., et al., *Immune cells within the tumor microenvironment: Biological functions and roles in cancer immunotherapy.* Cancer Lett, 2020. **470**: p. 126-133.

100. Gruosso, T., et al., *Spatially distinct tumor immune microenvironments stratify triple-negative breast cancers.* J Clin Invest, 2019. **129**(4): p. 1785-1800.

101. Savas, P., et al., *Single-cell profiling of breast cancer T cells reveals a tissue-resident memory subset associated with improved prognosis.* Nat Med, 2018. **24**(7): p. 986-993.

102. Gu-Trantien, C., et al., *CD4⁺ follicular helper T cell infiltration predicts breast cancer survival.* J Clin Invest, 2013. **123**(7): p. 2873-92.

103. Michea, P., et al., *Adjustment of dendritic cells to the breast-cancer microenvironment is subset specific.* Nat Immunol, 2018. **19**(8): p. 885-897.

104. Chung, W., et al., *Single-cell RNA-seq enables comprehensive tumour and immune cell profiling in primary breast cancer.* Nat Commun, 2017. **8**: p. 15081.

105. Zheng, C., et al., *Neutrophils in triple-negative breast cancer: an underestimated player with increasingly recognized importance.* Breast Cancer Res, 2023. **25**(1): p. 88.

106. Yu, J., et al., *Myeloid-derived suppressor cells suppress antitumor immune responses through IDO expression and correlate with lymph node metastasis in patients with breast cancer.* J Immunol, 2013. **190**(7): p. 3783-97.

107. Zhao, H., et al., *Identifying tumour microenvironment-related signature that correlates with prognosis and immunotherapy response in breast cancer.* Sci Data, 2023. **10**(1): p. 119.
108. Danenberg, E., et al., *Breast tumor microenvironment structures are associated with genomic features and clinical outcome.* Nat Genet, 2022. **54**(5): p. 660-669.
109. Diaz-Montero, C.M., et al., *Increased circulating myeloid-derived suppressor cells correlate with clinical cancer stage, metastatic tumor burden, and doxorubicin-cyclophosphamide chemotherapy.* Cancer Immunol Immunother, 2009. **58**(1): p. 49-59.
110. Jeong, H., et al., *Tumor-Associated Macrophages as Potential Prognostic Biomarkers of Invasive Breast Cancer.* J Breast Cancer, 2019. **22**(1): p. 38-51.
111. Stenström, J., I. Hedenfalk, and C. Hagerling, *Regulatory T lymphocyte infiltration in metastatic breast cancer-an independent prognostic factor that changes with tumor progression.* Breast Cancer Res, 2021. **23**(1): p. 27.
112. Mehraj, U., et al., *Tumor microenvironment promotes breast cancer chemoresistance.* Cancer Chemother Pharmacol, 2021. **87**(2): p. 147-158.
113. Denkert, C., et al., *Tumour-infiltrating lymphocytes and prognosis in different subtypes of breast cancer: a pooled analysis of 3771 patients treated with neoadjuvant therapy.* Lancet Oncol, 2018. **19**(1): p. 40-50.
114. Mehraj, U., et al., *The tumor microenvironment as driver of stemness and therapeutic resistance in breast cancer: New challenges and therapeutic opportunities.* Cell Oncol (Dordr), 2021. **44**(6): p. 1209-1229.
115. Wu, Q., et al., *Cancer-associated adipocytes: key players in breast cancer progression.* J Hematol Oncol, 2019. **12**(1): p. 95.

116. Mukherjee, A., A.J. Bilecz, and E. Lengyel, *The adipocyte microenvironment and cancer.* Cancer Metastasis Rev, 2022. **41**(3): p. 575-587.
117. Yang, D., et al., *Role of endothelial cells in tumor microenvironment.* Clin Transl Med, 2021. **11**(6): p. e450.
118. Fang, J., et al., *Exploring the crosstalk between endothelial cells, immune cells, and immune checkpoints in the tumor microenvironment: new insights and therapeutic implications.* Cell Death Dis, 2023. **14**(9): p. 586.
119. Kalluri, R., *The biology and function of fibroblasts in cancer.* Nat Rev Cancer, 2016. **16**(9): p. 582-98.
120. Chen, P.Y., et al., *Cancer-Associated Fibroblast Heterogeneity: A Factor That Cannot Be Ignored in Immune Microenvironment Remodeling.* Front Immunol, 2021. **12**: p. 671595.
121. Chen, Y., K.M. McAndrews, and R. Kalluri, *Clinical and therapeutic relevance of cancer-associated fibroblasts.* Nat Rev Clin Oncol, 2021. **18**(12): p. 792-804.
122. Houthuijzen, J.M. and J. Jonkers, *Cancer-associated fibroblasts as key regulators of the breast cancer tumor microenvironment.* Cancer Metastasis Rev, 2018. **37**(4): p. 577-597.
123. Kidd, S., et al., *Origins of the tumor microenvironment: quantitative assessment of adipose-derived and bone marrow-derived stroma.* PLoS One, 2012. **7**(2): p. e30563.
124. Karnoub, A.E., et al., *Mesenchymal stem cells within tumour stroma promote breast cancer metastasis.* Nature, 2007. **449**(7162): p. 557-63.
125. Dirat, B., et al., *Cancer-associated adipocytes exhibit an activated phenotype and contribute to breast cancer invasion.* Cancer Res, 2011. **71**(7): p. 2455-65.

126. Zeisberg, E.M., et al., *Discovery of endothelial to mesenchymal transition as a source for carcinoma-associated fibroblasts.* Cancer Res, 2007. **67**(21): p. 10123-8.
127. Hosaka, K., et al., *Pericyte-fibroblast transition promotes tumor growth and metastasis.* Proc Natl Acad Sci U S A, 2016. **113**(38): p. E5618-27.
128. Nair, N., et al., *A cancer stem cell model as the point of origin of cancer-associated fibroblasts in tumor microenvironment.* Sci Rep, 2017. **7**(1): p. 6838.
129. Avgustinova, A., et al., *Tumour cell-derived Wnt7a recruits and activates fibroblasts to promote tumour aggressiveness.* Nat Commun, 2016. **7**: p. 10305.
130. Kojima, Y., et al., *Autocrine TGF-beta and stromal cell-derived factor-1 (SDF-1) signaling drives the evolution of tumor-promoting mammary stromal myofibroblasts.* Proc Natl Acad Sci U S A, 2010. **107**(46): p. 20009-14.
131. Sharon, Y., et al., *Tumor-derived osteopontin reprograms normal mammary fibroblasts to promote inflammation and tumor growth in breast cancer.* Cancer Res, 2015. **75**(6): p. 963-73.
132. Li, K., et al., *Survivin in breast cancer-derived exosomes activates fibroblasts by up-regulating SOD1, whose feedback promotes cancer proliferation and metastasis.* J Biol Chem, 2020. **295**(40): p. 13737-13752.
133. Baroni, S., et al., *Exosome-mediated delivery of miR-9 induces cancer-associated fibroblast-like properties in human breast fibroblasts.* Cell Death Dis, 2016. **7**(7): p. e2312.
134. Vu, L.T., et al., *Tumor-secreted extracellular vesicles promote the activation of cancer-associated fibroblasts via the transfer of microRNA-125b.* J Extracell Vesicles, 2019. **8**(1): p. 1599680.

135. Chatterjee, A., et al., *MicroRNA-222 reprogrammed cancer-associated fibroblasts enhance growth and metastasis of breast cancer.* Br J Cancer, 2019. **121**(8): p. 679-689.

136. Dong, H., et al., *Breast cancer-derived exosomal lncRNA SNHG14 induces normal fibroblast activation to cancer-associated fibroblasts via the EBF1/FAM171A1 axis.* Breast Cancer, 2023. **30**(6): p. 1028-1040.

137. Raz, Y., et al., *Bone marrow-derived fibroblasts are a functionally distinct stromal cell population in breast cancer.* J Exp Med, 2018. **215**(12): p. 3075-3093.

138. Jotzu, C., et al., *Adipose tissue derived stem cells differentiate into carcinoma-associated fibroblast-like cells under the influence of tumor derived factors.* Cell Oncol (Dordr), 2011. **34**(1): p. 55-67.

139. Cho, J.A., et al., *Exosomes from breast cancer cells can convert adipose tissue-derived mesenchymal stem cells into myofibroblast-like cells.* Int J Oncol, 2012. **40**(1): p. 130-8.

140. Weber, C.E., et al., *Osteopontin mediates an MZF1-TGF-β1-dependent transformation of mesenchymal stem cells into cancer-associated fibroblasts in breast cancer.* Oncogene, 2015. **34**(37): p. 4821-33.

141. Bochet, L., et al., *Adipocyte-derived fibroblasts promote tumor progression and contribute to the desmoplastic reaction in breast cancer.* Cancer Res, 2013. **73**(18): p. 5657-68.

142. Sahai, E., et al., *A framework for advancing our understanding of cancer-associated fibroblasts.* Nat Rev Cancer, 2020. **20**(3): p. 174-186.

143. Nurmik, M., et al., *In search of definitions: Cancer-associated fibroblasts and their markers.* Int J Cancer, 2020. **146**(4): p. 895-905.

144. Bartoschek, M., et al., *Spatially and functionally distinct subclasses of breast cancer-associated fibroblasts revealed by single cell RNA sequencing.* Nat Commun, 2018. **9**(1): p. 5150.
145. Wu, X., et al., *Integrated analysis of single-cell RNA-seq and bulk RNA-seq unravels the heterogeneity of cancer-associated fibroblasts in TNBC.* Aging (Albany NY), 2023. **15**(21): p. 12674-12697.
146. Wu, S.Z., et al., *Stromal cell diversity associated with immune evasion in human triple-negative breast cancer.* Embo j, 2020. **39**(19): p. e104063.
147. Bagger, M.M., et al., *Evidence of steady-state fibroblast subtypes in the normal human breast as cells-of-origin for perturbed-state fibroblasts in breast cancer.* Breast Cancer Res, 2024. **26**(1): p. 11.
148. Ma, C., et al., *Pan-cancer spatially resolved single-cell analysis reveals the crosstalk between cancer-associated fibroblasts and tumor microenvironment.* Mol Cancer, 2023. **22**(1): p. 170.
149. Houthuijzen, J.M., et al., *CD26-negative and CD26-positive tissue-resident fibroblasts contribute to functionally distinct CAF subpopulations in breast cancer.* Nat Commun, 2023. **14**(1): p. 183.
150. Xu, A., et al., *Identification of prognostic cancer-associated fibroblast markers in luminal breast cancer using weighted gene co-expression network analysis.* Front Oncol, 2023. **13**: p. 1191660.
151. Wang, M., et al., *Identification of Cancer-Associated Fibroblast Subtype of Triple-Negative Breast Cancer.* J Oncol, 2022. **2022**: p. 6452636.
152. Wang, Y., et al., *A novel signature based on cancer-associated fibroblast genes to predict prognosis, immune feature, and*

therapeutic response in breast cancer. Aging (Albany NY), 2023. **15**(9): p. 3480-3497.

153. Park, S.Y., H.M. Kim, and J.S. Koo, *Differential expression of cancer-associated fibroblast-related proteins according to molecular subtype and stromal histology in breast cancer.* Breast Cancer Res Treat, 2015. **149**(3): p. 727-41.
154. Lee, J.H., H.M. Kim, and J.S. Koo, *Differential Expression of Cancer-Associated Fibroblast-Related Proteins in Ductal Carcinoma in situ According to Molecular Subtype and Stromal Histology.* Pathobiology, 2018. **85**(5-6): p. 311-321.
155. Tchou, J., et al., *Human breast cancer associated fibroblasts exhibit subtype specific gene expression profiles.* BMC Med Genomics, 2012. **5**: p. 39.
156. Fang, W.B., et al., *Transcriptome analysis reveals differences in cell cycle, growth and migration related genes that distinguish fibroblasts derived from pre-invasive and invasive breast cancer.* Front Oncol, 2023. **13**: p. 1130911.
157. Friedman, G., et al., *Cancer-associated fibroblast compositions change with breast cancer progression linking the ratio of S100A4(+) and PDPN(+) CAFs to clinical outcome.* Nat Cancer, 2020. **1**(7): p. 692-708.
158. Kim, H.M., W.H. Jung, and J.S. Koo, *Expression of cancer-associated fibroblast related proteins in metastatic breast cancer: an immunohistochemical analysis.* J Transl Med, 2015. **13**: p. 222.
159. Costa, A., et al., *Fibroblast Heterogeneity and Immunosuppressive Environment in Human Breast Cancer.* Cancer Cell, 2018. **33**(3): p. 463-479.e10.
160. Kieffer, Y., et al., *Single-Cell Analysis Reveals Fibroblast Clusters Linked to Immunotherapy Resistance in Cancer.* Cancer Discov, 2020. **10**(9): p. 1330-1351.

161. Pelon, F., et al., *Cancer-associated fibroblast heterogeneity in axillary lymph nodes drives metastases in breast cancer through complementary mechanisms.* Nat Commun, 2020. **11**(1): p. 404.
162. Bauer, M., et al., *Heterogeneity of gene expression in stromal fibroblasts of human breast carcinomas and normal breast.* Oncogene, 2010. **29**(12): p. 1732-40.
163. Peng, Q., et al., *Biological characteristics and genetic heterogeneity between carcinoma-associated fibroblasts and their paired normal fibroblasts in human breast cancer.* PLoS One, 2013. **8**(4): p. e60321.
164. Ping, Q., et al., *Cancer-associated fibroblasts: overview, progress, challenges, and directions.* Cancer Gene Ther, 2021. **28**(9): p. 984-999.
165. Pickup, M.W., J.K. Mouw, and V.M. Weaver, *The extracellular matrix modulates the hallmarks of cancer.* EMBO Rep, 2014. **15**(12): p. 1243-53.
166. Robertson, C., *The extracellular matrix in breast cancer predicts prognosis through composition, splicing, and crosslinking.* Exp Cell Res, 2016. **343**(1): p. 73-81.
167. Levental, K.R., et al., *Matrix crosslinking forces tumor progression by enhancing integrin signaling.* Cell, 2009. **139**(5): p. 891-906.
168. Tsunoda, T., et al., *Involvement of large tenascin-C splice variants in breast cancer progression.* Am J Pathol, 2003. **162**(6): p. 1857-67.
169. Dumont, N., et al., *Breast fibroblasts modulate early dissemination, tumorigenesis, and metastasis through alteration of extracellular matrix characteristics.* Neoplasia, 2013. **15**(3): p. 249-62.

170. Erdogan, B., et al., *Cancer-associated fibroblasts promote directional cancer cell migration by aligning fibronectin.* J Cell Biol, 2017. **216**(11): p. 3799-3816.
171. Oskarsson, T., et al., *Breast cancer cells produce tenascin C as a metastatic niche component to colonize the lungs.* Nat Med, 2011. **17**(7): p. 867-74.
172. Pein, M., et al., *Metastasis-initiating cells induce and exploit a fibroblast niche to fuel malignant colonization of the lungs.* Nat Commun, 2020. **11**(1): p. 1494.
173. De Francesco, E.M., et al., *HIF-1α/GPER signaling mediates the expression of VEGF induced by hypoxia in breast cancer associated fibroblasts (CAFs).* Breast Cancer Res, 2013. **15**(4): p. R64.
174. Ren, J., et al., *GPER in CAFs regulates hypoxia-driven breast cancer invasion in a CTGF-dependent manner.* Oncol Rep, 2015. **33**(4): p. 1929-37.
175. Al-Jomah, N., F.H. Al-Mohanna, and A. Aboussekhra, *Tocilizumab suppresses the pro-carcinogenic effects of breast cancer-associated fibroblasts through inhibition of the STAT3/AUF1 pathway.* Carcinogenesis, 2021. **42**(12): p. 1439-1448.
176. Lee, C.M., et al., *BRCA1 mutation promotes sprouting angiogenesis in inflammatory cancer-associated fibroblast of triple-negative breast cancer.* Cell Death Discov, 2024. **10**(1): p. 5.
177. O'Connell, J.T., et al., *VEGF-A and Tenascin-C produced by S100A4+ stromal cells are important for metastatic colonization.* Proc Natl Acad Sci U S A, 2011. **108**(38): p. 16002-7.
178. Orimo, A., et al., *Stromal fibroblasts present in invasive human breast carcinomas promote tumor growth and angiogenesis through elevated SDF-1/CXCL12 secretion.* Cell, 2005. **121**(3): p. 335-48.

179. Wan, X., et al., *FOSL2 promotes VEGF-independent angiogenesis by transcriptionnally activating Wnt5a in breast cancer-associated fibroblasts.* Theranostics, 2021. **11**(10): p. 4975-4991.
180. Ahirwar, D.K., et al., *Fibroblast-derived CXCL12 promotes breast cancer metastasis by facilitating tumor cell intravasation.* Oncogene, 2018. **37**(32): p. 4428-4442.
181. Sewell-Loftin, M.K., et al., *Cancer-associated fibroblasts support vascular growth through mechanical force.* Sci Rep, 2017. **7**(1): p. 12574.
182. An, Y., et al., *Crosstalk between cancer-associated fibroblasts and immune cells in cancer.* J Cell Mol Med, 2020. **24**(1): p. 13-24.
183. Kim, H.S., et al., *Cancer-Associated Fibroblasts Together with a Decline in CD8+ T Cells Predict a Worse Prognosis for Breast Cancer Patients.* Ann Surg Oncol, 2024. **31**(3): p. 2114-2126.
184. Liao, D., et al., *Cancer associated fibroblasts promote tumor growth and metastasis by modulating the tumor immune microenvironment in a 4T1 murine breast cancer model.* PLoS One, 2009. **4**(11): p. e7965.
185. Li, A., et al., *Histone deacetylase 6 regulates the immunosuppressive properties of cancer-associated fibroblasts in breast cancer through the STAT3-COX2-dependent pathway.* Oncogene, 2018. **37**(45): p. 5952-5966.
186. Zheng, S., et al., *Landscape of cancer-associated fibroblasts identifies the secreted biglycan as a protumor and immunosuppressive factor in triple-negative breast cancer.* Oncoimmunology, 2022. **11**(1): p. 2020984.
187. Gok Yavuz, B., et al., *Cancer associated fibroblasts sculpt tumour microenvironment by recruiting monocytes and inducing immunosuppressive PD-1(+) TAMs.* Sci Rep, 2019. **9**(1): p. 3172.

188. Timperi, E., et al., *Lipid-Associated Macrophages Are Induced by Cancer-Associated Fibroblasts and Mediate Immune Suppression in Breast Cancer.* Cancer Res, 2022. **82**(18): p. 3291-3306.
189. Allaoui, R., et al., *Cancer-associated fibroblast-secreted CXCL16 attracts monocytes to promote stroma activation in triple-negative breast cancers.* Nat Commun, 2016. **7**: p. 13050.
190. Silzle, T., et al., *Tumor-associated fibroblasts recruit blood monocytes into tumor tissue.* Eur J Immunol, 2003. **33**(5): p. 1311-20.
191. Qian, B.Z., et al., *CCL2 recruits inflammatory monocytes to facilitate breast-tumour metastasis.* Nature, 2011. **475**(7355): p. 222-5.
192. Pestell, T.G., et al., *Stromal cyclin D1 promotes heterotypic immune signaling and breast cancer growth.* Oncotarget, 2017. **8**(47): p. 81754-81775.
193. Chen, I.X., et al., *Blocking CXCR4 alleviates desmoplasia, increases T-lymphocyte infiltration, and improves immunotherapy in metastatic breast cancer.* Proc Natl Acad Sci U S A, 2019. **116**(10): p. 4558-4566.
194. Cohen, N., et al., *Fibroblasts drive an immunosuppressive and growth-promoting microenvironment in breast cancer via secretion of Chitinase 3-like 1.* Oncogene, 2017. **36**(31): p. 4457-4468.
195. Thomas, D.A. and J. Massagué, *TGF-beta directly targets cytotoxic T cell functions during tumor evasion of immune surveillance.* Cancer Cell, 2005. **8**(5): p. 369-80.
196. Acerbi, I., et al., *Human breast cancer invasion and aggression correlates with ECM stiffening and immune cell infiltration.* Integr Biol (Camb), 2015. **7**(10): p. 1120-34.

197. Fridlender, Z.G., et al., *Polarization of tumor-associated neutrophil phenotype by TGF-beta: "N1" versus "N2" TAN.* Cancer Cell, 2009. **16**(3): p. 183-94.

198. Dou, D., et al., *Cancer-Associated Fibroblasts-Derived Exosomes Suppress Immune Cell Function in Breast Cancer via the miR-92/PD-L1 Pathway.* Front Immunol, 2020. **11**: p. 2026.

199. Cremasco, V., et al., *FAP Delineates Heterogeneous and Functionally Divergent Stromal Cells in Immune-Excluded Breast Tumors.* Cancer Immunol Res, 2018. **6**(12): p. 1472-1485.

200. Hu, M., et al., *Regulation of in situ to invasive breast carcinoma transition.* Cancer Cell, 2008. **13**(5): p. 394-406.

201. Osuala, K.O., et al., *Il-6 signaling between ductal carcinoma in situ cells and carcinoma-associated fibroblasts mediates tumor cell growth and migration.* BMC Cancer, 2015. **15**: p. 584.

202. Bernard, S., et al., *CXCL1 Derived from Mammary Fibroblasts Promotes Progression of Mammary Lesions to Invasive Carcinoma through CXCR2 Dependent Mechanisms.* J Mammary Gland Biol Neoplasia, 2018. **23**(4): p. 249-267.

203. Jin, K., N.B. Pandey, and A.S. Popel, *Crosstalk between stromal components and tumor cells of TNBC via secreted factors enhances tumor growth and metastasis.* Oncotarget, 2017. **8**(36): p. 60210-60222.

204. Santolla, M.F., et al., *The AGEs/RAGE Transduction Signaling Prompts IL-8/CXCR1/2-Mediated Interaction between Cancer-Associated Fibroblasts (CAFs) and Breast Cancer Cells.* Cells, 2022. **11**(15): p. 2402.

205. Zellmer, V.R., et al., *Tumor-induced Stromal STAT1 Accelerates Breast Cancer via Deregulating Tissue Homeostasis.* Mol Cancer Res, 2017. **15**(5): p. 585-597.

206. Boesch, M., et al., *Interleukin 7-expressing fibroblasts promote breast cancer growth through sustenance of tumor cell stemness.* Oncoimmunology, 2018. **7**(4): p. e1414129.

207. Pinto, M.P., et al., *Malignant stroma increases luminal breast cancer cell proliferation and angiogenesis through platelet-derived growth factor signaling.* BMC Cancer, 2014. **14**: p. 735.

208. Gao, M.Q., et al., *Human breast cancer-associated fibroblasts enhance cancer cell proliferation through increased TGF-α cleavage by ADAM17.* Cancer Lett, 2013. **336**(1): p. 240-6.

209. Suh, J., et al., *Fibroblast growth factor-2, derived from cancer-associated fibroblasts, stimulates growth and progression of human breast cancer cells via FGFR1 signaling.* Mol Carcinog, 2020. **59**(9): p. 1028-1040.

210. Suh, J., et al., *Nuclear Localization of Fibroblast Growth Factor Receptor 1 in Breast Cancer Cells Interacting with Cancer Associated Fibroblasts.* J Cancer Prev, 2022. **27**(1): p. 68-76.

211. Tyan, S.W., et al., *Breast cancer cells induce cancer-associated fibroblasts to secrete hepatocyte growth factor to enhance breast tumorigenesis.* PLoS One, 2011. **6**(1): p. e15313.

212. Wang, B., et al., *Cancer-Associated Fibroblasts Promote Radioresistance of Breast Cancer Cells via the HGF/c-Met Signaling Pathway.* Int J Radiat Oncol Biol Phys, 2023. **116**(3): p. 640-654.

213. Nagel, A., et al., *ERα36-High Cancer-Associated Fibroblasts as an Unfavorable Factor in Triple-Negative Breast Cancer.* Cancers (Basel), 2022. **14**(8): p. 2005.

214. Al-Nasrallah, H.K., M.M. Al-Ansari, and A. Aboussekhra, *Osteoprotegerin (OPG) Upregulation Activates Breast Stromal Fibroblasts and Enhances Their Pro-Carcinogenic Effects through the STAT3/IL-6 Signaling.* Cells, 2022. **11**(21): p. 3369.

215. Avalle, L., et al., *STAT3 induces breast cancer growth via ANGPTL4, MMP13 and STC1 secretion by cancer associated fibroblasts.* Oncogene, 2022. **41**(10): p. 1456-1467.
216. Tsuyada, A., et al., *CCL2 mediates cross-talk between cancer cells and stromal fibroblasts that regulates breast cancer stem cells.* Cancer Res, 2012. **72**(11): p. 2768-79.
217. Zhao, X.L., et al., *High-mobility group box 1 released by autophagic cancer-associated fibroblasts maintains the stemness of luminal breast cancer cells.* J Pathol, 2017. **243**(3): p. 376-389.
218. Dang, T.T., A.M. Prechtl, and G.W. Pearson, *Breast cancer subtype-specific interactions with the microenvironment dictate mechanisms of invasion.* Cancer Res, 2011. **71**(21): p. 6857-66.
219. Yu, Y., et al., *Cancer-associated fibroblasts induce epithelial-mesenchymal transition of breast cancer cells through paracrine TGF-β signalling.* Br J Cancer, 2014. **110**(3): p. 724-32.
220. Takai, K., et al., *Targeting the cancer-associated fibroblasts as a treatment in triple-negative breast cancer.* Oncotarget, 2016. **7**(50): p. 82889-82901.
221. Ren, Y., et al., *Paracrine and epigenetic control of CAF-induced metastasis: the role of HOTAIR stimulated by TGF-ß1 secretion.* Mol Cancer, 2018. **17**(1): p. 5.
222. Soon, P.S., et al., *Breast cancer-associated fibroblasts induce epithelial-to-mesenchymal transition in breast cancer cells.* Endocr Relat Cancer, 2013. **20**(1): p. 1-12.
223. Dvorak, K.M., et al., *Carcinoma associated fibroblasts (CAFs) promote breast cancer motility by suppressing mammalian Diaphanous-related formin-2 (mDia2).* PLoS One, 2018. **13**(3): p. e0195278.
224. Farmaki, E., et al., *A CCL8 gradient drives breast cancer cell dissemination.* Oncogene, 2016. **35**(49): p. 6309-6318.

225. Liu, Y., et al., *Down-regulation of miR-29b in carcinoma associated fibroblasts promotes cell growth and metastasis of breast cancer.* Oncotarget, 2017. **8**(24): p. 39559-39570.
226. Chan, T.S., et al., *Metronomic chemotherapy prevents therapy-induced stromal activation and induction of tumor-initiating cells.* J Exp Med, 2016. **213**(13): p. 2967-2988.
227. Studebaker, A.W., et al., *Fibroblasts isolated from common sites of breast cancer metastasis enhance cancer cell growth rates and invasiveness in an interleukin-6-dependent manner.* Cancer Res, 2008. **68**(21): p. 9087-95.
228. Louault, K., et al., *Interactions between cancer-associated fibroblasts and tumor cells promote MCL-1 dependency in estrogen receptor-positive breast cancers.* Oncogene, 2019. **38**(17): p. 3261-3273.
229. Liao, H., et al., *Melatonin blunts the tumor-promoting effect of cancer-associated fibroblasts by reducing IL-8 expression and reversing epithelial-mesenchymal transition.* Int Immunopharmacol, 2023. **119**: p. 110194.
230. Wen, S., et al., *Cancer-associated fibroblast (CAF)-derived IL32 promotes breast cancer cell invasion and metastasis via integrin β3-p38 MAPK signalling.* Cancer Lett, 2019. **442**: p. 320-332.
231. Ershaid, N., et al., *NLRP3 inflammasome in fibroblasts links tissue damage with inflammation in breast cancer progression and metastasis.* Nat Commun, 2019. **10**(1): p. 4375.
232. Muchlińska, A., et al., *Alpha-smooth muscle actin-positive cancer-associated fibroblasts secreting osteopontin promote growth of luminal breast cancer.* Cell Mol Biol Lett, 2022. **27**(1): p. 45.
233. Xu, K., et al., *The fibroblast Tiam1-osteopontin pathway modulates breast cancer invasion and metastasis.* Breast Cancer Res, 2016. **18**(1): p. 14.

234. Tyan, S.W., et al., *Breast cancer cells induce stromal fibroblasts to secrete ADAMTS1 for cancer invasion through an epigenetic change.* PLoS One, 2012. **7**(4): p. e35128.

235. Dittmer, A. and J. Dittmer, *A CAF-Fueled TIMP-1/CD63/ITGB1/STAT3 Feedback Loop Promotes Migration and Growth of Breast Cancer Cells.* Cancers (Basel), 2022. **14**(20): p. 4983.

236. Ren, J., et al., *Cancer-associated fibroblast-derived Gremlin 1 promotes breast cancer progression.* Breast Cancer Res, 2019. **21**(1): p. 109.

237. Li, H., et al., *Cancer-associated fibroblast-secreted collagen triple helix repeat containing-1 promotes breast cancer cell migration, invasiveness and epithelial-mesenchymal transition by activating the Wnt/β-catenin pathway.* Oncol Lett, 2021. **22**(6): p. 814.

238. Adhikari, E., et al., *Brain metastasis-associated fibroblasts secrete fucosylated PVR/CD155 that induces breast cancer invasion.* Cell Rep, 2023. **42**(12): p. 113463.

239. Pavlides, S., et al., *The reverse Warburg effect: aerobic glycolysis in cancer associated fibroblasts and the tumor stroma.* Cell Cycle, 2009. **8**(23): p. 3984-4001.

240. Demircioglu, F., et al., *Cancer associated fibroblast FAK regulates malignant cell metabolism.* Nat Commun, 2020. **11**(1): p. 1290.

241. Guido, C., et al., *Metabolic reprogramming of cancer-associated fibroblasts by TGF-β drives tumor growth: connecting TGF-β signaling with "Warburg-like" cancer metabolism and L-lactate production.* Cell Cycle, 2012. **11**(16): p. 3019-35.

242. Yan, W., et al., *Cancer-cell-secreted exosomal miR-105 promotes tumour growth through the MYC-dependent metabolic reprogramming of stromal cells.* Nat Cell Biol, 2018. **20**(5): p. 597-609.

243. Becker, L.M., et al., *Epigenetic Reprogramming of Cancer-Associated Fibroblasts Deregulates Glucose Metabolism and Facilitates Progression of Breast Cancer.* Cell Rep, 2020. **31**(9): p. 107701.

244. Bonuccelli, G., et al., *Ketones and lactate "fuel" tumor growth and metastasis: Evidence that epithelial cancer cells use oxidative mitochondrial metabolism.* Cell Cycle, 2010. **9**(17): p. 3506-14.

245. Martinez-Outschoorn, U.E., et al., *Ketones and lactate increase cancer cell "stemness," driving recurrence, metastasis and poor clinical outcome in breast cancer: achieving personalized medicine via Metabolo-Genomics.* Cell Cycle, 2011. **10**(8): p. 1271-86.

246. Yu, T., et al., *Cytoplasmic GPER translocation in cancer-associated fibroblasts mediates cAMP/PKA/CREB/glycolytic axis to confer tumor cells with multidrug resistance.* Oncogene, 2017. **36**(15): p. 2131-2145.

247. Sun, K., et al., *Oxidized ATM-mediated glycolysis enhancement in breast cancer-associated fibroblasts contributes to tumor invasion through lactate as metabolic coupling.* EBioMedicine, 2019. **41**: p. 370-383.

248. Yi, Y., et al., *Tumor-Derived Exosomal Non-Coding RNAs: The Emerging Mechanisms and Potential Clinical Applications in Breast Cancer.* Front Oncol, 2021. **11**: p. 738945.

249. Donnarumma, E., et al., *Cancer-associated fibroblasts release exosomal microRNAs that dictate an aggressive phenotype in breast cancer.* Oncotarget, 2017. **8**(12): p. 19592-19608.

250. Boelens, M.C., et al., *Exosome transfer from stromal to breast cancer cells regulates therapy resistance pathways.* Cell, 2014. **159**(3): p. 499-513.

251. Luga, V., et al., *Exosomes mediate stromal mobilization of autocrine Wnt-PCP signaling in breast cancer cell migration.* Cell, 2012. **151**(7): p. 1542-56.
252. Tao, S., et al., *Extracellular vesicles released by hypoxia-induced tumor-associated fibroblasts impart chemoresistance to breast cancer cells via long noncoding RNA H19 delivery.* Faseb j, 2024. **38**(2): p. e23165.
253. Farmer, P., et al., *A stroma-related gene signature predicts resistance to neoadjuvant chemotherapy in breast cancer.* Nat Med, 2009. **15**(1): p. 68-74.
254. Li, C., et al., *Integrating single-cell and bulk transcriptomic analyses to develop a cancer-associated fibroblast-derived biomarker for predicting prognosis and therapeutic response in breast cancer.* Front Immunol, 2023. **14**: p. 1307588.
255. Brechbuhl, H.M., et al., *Fibroblast Subtypes Regulate Responsiveness of Luminal Breast Cancer to Estrogen.* Clin Cancer Res, 2017. **23**(7): p. 1710-1721.
256. Rivas, E.I., et al., *Targeted immunotherapy against distinct cancer-associated fibroblasts overcomes treatment resistance in refractory HER2+ breast tumors.* Nat Commun, 2022. **13**(1): p. 5310.
257. Giussani, M., et al., *Tumor-extracellular matrix interactions: Identification of tools associated with breast cancer progression.* Semin Cancer Biol, 2015. **35**: p. 3-10.
258. Lin, C.H., et al., *Microenvironment rigidity modulates responses to the HER2 receptor tyrosine kinase inhibitor lapatinib via YAP and TAZ transcription factors.* Mol Biol Cell, 2015. **26**(22): p. 3946-53.
259. Yuan, J., et al., *Acquisition of epithelial-mesenchymal transition phenotype in the tamoxifen-resistant breast cancer cell: a new role for G protein-coupled estrogen receptor in mediating tamoxifen*

resistance through cancer-associated fibroblast-derived fibronectin and β1-integrin signaling pathway in tumor cells. Breast Cancer Res, 2015. **17**(1): p. 69.

260. Cui, Q., et al., *Upregulating MMP-1 in carcinoma-associated fibroblasts reduces the efficacy of Taxotere on breast cancer synergized by Collagen IV.* Oncol Lett, 2018. **16**(3): p. 3537-3544.
261. Miroshnychenko, D., et al., *Stroma-Mediated Breast Cancer Cell Proliferation Indirectly Drives Chemoresistance by Accelerating Tumor Recovery between Chemotherapy Cycles.* Cancer Res, 2023. **83**(22): p. 3681-3692.
262. Amornsupak, K., et al., *Cancer-associated fibroblasts induce high mobility group box 1 and contribute to resistance to doxorubicin in breast cancer cells.* BMC Cancer, 2014. **14**: p. 955.
263. Hogstrom, J.M., et al., *Simultaneous isolation of hormone receptor-positive breast cancer organoids and fibroblasts reveals stroma-mediated resistance mechanisms.* J Biol Chem, 2023. **299**(8): p. 105021.
264. Chuangchot, N., et al., *Enhancement of PD-L1-attenuated CAR-T cell function through breast cancer-associated fibroblasts-derived IL-6 signaling via STAT3/AKT pathways.* Breast Cancer Res, 2023. **25**(1): p. 86.
265. Guo, Z., et al., *Cancer-associated fibroblasts induce growth and radioresistance of breast cancer cells through paracrine IL-6.* Cell Death Discov, 2023. **9**(1): p. 6.
266. Nandi, A., et al., *Dll1-Mediated Notch Signaling Drives Tumor Cell Cross-talk with Cancer-Associated Fibroblasts to Promote Radioresistance in Breast Cancer.* Cancer Res, 2022. **82**(20): p. 3718-3733.

267. Fernández-Nogueira, P., et al., *Tumor-Associated Fibroblasts Promote HER2-Targeted Therapy Resistance through FGFR2 Activation.* Clin Cancer Res, 2020. **26**(6): p. 1432-1448.

268. Zervantonakis, I.K., et al., *Fibroblast-tumor cell signaling limits HER2 kinase therapy response via activation of MTOR and antiapoptotic pathways.* Proc Natl Acad Sci U S A, 2020. **117**(28): p. 16500-16508.

269. Du, R., et al., *PDPN positive CAFs contribute to HER2 positive breast cancer resistance to trastuzumab by inhibiting antibody-dependent NK cell-mediated cytotoxicity.* Drug Resist Updat, 2023. **68**: p. 100947.

270. Sansone, P., et al., *Packaging and transfer of mitochondrial DNA via exosomes regulate escape from dormancy in hormonal therapy-resistant breast cancer.* Proc Natl Acad Sci U S A, 2017. **114**(43): p. E9066-e9075.

271. Su, S., et al., *CD10(+)GPR77(+) Cancer-Associated Fibroblasts Promote Cancer Formation and Chemoresistance by Sustaining Cancer Stemness.* Cell, 2018. **172**(4): p. 841-856.e16.

272. Peiris-Pagès, M., F. Sotgia, and M.P. Lisanti, *Chemotherapy induces the cancer-associated fibroblast phenotype, activating paracrine Hedgehog-GLI signalling in breast cancer cells.* Oncotarget, 2015. **6**(13): p. 10728-45.

273. Al-Tweigeri, T., et al., *High AUF1 level in stromal fibroblasts promotes carcinogenesis and chemoresistance and predicts unfavorable prognosis among locally advanced breast cancer patients.* Breast Cancer Res, 2022. **24**(1): p. 46.

274. Cazet, A.S., et al., *Targeting stromal remodeling and cancer stem cell plasticity overcomes chemoresistance in triple negative breast cancer.* Nat Commun, 2018. **9**(1): p. 2897.

275. Joseph, T.M., et al., *Nanoparticles: Taking a Unique Position in Medicine.* Nanomaterials (Basel), 2023. **13**(3): p. 574.

276. Sim, S. and N.K. Wong, *Nanotechnology and its use in imaging and drug delivery* Biomed Rep, 2021. **14**(5): p. 42.

277. Rodríguez, F., et al., *Nano-Based Approved Pharmaceuticals for Cancer Treatment: Present and Future Challenges.* Biomolecules, 2022. **12**(6): p. 784.

278. Palazzolo, S., et al., *The Clinical Translation of Organic Nanomaterials for Cancer Therapy: A Focus on Polymeric Nanoparticles, Micelles, Liposomes and Exosomes.* Curr Med Chem, 2018. **25**(34): p. 4224-4268.

279. Yao, Y., et al., *Nanoparticle-Based Drug Delivery in Cancer Therapy and Its Role in Overcoming Drug Resistance.* Front Mol Biosci, 2020. **7**: p. 193.

280. Kipp, J.E., *The role of solid nanoparticle technology in the parenteral delivery of poorly water-soluble drugs.* Int J Pharm, 2004. **284**(1-2): p. 109-22.

281. Shi, D., et al., *To PEGylate or not to PEGylate: Immunological properties of nanomedicine's most popular component, polyethylene glycol and its alternatives.* Adv Drug Deliv Rev, 2022. **180**(1): p. 114079.

282. Mitchell, M.J., et al., *Engineering precision nanoparticles for drug delivery.* Nat Rev Drug Discov, 2021. **20**(2): p. 101-124.

283. Chen, Y., D.Y. Gao, and L. Huang, *In vivo delivery of miRNAs for cancer therapy: challenges and strategies.* Adv Drug Deliv Rev, 2015. **81**: p. 128-41.

284. Cheng, R. and H.A. Santos, *Smart Nanoparticle-Based Platforms for Regulating Tumor Microenvironment and Cancer Immunotherapy.* Adv Healthc Mater, 2023. **12**(8): p. e2202063.

285. Alshammari, B.H., et al., *Organic and inorganic nanomaterials: fabrication, properties and applications.* RSC Adv, 2023. **13**(20): p. 13735-13785.

286. Romero, G. and S.E. Moya, *Synthesis of organic nanoparticles*, in *Frontiers of nanoscience*. 2012, Elsevier. p. 115-141.

287. Sheoran, S., et al., *Lipid-based nanoparticles for treatment of cancer.* Heliyon, 2022. **8**(5): p. e09403.

288. Mehta, M., et al., *Lipid-Based Nanoparticles for Drug/Gene Delivery: An Overview of the Production Techniques and Difficulties Encountered in Their Industrial Development.* ACS Mater Au, 2023. **3**(6): p. 600-619.

289. Zhang, Z., et al., *Application of lipid-based nanoparticles in cancer immunotherapy.* Front Immunol, 2022. **13**: p. 967505.

290. Anselmo, A.C. and S. Mitragotri, *Nanoparticles in the clinic: An update.* Bioeng Transl Med, 2019. **4**(3): p. e10143.

291. O'Brien, M.E., et al., *Reduced cardiotoxicity and comparable efficacy in a phase III trial of pegylated liposomal doxorubicin HCl (CAELYX/Doxil) versus conventional doxorubicin for first-line treatment of metastatic breast cancer.* Ann Oncol, 2004. **15**(3): p. 440-9.

292. Batist, G., et al., *Reduced cardiotoxicity and preserved antitumor efficacy of liposome-encapsulated doxorubicin and cyclophosphamide compared with conventional doxorubicin and cyclophosphamide in a randomized, multicenter trial of metastatic breast cancer.* J Clin Oncol, 2001. **19**(5): p. 1444-54.

293. Elmowafy, M., et al., *Polymeric Nanoparticles for Delivery of Natural Bioactive Agents: Recent Advances and Challenges.* Polymers (Basel), 2023. **15**(5): p. 1123.

294. Xiao, X., et al., *Polymeric nanoparticles-Promising carriers for cancer therapy.* Front Bioeng Biotechnol, 2022. **10**: p. 1024143.

295. Zielińska, A., et al., *Polymeric Nanoparticles: Production, Characterization, Toxicology and Ecotoxicology.* Molecules, 2020. **25**(16): p. 3731.

296. Stevanović, M., et al., *Biomedical inorganic nanoparticles: preparation, properties, and perspectives*, in *Materials for Biomedical Engineering*. 2019, Elsevier. p. 1-46.

297. Hu, X., et al., *Multifunctional Gold Nanoparticles: A Novel Nanomaterial for Various Medical Applications and Biological Activities.* Front Bioeng Biotechnol, 2020. **8**: p. 990.

298. Cheng, J., et al., *Surface functionalized gold nanoparticles for drug delivery.* J Biomed Nanotechnol, 2013. **9**(8): p. 1362-9.

299. Mody, V.V., et al., *Introduction to metallic nanoparticles.* J Pharm Bioallied Sci, 2010. **2**(4): p. 282-9.

300. Arias, L.S., et al., *Iron Oxide Nanoparticles for Biomedical Applications: A Perspective on Synthesis, Drugs, Antimicrobial Activity, and Toxicity.* Antibiotics (Basel), 2018. **7**(2): p. 46.

301. Mandriota, G., et al., *Design and Application of Cisplatin-Loaded Magnetic Nanoparticle Clusters for Smart Chemotherapy.* ACS Appl Mater Interfaces, 2019. **11**(2): p. 1864-1875.

302. Basoglu, H., B. Goncu, and F. Akbas, *Magnetic nanoparticle-mediated gene therapy to induce Fas apoptosis pathway in breast cancer.* Cancer Gene Ther, 2018. **25**(5-6): p. 141-147.

303. Meng, J., et al., *LHRH-functionalized superparamagnetic iron oxide nanoparticles for breast cancer targeting and contrast enhancement in MRI.* Materials Science and Engineering: C, 2009. **29**(4): p. 1467-1479.

304. Wagner, A.M., et al., *Quantum dots in biomedical applications.* Acta Biomater, 2019. **94**: p. 44-63.

305. Jamieson, T., et al., *Biological applications of quantum dots.* Biomaterials, 2007. **28**(31): p. 4717-32.

306. Madani, S.Y., et al., *A new era of cancer treatment: carbon nanotubes as drug delivery tools.* Int J Nanomedicine, 2011. **6**: p. 2963-79.

307. Luo, E., et al., *The toxicity and pharmacokinetics of carbon nanotubes as an effective drug carrier.* Curr Drug Metab, 2013. **14**(8): p. 879-90.

308. Huang, Y., et al., *Silica nanoparticles: Biomedical applications and toxicity.* Biomed Pharmacother, 2022. **151**: p. 113053.

309. Slowing, II, et al., *Mesoporous silica nanoparticles as controlled release drug delivery and gene transfection carriers.* Adv Drug Deliv Rev, 2008. **60**(11): p. 1278-1288.

310. Garrido-Cano, I., et al., *Biocompatibility and internalization assessment of bare and functionalised mesoporous silica nanoparticles.* Microporous and Mesoporous Materials, 2021. **310**: p. 110593.

311. Yu, A., et al., *Recent Advances of Mesoporous Silica as a Platform for Cancer Immunotherapy.* Biosensors (Basel), 2022. **12**(2): p. 109.

312. Rajana, N., et al., *Multifunctional hybrid nanoparticles in diagnosis and therapy of breast cancer.* J Control Release, 2022. **352**: p. 1024-1047.

313. Butler, K.S., et al., *Protocells: Modular Mesoporous Silica Nanoparticle-Supported Lipid Bilayers for Drug Delivery.* Small, 2016. **12**(16): p. 2173-85.

314. Gajbhiye, K.R., et al., *Lipid polymer hybrid nanoparticles: a custom-tailored next-generation approach for cancer therapeutics.* Mol Cancer, 2023. **22**(1): p. 160.

315. Fang, R.H., et al., *Cell Membrane Coating Nanotechnology.* Adv Mater, 2018. **30**(23): p. e1706759.

316. Watermann, A. and J. Brieger, *Mesoporous Silica Nanoparticles as Drug Delivery Vehicles in Cancer.* Nanomaterials (Basel), 2017. **7**(7): p. 189.

317. Castillo, R.R., et al., *Advances in mesoporous silica nanoparticles for targeted stimuli-responsive drug delivery: an update.* Expert Opin Drug Deliv, 2019. **16**(4): p. 415-439.

318. Croissant, J.G., et al., *Mesoporous Silica and Organosilica Nanoparticles: Physical Chemistry, Biosafety, Delivery Strategies, and Biomedical Applications.* Adv Healthc Mater, 2018. **7**(4): p. 1700831.

319. Hoang Thi, T.T., et al., *Functionalized mesoporous silica nanoparticles and biomedical applications.* Mater Sci Eng C Mater Biol Appl, 2019. **99**: p. 631-656.

320. Slowing, I., B.G. Trewyn, and V.S. Lin, *Effect of surface functionalization of MCM-41-type mesoporous silica nanoparticles on the endocytosis by human cancer cells.* J Am Chem Soc, 2006. **128**(46): p. 14792-3.

321. Xu, B., et al., *Multifunctional mesoporous silica nanoparticles for biomedical applications.* Signal Transduct Target Ther, 2023. **8**(1): p. 435.

322. Ernsting, M.J., et al., *Factors controlling the pharmacokinetics, biodistribution and intratumoral penetration of nanoparticles.* J Control Release, 2013. **172**(3): p. 782-94.

323. Zhu, G.H., A.B.C. Gray, and H.K. Patra, *Nanomedicine: controlling nanoparticle clearance for translational success.* Trends Pharmacol Sci, 2022. **43**(9): p. 709-711.

324. Li, S.D. and L. Huang, *Nanoparticles evading the reticuloendothelial system: role of the supported bilayer.* Biochim Biophys Acta, 2009. **1788**(10): p. 2259-66.

325. Kalyane, D., et al., *Employment of enhanced permeability and retention effect (EPR): Nanoparticle-based precision tools for targeting of therapeutic and diagnostic agent in cancer.* Mater Sci Eng C Mater Biol Appl, 2019. **98**: p. 1252-1276.
326. Gao, Y., et al., *Simulation study of the effects of interstitial fluid pressure and blood flow velocity on transvascular transport of nanoparticles in tumor microenvironment.* Comput Methods Programs Biomed, 2020. **193**: p. 105493.
327. Tagami, T. and T. Ozeki, *Recent Trends in Clinical Trials Related to Carrier-Based Drugs.* J Pharm Sci, 2017. **106**(9): p. 2219-2226.
328. Jain, R.K. and T. Stylianopoulos, *Delivering nanomedicine to solid tumors.* Nat Rev Clin Oncol, 2010. **7**(11): p. 653-64.
329. Wu, D., et al., *Nanomedicine applications in the treatment of breast cancer: current state of the art.* Int J Nanomedicine, 2017. **12**: p. 5879-5892.
330. Torrisi, R., et al., *Phase II trial of combination of pegylated liposomal doxorubicin, cisplatin, and infusional 5-fluorouracil (CCF) plus trastuzumab as preoperative treatment for locally advanced and inflammatory breast cancer.* Clin Breast Cancer, 2010. **10**(6): p. 483-8.
331. Torrisi, R., et al., *Neoadjuvant pegylated liposomal doxorubicin in combination with cisplatin and infusional fluoruracil (CCF) with and without endocrine therapy in locally advanced primary or recurrent breast cancer.* Breast, 2011. **20**(1): p. 34-8.
332. Gil-Gil, M.J., et al., *Pegylated liposomal doxorubicin plus cyclophosphamide followed by paclitaxel as primary chemotherapy in elderly or cardiotoxicity-prone patients with high-risk breast cancer: results of the phase II CAPRICE study.* Breast Cancer Res Treat, 2015. **151**(3): p. 597-606.

333. Rau, K.M., et al., *Pegylated liposomal doxorubicin (Lipo-Dox®) combined with cyclophosphamide and 5-fluorouracil is effective and safe as salvage chemotherapy in taxane-treated metastatic breast cancer: an open-label, multi-center, non-comparative phase II study.* BMC Cancer, 2015. **15**: p. 423.

334. Gradishar, W.J., et al., *Phase III trial of nanoparticle albumin-bound paclitaxel compared with polyethylated castor oil-based paclitaxel in women with breast cancer.* J Clin Oncol, 2005. **23**(31): p. 7794-803.

335. Untch, M., et al., *Nab-paclitaxel versus solvent-based paclitaxel in neoadjuvant chemotherapy for early breast cancer (GeparSepto-GBG 69): a randomised, phase 3 trial.* Lancet Oncol, 2016. **17**(3): p. 345-356.

336. Nahleh, Z.A., et al., *SWOG S0800 (NCI CDR0000636131): addition of bevacizumab to neoadjuvant nab-paclitaxel with dose-dense doxorubicin and cyclophosphamide improves pathologic complete response (pCR) rates in inflammatory or locally advanced breast cancer.* Breast Cancer Res Treat, 2016. **158**(3): p. 485-95.

337. Tezuka, K., et al., *Phase I study of nanoparticle albumin-bound paclitaxel, carboplatin and trastuzumab in women with human epidermal growth factor receptor 2-overexpressing breast cancer.* Mol Clin Oncol, 2017. **6**(4): p. 534-538.

338. Xia, T., et al., *Polyethyleneimine coating enhances the cellular uptake of mesoporous silica nanoparticles and allows safe delivery of siRNA and DNA constructs.* ACS Nano, 2009. **3**(10): p. 3273-86.

339. Garrido-Cano, I., et al., *Delivery of miR-200c-3p Using Tumor-Targeted Mesoporous Silica Nanoparticles for Breast Cancer*

Therapy. ACS Appl Mater Interfaces, 2023. **15**(32): p. 38323-38334.

340. Garrido-Cano, I., et al., *miR-99a-5p modulates doxorubicin resistance via the COX-2/ABCG2 axis in triple-negative breast cancer: from the discovery to in vivo studies.* Cancer Commun (Lond), 2022. **42**(12): p. 1412-1416.
341. Ovais, M., et al., *Designing Stimuli-Responsive Upconversion Nanoparticles that Exploit the Tumor Microenvironment.* Adv Mater, 2020. **32**(22): p. e2000055.
342. Vander Heiden, M.G., L.C. Cantley, and C.B. Thompson, *Understanding the Warburg effect: the metabolic requirements of cell proliferation.* Science, 2009. **324**(5930): p. 1029-33.
343. Kanamala, M., et al., *Mechanisms and biomaterials in pH-responsive tumour targeted drug delivery: A review.* Biomaterials, 2016. **85**: p. 152-67.
344. Wang, C., et al., *Investigation of endosome and lysosome biology by ultra pH-sensitive nanoprobes.* Adv Drug Deliv Rev, 2017. **113**: p. 87-96.
345. Shen, Q., et al., *A tumor microenvironment (TME)-responsive nanoplatform for systemic saporin delivery and effective breast cancer therapy.* Chem Commun (Camb), 2021. **57**(20): p. 2563-2566.
346. Gong, C., et al., *Regulating the immunosuppressive tumor microenvironment to enhance breast cancer immunotherapy using pH-responsive hybrid membrane-coated nanoparticles.* J Nanobiotechnology, 2021. **19**(1): p. 58.
347. Liu, Y., et al., *Dual pH-responsive multifunctional nanoparticles for targeted treatment of breast cancer by combining immunotherapy and chemotherapy.* Acta Biomater, 2018. **66**: p. 310-324.

348. Panieri, E. and M.M. Santoro, *ROS homeostasis and metabolism: a dangerous liason in cancer cells.* Cell Death Dis, 2016. **7**(6): p. e2253.

349. Glass, S.B., et al., *Redox Potential and ROS-Mediated Nanomedicines for Improving Cancer Therapy.* Antioxid Redox Signal, 2019. **30**(5): p. 747-761.

350. Yang, N., et al., *Recent Advances in Tumor Microenvironment Hydrogen Peroxide-Responsive Materials for Cancer Photodynamic Therapy.* Nanomicro Lett, 2020. **12**(1): p. 15.

351. Zhang, Z., et al., *ROS-Responsive and active targeted drug delivery based on conjugated polymer nanoparticles for synergistic chemo-/photodynamic therapy.* J Mater Chem B, 2021. **9**(9): p. 2240-2248.

352. Qin, Y., et al., *Self-delivered supramolecular nanomedicine with transformable shape for ferrocene-amplified photodynamic therapy of breast cancer and bone metastases.* Advanced Functional Materials, 2021. **31**(42): p. 2104645.

353. Zhang, J., et al., *Fenton-reaction-stimulative nanoparticles decorated with a reactive-oxygen-species (ROS)-responsive molecular switch for ROS amplification and triple negative breast cancer therapy.* J Mater Chem B, 2019. **7**(45): p. 7141-7151.

354. Wan, W.J., et al., *Doxorubicin and siRNA-PD-L1 co-delivery with T7 modified ROS-sensitive nanoparticles for tumor chemoimmunotherapy.* Int J Pharm, 2019. **566**: p. 731-744.

355. Jian, H., et al., *Tumor microcalcification-mediated relay drug delivery for photodynamic immunotherapy of breast cancer.* Acta Biomater, 2022. **140**: p. 518-529.

356. Yin, T., et al., *Co-delivery of hydrophobic paclitaxel and hydrophilic AURKA specific siRNA by redox-sensitive micelles for effective treatment of breast cancer.* Biomaterials, 2015. **61**: p. 10-25.

357. Chung, C.H., et al., *Fucoidan-based, tumor-activated nanoplatform for overcoming hypoxia and enhancing photodynamic therapy and antitumor immunity.* Biomaterials, 2020. **257**: p. 120227.

358. Liu, D., et al., *Redox-Activated Porphyrin-Based Liposome Remote-Loaded with Indoleamine 2,3-Dioxygenase (IDO) Inhibitor for Synergistic Photoimmunotherapy through Induction of Immunogenic Cell Death and Blockage of IDO Pathway.* Nano Lett, 2019. **19**(10): p. 6964-6976.

359. Li, K., et al., *Engineering of Cascade-Responsive Nanoplatform to Inhibit Lactate Efflux for Enhanced Tumor Chemo-Immunotherapy.* ACS Nano, 2020. **14**(10): p. 14164-14180.

360. Yang, X., et al., *Tumor microenvironment-responsive dual drug dimer-loaded pegylated bilirubin nanoparticles for improved drug delivery and enhanced immune-chemotherapy of breast cancer.* Advanced Functional Materials, 2019. **29**(32): p. 1901896.

361. Sun, W. and Z. Gu, *ATP-Responsive Drug Delivery Systems.* Expert Opin Drug Deliv, 2016. **13**(3): p. 311-4.

362. Abnous, K., et al., *A smart ATP-responsive chemotherapy drug-free delivery system using a DNA nanostructure for synergistic treatment of breast cancer in vitro and in vivo.* J Drug Target, 2020. **28**(7-8): p. 852-859.

363. Eales, K.L., K.E. Hollinshead, and D.A. Tennant, *Hypoxia and metabolic adaptation of cancer cells.* Oncogenesis, 2016. **5**(1): p. e190.

364. Kumari, R., D. Sunil, and R.S. Ningthoujam, *Hypoxia-responsive nanoparticle based drug delivery systems in cancer therapy: An up-to-date review.* J Control Release, 2020. **319**: p. 135-156.

365. Li, X., et al., *In Vivo-assembled phthalocyanine/albumin supramolecular complexes combined with a hypoxia-activated*

prodrug for enhanced photodynamic immunotherapy of cancer. Biomaterials, 2021. **266**: p. 120430.

366. Yang, D., et al., *In vivo targeting of metastatic breast cancer via tumor vasculature-specific nano-graphene oxide.* Biomaterials, 2016. **104**: p. 361-71.
367. Shahriari, M., et al., *Enzyme responsive drug delivery systems in cancer treatment.* J Control Release, 2019. **308**: p. 172-189.
368. Li, H., et al., *The relationship between MMP-2 and MMP-9 expression levels with breast cancer incidence and prognosis.* Oncol Lett, 2017. **14**(5): p. 5865-5870.
369. Wei, Z., et al., *Selenopeptide Nanomedicine Activates Natural Killer Cells for Enhanced Tumor Chemoimmunotherapy.* Adv Mater, 2022. **34**(17): p. e2108167.
370. Zhang, J., et al., *Tumor-permeated ATP-based size-controllable immunogenic cell death amplifier remodel immunosuppressive microenvironment to boost cancer immunotherapy.* Applied Materials Today, 2022. **28**: p. 101518.
371. Xu, C., et al., *Transformable nanoparticle-enabled synergistic elicitation and promotion of immunogenic cell death for triple-negative breast cancer immunotherapy.* Advanced Functional Materials, 2019. **29**(45): p. 1905213.
372. Park, J., et al., *Combination delivery of TGF-β inhibitor and IL-2 by nanoscale liposomal polymeric gels enhances tumour immunotherapy.* Nat Mater, 2012. **11**(10): p. 895-905.
373. Ye, Y., et al., *Synergistic Transcutaneous Immunotherapy Enhances Antitumor Immune Responses through Delivery of Checkpoint Inhibitors.* ACS Nano, 2016. **10**(9): p. 8956-63.
374. Huai, Y., et al., *Nanoparticle Interactions with the Tumor Microenvironment.* Bioconjug Chem, 2019. **30**(9): p. 2247-2263.

375. Gao, J., Y. Liang, and L. Wang, *Shaping Polarization Of Tumor-Associated Macrophages In Cancer Immunotherapy.* Front Immunol, 2022. **13**: p. 888713.

376. Andón, F.T., et al., *Targeting tumor associated macrophages: The new challenge for nanomedicine.* Semin Immunol, 2017. **34**: p. 103-113.

377. Wang, Y., et al., *Engineering Endogenous Tumor-Associated Macrophage-Targeted Biomimetic Nano-RBC to Reprogram Tumor Immunosuppressive Microenvironment for Enhanced Chemo-Immunotherapy.* Advanced Materials, 2021. **33**(39): p. 2103497.

378. Niu, M., et al., *Tumor-Associated Macrophage-Mediated Targeted Therapy of Triple-Negative Breast Cancer.* Mol Pharm, 2016. **13**(6): p. 1833-42.

379. Li, Z., et al., *Depletion of tumor associated macrophages enhances local and systemic platelet-mediated anti-PD-1 delivery for post-surgery tumor recurrence treatment.* Nat Commun, 2022. **13**(1): p. 1845.

380. Figueiredo, P., et al., *Peptide-guided resiquimod-loaded lignin nanoparticles convert tumor-associated macrophages from M2 to M1 phenotype for enhanced chemotherapy.* Acta Biomater, 2021. **133**: p. 231-243.

381. Liu, Y. and X. Cao, *Intratumoral dendritic cells in the anti-tumor immune response.* Cell Mol Immunol, 2015. **12**(4): p. 387-90.

382. Stead, S.O., et al., *Manipulating human dendritic cell phenotype and function with targeted porous silicon nanoparticles.* Biomaterials, 2018. **155**: p. 92-102.

383. Bol, K.F., et al., *Dendritic Cell-Based Immunotherapy: State of the Art and Beyond.* Clin Cancer Res, 2016. **22**(8): p. 1897-906.

384. Mody, K.T., et al., *Mesoporous silica nanoparticles as antigen carriers and adjuvants for vaccine delivery.* Nanoscale, 2013. **5**(12): p. 5167-79.

385. Fang, R.H., et al., *Cancer cell membrane-coated nanoparticles for anticancer vaccination and drug delivery.* Nano Lett, 2014. **14**(4): p. 2181-8.

386. Perica, K., et al., *Nanoscale artificial antigen presenting cells for T cell immunotherapy.* Nanomedicine, 2014. **10**(1): p. 119-29.

387. Speiser, D.E., P.C. Ho, and G. Verdeil, *Regulatory circuits of T cell function in cancer.* Nat Rev Immunol, 2016. **16**(10): p. 599-611.

388. Tay, R.E., E.K. Richardson, and H.C. Toh, *Revisiting the role of CD4(+) T cells in cancer immunotherapy-new insights into old paradigms.* Cancer Gene Ther, 2021. **28**(1-2): p. 5-17.

389. Haist, M., V. Mailänder, and M. Bros, *Nanodrugs Targeting T Cells in Tumor Therapy.* Front Immunol, 2022. **13**: p. 912594.

390. Nishikawa, H. and S. Sakaguchi, *Regulatory T cells in cancer immunotherapy.* Curr Opin Immunol, 2014. **27**: p. 1-7.

391. Esmaily, M., et al., *Blockade of CTLA-4 increases anti-tumor response inducing potential of dendritic cell vaccine.* J Control Release, 2020. **326**: p. 63-74.

392. Wu, Y., et al., *Silencing PD-1 and PD-L1 with nanoparticle-delivered small interfering RNA increases cytotoxicity of tumor-infiltrating lymphocytes.* Nanomedicine (Lond), 2019. **14**(8): p. 955-967.

393. Du, B., et al., *Simultaneous innate immunity activation and immunosuppression improvement by biodegradable nanoplatform for boosting antitumor chemo-immunotherapy.* Chemical Engineering Journal, 2022. **441**: p. 136093.

394. Feng, B., et al., *Binary Cooperative Prodrug Nanoparticles Improve Immunotherapy by Synergistically Modulating Immune Tumor Microenvironment.* Adv Mater, 2018. **30**(38): p. e1803001.

395. Hu, D., et al., *Cancer-associated fibroblasts in breast cancer: Challenges and opportunities.* Cancer Commun (Lond), 2022. **42**(5): p. 401-434.

396. Chen, X. and E. Song, *Turning foes to friends: targeting cancer-associated fibroblasts.* Nat Rev Drug Discov, 2019. **18**(2): p. 99-115.

397. Liu, Y., et al., *A triple enhanced permeable gold nanoraspberry designed for positive feedback interventional therapy.* J Control Release, 2022. **345**: p. 120-137.

398. Hu, M., et al., *Salvianolic acid B-loaded polydopamine-modified hollow mesoporous organic silica nanoparticles for treatment of breast cancer metastasis via suppressing cancer-associated fibroblasts.* Eur J Pharm Sci, 2024. **192**: p. 106641.

399. Zhang, H., et al., *Relaxin-encapsulated polymeric metformin nanoparticles remodel tumor immune microenvironment by reducing CAFs for efficient triple-negative breast cancer immunotherapy.* Asian J Pharm Sci, 2023. **18**(2): p. 100796.

400. Xin, L., et al., *Fibroblast Activation Protein-α as a Target in the Bench-to-Bedside Diagnosis and Treatment of Tumors: A Narrative Review.* Front Oncol, 2021. **11**: p. 648187.

401. Zhen, Z., et al., *Protein Nanocage Mediated Fibroblast-Activation Protein Targeted Photoimmunotherapy To Enhance Cytotoxic T Cell Infiltration and Tumor Control.* Nano Lett, 2017. **17**(2): p. 862-869.

402. Jian, C., et al., *Biomimetic Nanoplatform for Dual-Targeted Clearance of Activated and Senescent Cancer-Associated*

Fibroblasts to Improve Radiation Resistance in Breast Cancer. Small, 2024. **20**(25): p. e2309279.

403. Ji, T., et al., *Transformable Peptide Nanocarriers for Expeditious Drug Release and Effective Cancer Therapy via Cancer-Associated Fibroblast Activation.* Angew Chem Int Ed Engl, 2016. **55**(3): p. 1050-5.
404. Loeffler, M., et al., *Targeting tumor-associated fibroblasts improves cancer chemotherapy by increasing intratumoral drug uptake.* J Clin Invest, 2006. **116**(7): p. 1955-62.
405. Zhang, F.F., et al., *Epitope-based minigene vaccine targeting fibroblast activation protein α induces specific immune responses and anti-tumor effects in 4 T1 murine breast cancer model.* Int Immunopharmacol, 2022. **112**: p. 109237.
406. Jia, J., et al., *FAP-α (Fibroblast activation protein-α) is involved in the control of human breast cancer cell line growth and motility via the FAK pathway.* BMC Cell Biol, 2014. **15**: p. 16.
407. Tchou, J., et al., *Fibroblast activation protein expression by stromal cells and tumor-associated macrophages in human breast cancer.* Hum Pathol, 2013. **44**(11): p. 2549-57.
408. Stefanescu, M., M. Stoia, and O. Stefanescu, *Thermal and FT-IR study of the hybrid ethylene-glycol–silica matrix.* Journal of sol-gel science and technology, 2007. **41**(1): p. 71-78.
409. Cui, C.Y., B. Li, and X.C. Su, *Real-Time Monitoring of the Level and Activity of Intracellular Glutathione in Live Cells at Atomic Resolution by (19)F-NMR.* ACS Cent Sci, 2023. **9**(8): p. 1623-1632.
410. Lérida-Viso, A., et al., *Biosafety of mesoporous silica nanoparticles; towards clinical translation.* Adv Drug Deliv Rev, 2023. **201**: p. 115049.

411. Bej, R. and S. Ghosh, *Glutathione Triggered Cascade Degradation of an Amphiphilic Poly(disulfide)-Drug Conjugate and Targeted Release.* Bioconjug Chem, 2019. **30**(1): p. 101-110.

412. Moorman, A.M., et al., *The prognostic value of tumour-stroma ratio in triple-negative breast cancer.* Eur J Surg Oncol, 2012. **38**(4): p. 307-13.

413. Murakami, M., et al., *Docetaxel conjugate nanoparticles that target α-smooth muscle actin-expressing stromal cells suppress breast cancer metastasis.* Cancer Res, 2013. **73**(15): p. 4862-71.

414. Carvalho, C., et al., *Doxorubicin: the good, the bad and the ugly effect.* Curr Med Chem, 2009. **16**(25): p. 3267-85.

415. Favreau-Lessard, A.J., et al., *Systemic and cardiac susceptibility of immune compromised mice to doxorubicin.* Cardiooncology, 2019. **5**: p. 2.

APPENDIX

Supplementary figures

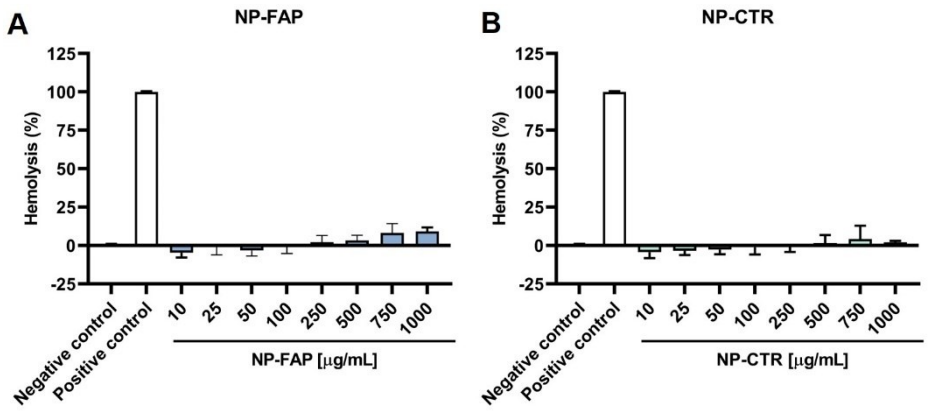

Figure S1. Mesoporous silica nanoparticles biocompatibility. Hemolytic activity of the **(A)** NP-FAP and **(B)** NP-CTR. Red blood cells were incubated with PBS (negative control), 1% Triton X-100 (positive control), or NPs at different concentrations for 1 hour at 37 °C. Mean ± SD.

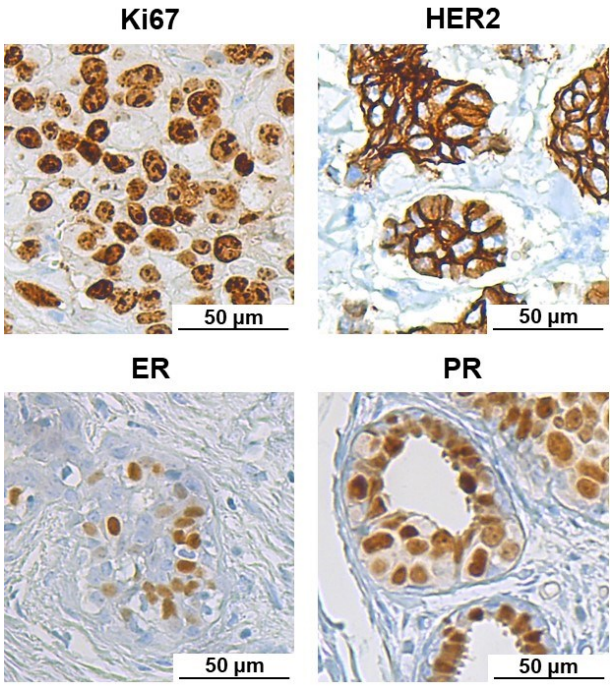

Figure S2. Immunohistochemistry positive controls. Representative images of immunocytochemistry staining of Ki67, human epidermal growth factor receptor 2 (HER2), estrogen receptor (ER), and progesterone receptor (PR) positive controls. Scale bar: 50 µm.

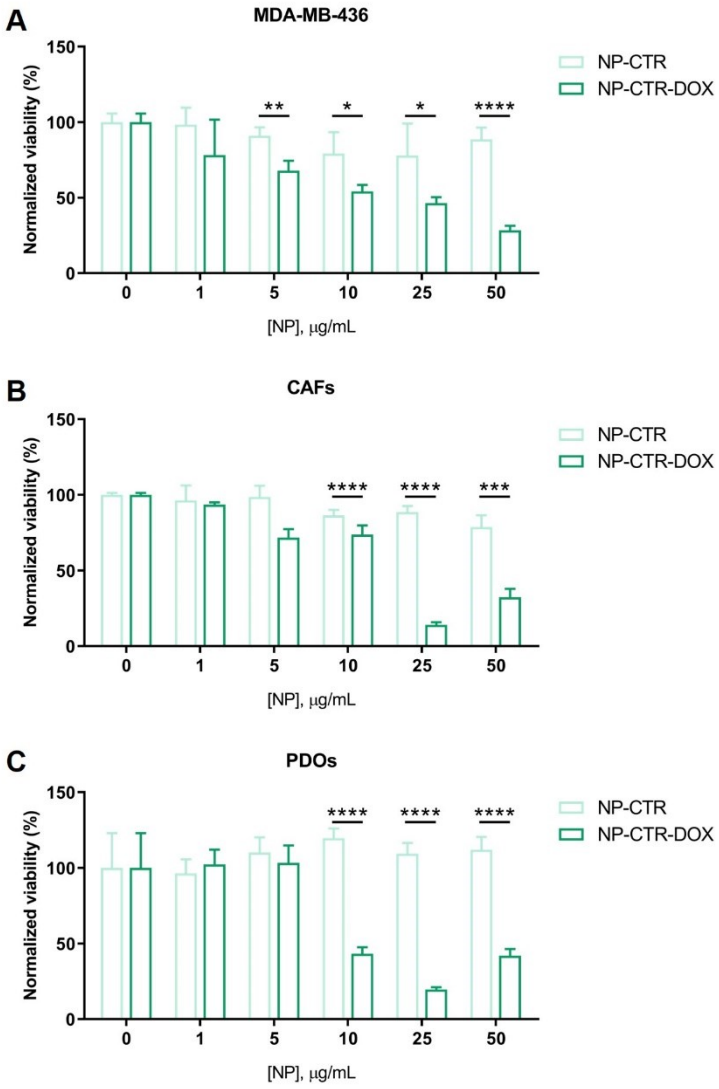

Figure S3. NP-CTR-DOX cytotoxic effect on breast cancer FAP-α positive cells, cancer-associated fibroblasts, and patient-derived organoids. Cellular cytotoxicity of NP-CTR and NP-CTR-DOX in **(A)** MDA-MB-436 cell line, **(B)** CAFs, and **(C)** PDOs. Cells were treated with 0, 1, 5, 10, 25, and 50 μg/mL for 72 hours and viability was determined. Mean ± SD, *$p < 0.05$, **$p < 0.01$, ***$p < 0.001$, ****$p < 0.0001$.

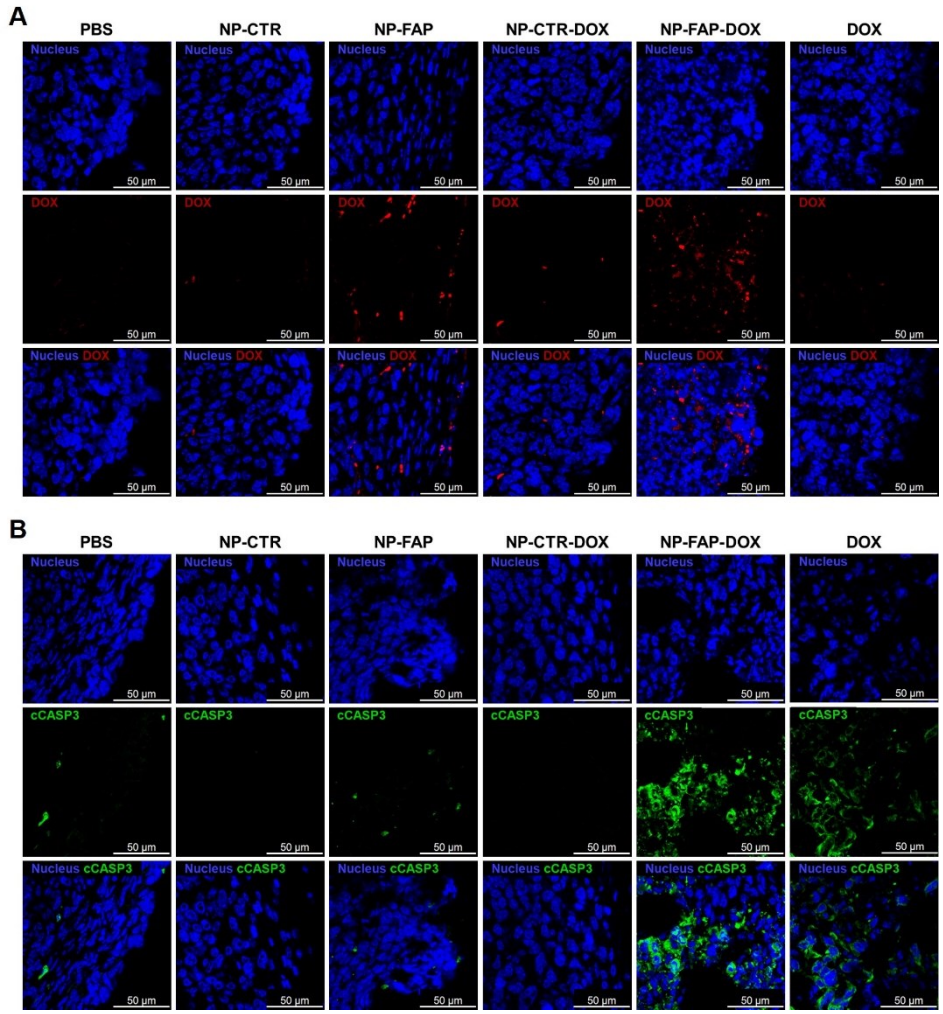

Figure S4. NP-FAP-DOX's *in vivo* antitumoral efficacy. (A) Representative images of internalized DOX in paraffin-embedded tumor sections at the treatment endpoint. Blue: DAPI, Red: DOX. Scale bar: 50 µm. **(B)** Representative images of immunofluorescence staining of cleaved-caspase 3 (cCASP3) in paraffin-embedded tumor sections at the treatment endpoint. Blue: DAPI, Green: cCASP3. Scale bar: 50 µm.

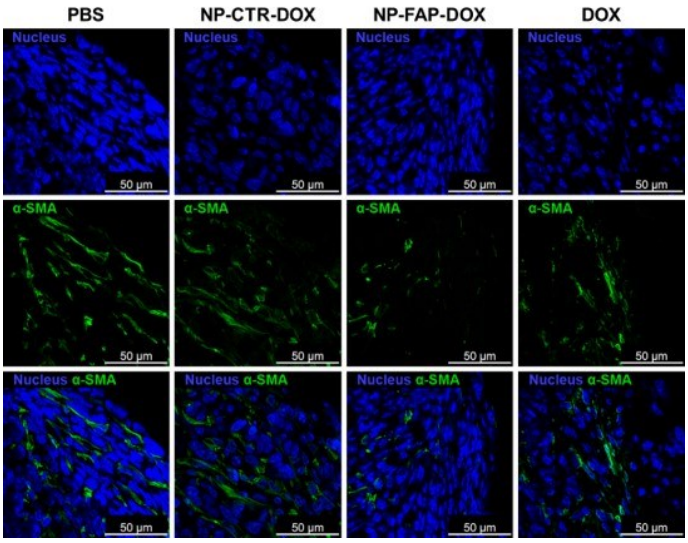

Figure S5. NP-FAP-DOX's *in vivo* targeting of cancer-associated fibroblasts. Representative images of immunofluorescence staining of α-SMA in paraffin-embedded tumor sections at the treatment endpoint. Blue: DAPI, Green: α-SMA. Scale bar: 50 μm.

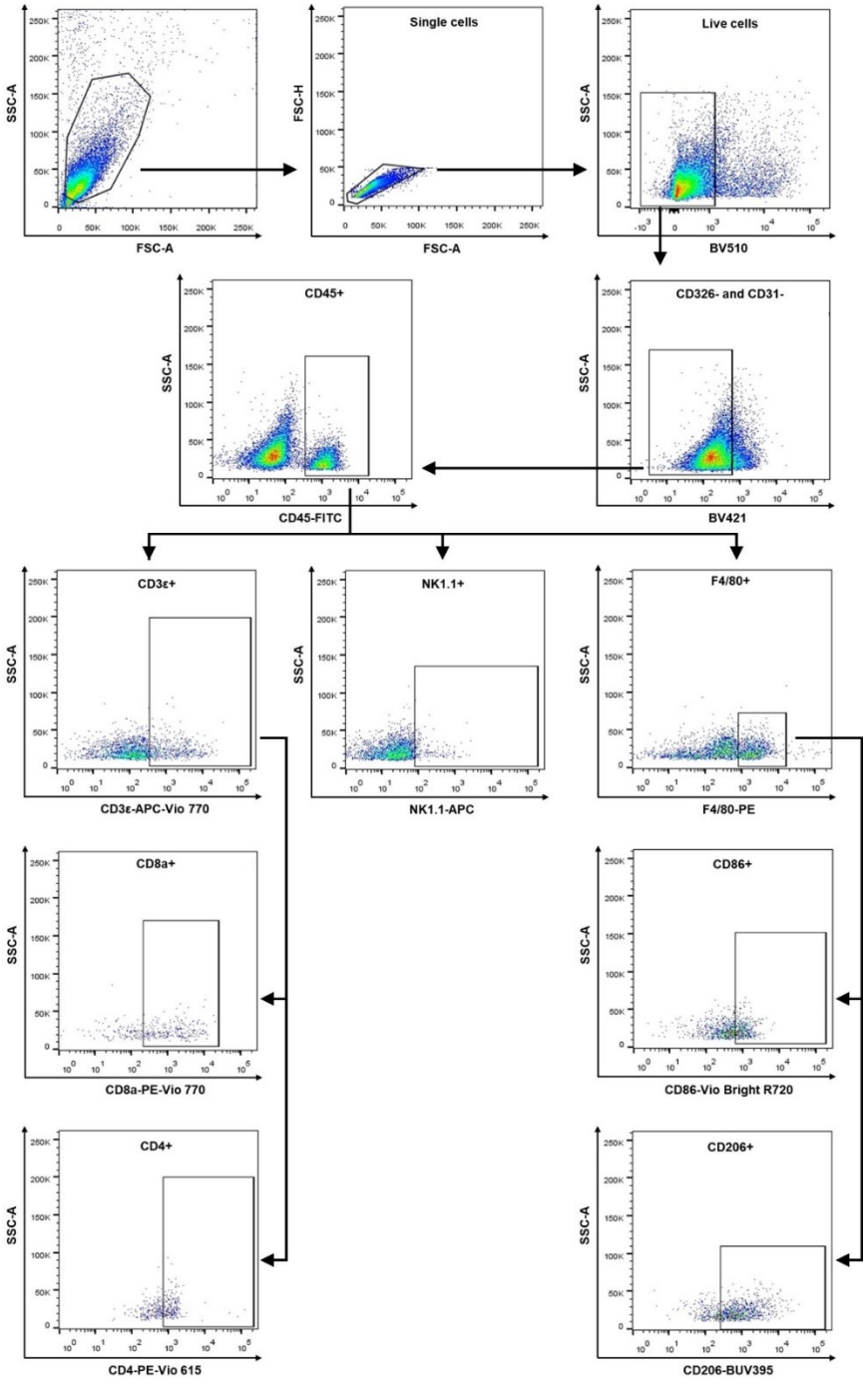

Figure S6. Flow chart of flow cytometry analysis of T lymphocytes (CD45+CD3ε+), cytotoxic T cells (CD45+CD3ε+CD8a+), helper T cells

(CD45+CD3ε+CD4+), NK cells (CD45+NK1.1+), M1-like macrophages (CD45+F4/80+CD86+), and M2-like macrophages (CD45+F4/80+CD206+) in the treated tumor.

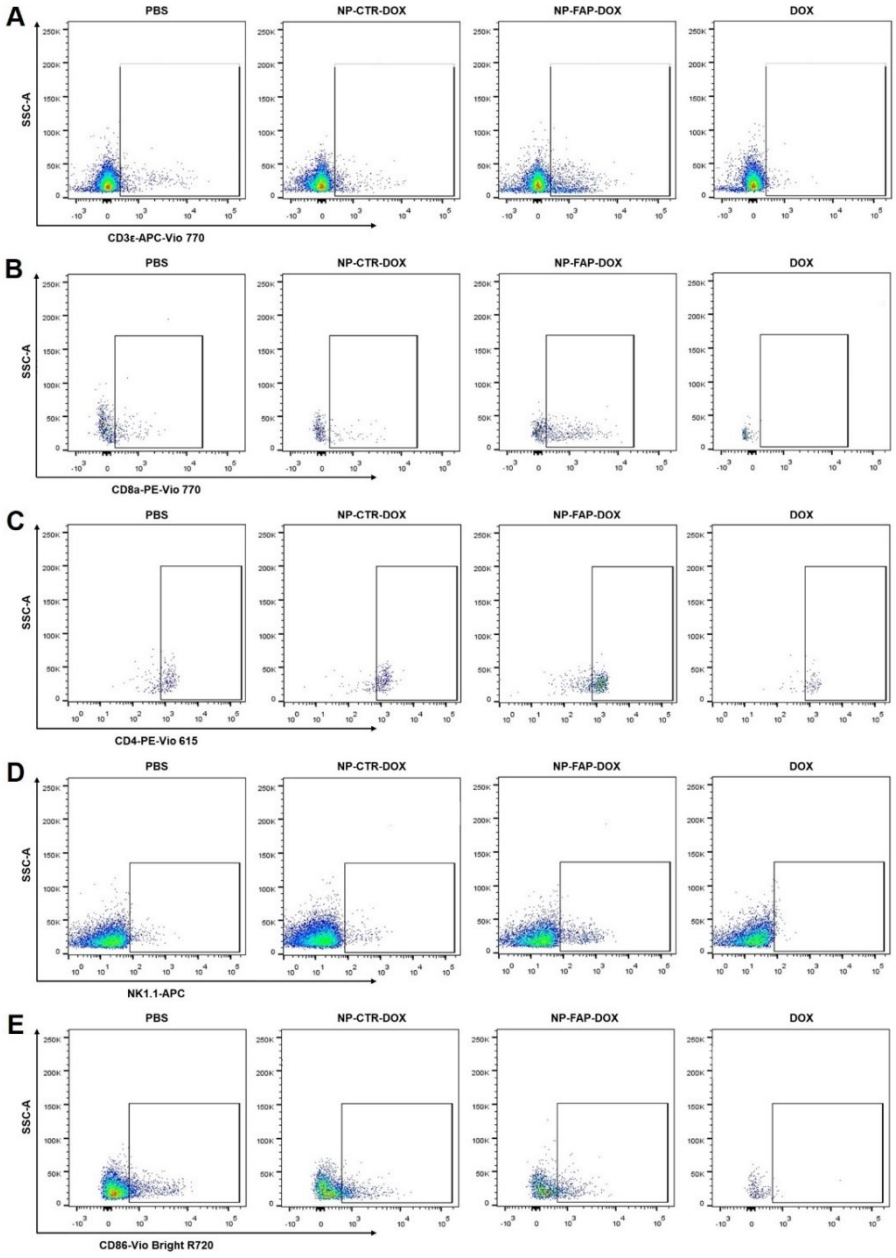

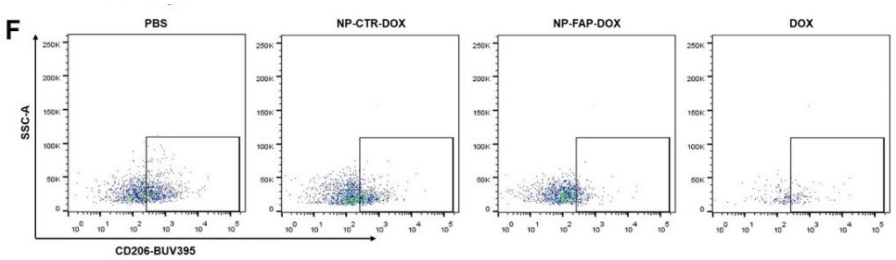

Figure S7. NP-FAP-DOX's *in vivo* tumor microenvironment modulation. Representative flow cytometry analysis of **(A)** T lymphocytes ($CD45^+/CD3\varepsilon^+$), **(B)** cytotoxic T cells ($CD45^+/CD3\varepsilon^+/CD8a^+$), **(C)** helper T cells ($CD45^+/CD3\varepsilon^+/CD4^+$), **(D)** natural killer cells ($CD45^+/NK1.1^+$), **(E)** M1-like macrophages ($CD45^+/F4/80^+/CD86^+$), and **(F)** M2-like macrophages ($CD45^+/F4/80^+/CD206^+$) in xenograft tumors analyzed at the treatment endpoint.